Quantum Dynamical Approach to Ultrafast Molecular Desorption from Surfaces

Peter Saalfrank

Theoretische Chemie, Institut für Chemie, Universität Potsdam, Karl-Liebknecht-Strasse 24-25, D-14476 Potsdam-Golm, Germany

Contents

1. Introduction

1.1. General

The desorption of atoms or molecules from solid surfaces is a key step in heterogeneous catalysis, photocatalysis, electrochemistry, and surface nanochemistry. The breaking of a bond between an adsorbate and a surface can be extremely fast (i.e., femtoseconds, 10^{-15} s, and below) but also very slow (i.e., seconds and above), depending on the enforcing conditions and on the specific system under consideration.

In this review, I will mostly be concerned with ultrafast desorption on the (sub-) picosecond time scale, enforced with photons. Occasionally, however, slower reactions will also be considered. Photodesorption continues to attract attention from both experiment[1] and theory.[2] Photodesorption is interesting not only per se but also as a prototypical example for a wider class of nonadiabatic surface reactions.[3] Among

Peter Saalfrank studied chemistry at the University of Erlangen-Nürnberg in Germany, where he graduated in 1988. He received his Ph.D. from the same institution under J. Ladik in 1991, with a topic from the theory of electronic structure of solids. From 1992 to 1993, he was a DFG postdoctoral research fellow at the University of California at Berkeley with W. H. Miller, then a scientific co-worker at the Fritz-Haber-Instiut in Berlin (1993) and at the Freie Universität Berlin (1993–1998), where he finished his habilitation in Theoretical Chemistry in 1996. From 1998 to 2000, he was Senior Lecturer for Theoretical Chemistry at University College London, and from 2000 to 2003, he was Professor for Theoretical Chemistry at the University of Regensburg, Bavaria. Since 2003, he has held the Chair of Theoretical Chemistry at the University of Potsdam, Germany. He is presently "Fachkollegiat" (referee) of the German Research Council (DFG) for Theoretical Solid State Chemistry. The main research topics of Dr. Saalfrank are theoretical surface science, reaction dynamics and femtochemistry, and electronic structures of molecules and solids.

these are simple vibrational[4] and rotational excitation of molecules, photodissociation,[5] photoassociation,[6,7] photo-diffusion,[8,9] and more complex photoreactions[10] of adsorbed species, with potential implications for molecular machines,[11-13] molecular rotors,[14,15] and molecular switches.[16] Some of these reactions will be covered by other authors in this thematic issue of *Chemical Reviews*.

1.2. Mechanisms of Photodesorption

Photodesorption, the simplest of all photoreactions at a surface, can be enforced either directly or indirectly, i.e., substrate-mediated. In the first case, either infrared (IR)[17] or, more commonly, ultraviolet/visible (UV/vis) photons[1] couple directly to the dipole or transition dipole moment of the adsorbate–substrate complex. For weakly bound adsorbates, the black body radiation at ambient temperatures suffices to induce direct desorption.[18,19] Direct excitation is also the rule for IR excitation, even at metal surfaces, which frequently act as "mirrors" for IR photons. On the other hand, in UV/vis, direct excitation only dominates for semiconductor or insulating surfaces. In contrast, metal surfaces have a large absorptivity at these shorter wavelengths, thus preferring the indirect route. In this case, desorption is a two-step process, i.e., initial absorption by the surface and subsequent transfer of energy to the adsorbate–substrate complex. Direct and indirect routes can experimentally be discriminated by a dependence, or lack thereof, of the desorption yield and other observables on the polarization of the incoming light: For direct excitation, the cross-section is largest with light polarized along the (transition) dipole of the bond to be broken, while for substrate-mediated excitation, the polarization plays only a minor role.

An example for the first scenario is H:Si(100)2 × 1, where a strong dependence of the UV laser-induced desorption of

hydrogen atoms on the polarization was observed, with polarization along the H−Si bond favoring the reaction.[20] An example for the second class is photodesorption of NO from Pt(111), where no such dependence on laser polarization was found.[21,22]

The indirect, substrate-mediated excitation can further be categorized according to the photon density of the exciting light source. With low-fluence light, typically realized with continuous wave (cw) or nanosecond-pulse lasers, one observes, in the context of photodesorption, so-called DIET, desorption induced by electronic transitions. Experimentally, DIET of adsorbates from metals is characterized by comparatively small desorption probabilities Y per absorbed photon and by a yield that increases *linearly* with laser fluence. In contrast, with intense light sources such as femtosecond lasers (FLs), one observes so-called DIMET, desorption induced by multiple electronic transitions. For this reaction, which was pioneered by Heinz and co-workers,[23-26] a number of "hallmarks" have been identified, which distinguish it from DIET. These hallmarks are as follows: (i) The desorption yield is usually, at the same wavelength, larger in DIMET than in DIET. (ii) The desorption yield increases *superlinearly* with laser fluence, F. Often, an empirical power law

$$Y = A\,F^n \tag{1}$$

is observed with $n > 1$ (typically $2-10$). An illustrative example is, again, NO/Pt(111), where at low absorbed fluences up to about 1.5 mJ/cm^2, a linear increase $Y \propto F$ was found and a power law $Y \propto F^{6\pm1}$ was found at higher fluences[27]—See Figure 1.
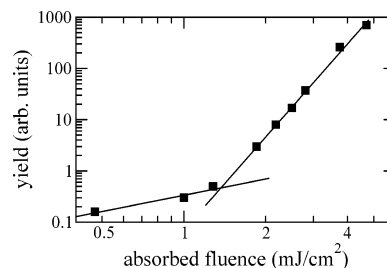
Figure 1. Desorption of NO from Pt(111). Desorption yield Y as a function of absorbed laser fluence F; after ref 27 (one data set). The two lines are curves $Y \propto F$ and $Y \propto F^6$, respectively.

The nonlinear scaling (1) has been observed in a number of FL-induced desorption (FLD) experiments, such as NO/Pd(111)[23] (exponent, $n \sim 3.3$), CO/Cu(111)[28] ($n \sim 3.7$), CO/Cu(100)[29] ($n \sim 8$), or O$_2$/Pd(111)[30,31] ($n \sim 6$). Nonlinear scalings were also observed for several other photoreactions, such as photodissociation of O$_2$ on Pt(111)[32-34] or the photodiffusion of O$_2$ on Pt(110).[9]

Besides the desorption yield, other properties of the desorbates may be different under DIMET conditions. For example, the amount of vibrational excitation of NO desorbing from Pt(111), as well as the translational energy, increase with increasing laser fluence.[27]

Under DIMET or more general, under FL conditions, the *branching ratios* of possible, concuring reactions can be different to DIET conditions. As an example, for O$_2$ adsorbed on Pt(111), the preferred reaction is dissociation when nanosecond lasers are used, whereas molecular desorption dominates under FL excitation conditions.[32-34]

DIET is brought about by infrequent, uncorrelated electronic excitations of the adsorbate−substrate complex. On the excited-state potential energy surface(s) (PES), the nuclear wave packet is nonstationary and feels forces, which are absent in the ground state. The enforced nuclear motion may eventually lead to the breaking of a bond, as will be outlined in greater detail below. It is important to note that the excited state(s) often couples efficiently to the internal degrees of freedom of the substrate, in particular to electron−hole pairs of a metal. As a consequence, the excited states are *resonances*, i.e., short-lived intermediates rather than stationary states, with lifetimes, τ_{el}, often on the time scale of femtoseconds. Once in the ground state again, from where desorption occurs, the adsorbate also relaxes vibrationally, on a somewhat longer time scale, τ_{vib}—typically within picoseconds when the adsorbate vibration couples to electron−hole pairs. This time scale holds for the molecule−surface bond but also for internal modes—For desorption, the former is more relevant. DIET is realized if the average time between two subsequent electronic excitations, t_{exc}, is long as compared to the lifetimes, τ_{el} and τ_{vib}. The individual excitation/deexcitation processes have no memory of each other; therefore, the reaction yield Y increases proportional to F.

In contrast, in DIMET, short, intense laser pulses cause more than one, i.e., multiple, excitations of the adsorbate on the time scales of electronic and vibrational relaxation. This is due to a high density of "hot electrons" created in the metal surface. Often, the hot electrons are attached to the adsorbate and a "negative ion resonance" is formed. During action of the laser pulse, by vibration−electron coupling, the adsorbate−surface bond becomes "vibrationally hot", thus leading to "ladder climbing" in the electronic ground state and desorption. This is a complicated, correlated process, with the result that the desorption yield increases nonlinearly with F according to eq 1.

Intense laser pulses heat not only the metal electrons but also the substrate phonons by electron−phonon coupling. Also, because the adsorbate−surface vibrations are coupled to the phonons, there is the possibility that intense laser pulses cause *thermal desorption* in the ground state. In general, both mechanisms, "electronic" and "phononic", occur simultaneously, with different weights. Experimentally, one can discriminate between phonon and electron mechanisms by *two-pulse correlation* (2PC) traces.[24] Accordingly, one records observables, such as the desorption yield Y, as a function of the delay time $\Delta\tau$ between two laser pulses. As a result of the nonlinear increase of Y with F according to eq 1, one typically obtains a signal Y vs $\Delta\tau$, which peaks sharply around $\Delta\tau = 0$, gradually falling off at $\Delta\tau \rightarrow \pm\infty$. If the half width at half maximum (hwhm) of the $Y(\Delta t)$ curve is in the nanosecond range; this is indicative of a dominant phononic mechanism. A hwhm $\sim$ picosecond suggests an electronic mechanism (vide infra). The ultrafast response in hot-electron-mediated FLD is therefore another "hallmark" of DIMET.[24]

In Figure 2, I summarize various photon-stimulated desorption (PSD) processes, which will be covered in this paper.

1.3. Related Phenomena

It has been mentioned that photochemistry at surfaces is not restricted to desorption. Furthermore, all of the above reactions can also be initiated by energy sources other than electromagnetic radiation. The most prominent example is
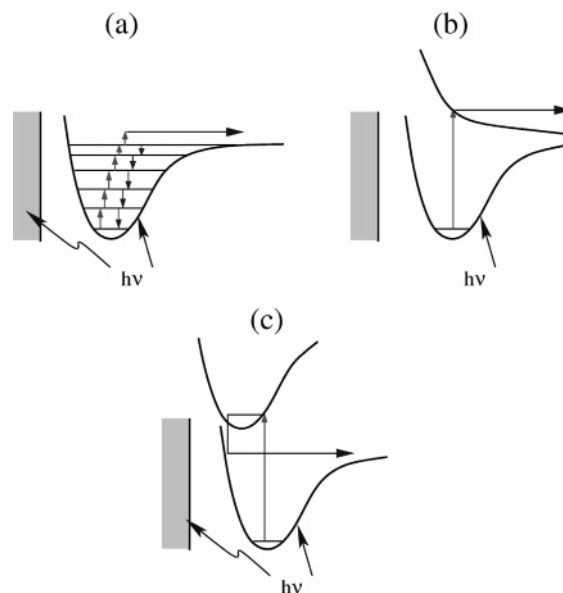

Figure 2. Various PSD processes. (a) Ladder climbing by direct (IR photons) or substrate-mediated (phonon) excitation. (b) Desorption in a long-lived excited state after direct excitation, typically realized for insulators. (c) Desorption in the ground state after intermediate population of a short-lived excited state, typically realized for metal surfaces. In this case, multiple excitation−deexcitation cycles may occur, leading to DIMET (see the text).

the scanning tunneling microscope (STM), by which—depending on the polarity of the applied voltage—electrons or holes tunneling from the STM tip enforce molecular dynamics (MD).

Similar to photochemistry, different regimes exist in which the desorption yield, for example, increases either linearly with the tunneling current I or in a nonlinear fashion. The linear and nonlinear regimes can be realized by choosing the bias voltage above or below a threshold for electronic excitation, respectively. The "above threshold" regime, where $Y \propto I$, corresponds to DIET and arises from singular and uncorrelated excitations of the adsorbate. A single charge carrier emitted from the STM tip provides enough energy to reach the excited state. For semiconductor surfaces, this is sometimes several electronvolts, and consequently, a voltage of several volts has to be applied.

At lower bias voltages, in the "below threshold regime", the charge carriers are energetically unable to directly reach the resonance. Nevertheless, similar to DIMET, a gradual "heating" of the adsorbate−surface bond can occur, by inelastic electron tunneling (IET), leading eventually to bond breaking. For the desorption or other reaction, the yield is typically much smaller than in the "above threshold" case and increases nonlinearly with the tunneling current.[35]

An experimental example is the STM-induced desorption of H and D atoms from hydrogen-covered Si(100)2 × 1 surfaces. At positive sample biases below 7 V or so, the desorption yield is low ($<10^{-6}$ per tunneling electron) and increases according to a power law I^n with the STM current by "ladder climbing".[36,37] Above a threshold of about 7 V, the $\sigma \rightarrow \sigma*$ excitation energy for the Si−H bond is met, leading to a DIET reaction with a larger yield of about 3 × 10^{-6} per tunneling electron for H/Si. In this regime, a linear dependence of Y on I is found.[35,38] There are also examples where desorption of molecular systems has been achieved with an STM, e.g., of benzene from Si(100)2 × 1,[39,40] chlorobenzene from Si(111)7 × 7,[41] or NH_3 from Cu(100).[42]

The STM thus offers, as additional control parameters, the current, the voltage, and the polarity of the bias. At positive bias voltage, $V_s > 0$ electrons tunnel from the tip to the surface, inelastically scattering at empty orbitals of an adsorbate in between. At negative sample bias voltages, $V_s < 0$ electrons tunnel from the surface to the tip (or equivalently holes in the opposite direction), inelastically scattering at occupied orbitals of the adsorbate. As a result, the reaction can proceed, besides via neutral excited states, through negative ion and positive ion resonances, respectively, with possibly different outcomes. For example, at positive sample bias, desorption of H is observed (see above). At negative sample bias, both desorption and the lateral "switching" of a hydrogen atom from one side of a Si_2 dimer to a neighboring, empty, dangling bond site at the same dimer has been realized.[43−45] Lateral switching of adsorbates had earlier been observed, on metal surfaces, by Eigler and co-workers[46,47] and Rieder and co-workers.[48] Also, vertical "switches" (between a surface and the STM tip) are known.[49,50]

In addition to resonant processes, the STM offers in principle also the route to tip−field-induced manipulations. In particular, at semiconductor or oxide surfaces, the field strengths may become quite large (in the order of 1 V/Å), leading to a distorted ground-state potential and molecular motion.[51,52]

Apart from switching and desorption, there are a number of other processes, which can be triggered by an STM.[53] The vibrational excitation of adsorbates by inelastically tunneling electrons is used in scanning tunneling spectroscopy (STS).[54−56] Other examples are STM-induced diffusion,[48,57] STM-induced rotation of molecules[55,58] or of individual units of large molecules,[59] STM-induced dissociation,[60−64] STM-induced reactions,[65] and STM-induced isomerization.[42,66] In ref 42, it was also demonstrated that it is possible, by varying current and voltage, to influence the outcome of IET. Specifically, the tunneling electrons were tuned to either desorb NH_3 molecules from a Cu(100) surface or translate them laterally.

Because current-induced surface reactions arise from inelastic electron−molecule scattering, similar to substrate-mediated, hot-electron chemistry, photon- and current-induced reactions are frequently treated with very similar models and methods. Similarities exist also to problems related to the transport of electrons (or holes) through molecular junctions and in molecular electronics[67−71]—in this case, STM tips and substrates are simply replaced by electrodes.

Finally, nonadiabatic surface reactions can also be induced by electrons coming from other sources. In electron stimulated desorption (ESD), for example, an electron beam enforces the desired reaction. While electrons created by FLs or emanating from an STM are low in energy (typically in the order of one to a few eV), electrons from a beam can have energies in the kiloelectronvolt regime. Even if not all of that energy is transferred to the adsorbate, high-energy excitations are possible; therefore, the outcome of an ESD experiment is qualitatively different from a UV/vis photon-stimulated process or an STM-induced process. For example, by using 150 keV electrons, Menzel and co-workers desorbed CO molecules from a Ru(0001) surface.[72,73] In contrast to the milder conditions of typical PSD experiments, it was observed that the desorbing molecules are vibrationally extremely excited.
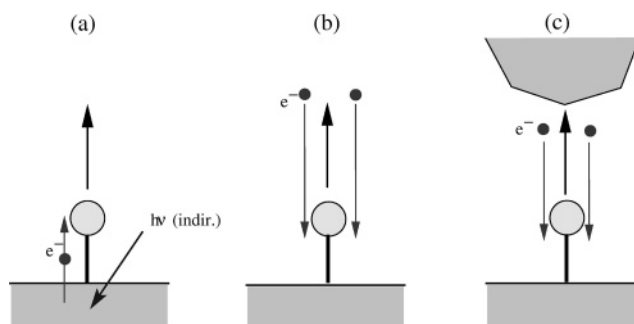

Figure 3. Various electron-mediated desorption processes: Hot-electron-mediated PSD, ESD, and STM-induced desorption.

In Figure 3, I schematically indicate different "electron-mediated" desorption processes, PSD via hot electrons (panel a), ESD (panel b), and STM-induced desorption (panel c).

In passing, I note that other high-energy projectiles such as atoms or ions may also be used to enforce desorption and other nonadiabatic surface reactions.[74] Finally, there is a close connection of the physics and techniques to be covered by this review and nonadiabatic gas−surface scattering.[75]

1.4. Focus and Outline of This Review

In this overview, I focus on recent advances in the *quantum theory* and in particular of the *dynamics* of processes at surfaces that are driven by photons and that lead to bond breaking. The molecular manipulation via atomic force microscopes and static-field manipulation via an STM will not be reviewed. Resonance-mediated, STM-induced processes such as IET and subsequent reactions will only be treated to an extent that allows one to make connections to photon-induced chemistry. Finally, I emphasize *nuclear dynamics* in the following. The focus is also on a *time-dependent* description, despite the fact that time-independent approaches can be very useful.[76,77]

This review is organized as follows. In the next section, I will present the most common *models* and *methods* for photodesorption. I will distinguish here between electronically adiabatic (section 2.1), weakly nonadiabatic (section 2.2), and strongly nonadiabatic dynamics (section 2.3). This encompasses situations/models in which desorption occurs in the ground state, by excited-state-driven ladder climbing in the ground state, and by explicit, active participation of one or several electronically excited states, respectively. The discrimination between "weak" and "strong" nonadiabaticity is somewhat arbitrary.

The theoretical and numerical tools to treat the nuclear dynamics within a given model will also be outlined in section 2, for the three "limits" mentioned above. In many, but not all, models of photodesorption, the Born−Oppenheimer separation between electronic and nuclear motion is central, with nonadiabatic couplings being treated a posteriori, either explicitly or in some effective, reduced dynamics way. The most frequently used techniques here are classical trajectory (possibly with electronic friction) methods, semiclassical surface hopping, and wave packet and reduced density matrix methods. Several of these methods come together with model Hamiltonians—Some of them will also be presented in section 2.

A first step toward dynamics is the determination of ground- and excited-state potentials of the adsorbate−surface system. Methods to calculate those will be treated in section 3. In reduced dynamics models, the electronically (and

vibrationally) excited states are nonstationary, thus accounting for the coupling to a "bath" of substrate phonons and electron−hole pairs. The computation of electronic and vibrational lifetimes, and corresponding resonance widths, will be surveyed in section 4.

In section 5, I will review recent theory in the field of direct, IR photon-induced desorption and vibrational excitation of molecules at surfaces. In section 6, I will give concrete examples of theoretical models for photodesorption from insulating surfaces, when UV/vis light is used instead. Here, the adsorbates can be treated as "weakly coupled" to the substrate, with the consequence that the physics is similar to gas-phase dissociation. Strong coupling between adsorbate and surface modes is the rule for metal surfaces and sometimes for semiconductors. This leads to short lifetimes of excited states, which cannot be neglected. Photodesorption from semiconductor and metal surfaces will be covered in section 7. I will distinguish here between direct DIET (section 7.1), substrate-mediated DIET (section 7.2), and DIMET by FLs (section 7.3). In section 8, related reactions will briefly be considered, e.g., STM-induced desorption and ESD. Section 9 describes attempts to control surface photoreactivity, either by nanostructuring the substrate or by lasers. This review covers the last 8 years or so; however, it sometimes digs deeper into history.

2. Models and Methods for Desorption

2.1. Adiabatic Dynamics

2.1.1. The Born–Oppenheimer Approximation

Most of the theoretical models start with the Born−Oppenheimer approximation, in which the electronic and nuclear motion are separated from each other, i.e., by solving an electronic Schrödinger equation

$$\hat{H}_r \Psi_i(r, R) = E_i(R)\, \Psi_i(r, R) \tag{2}$$

I obtain, for various electronic states i, the electronic energy $E_i = \langle \Psi_i | \hat{H}_r | \Psi_i \rangle_r$ and the electronic wave functions $\Psi_i(r; R)$. The latter depend on the coordinates of the N electrons, $\underline{r} = (\underline{r}_1, \underline{r}_2, ..., \underline{r}_N)$, denoted by r for compactness and, parametrically, also on the coordinates of N_A nuclei, $\underline{R} = (\underline{R}_1, \underline{R}_2, ..., \underline{R}_{N_A})$, denoted here as R. $\hat{H}_r = \hat{T}_r + V_{rr} + V_{rR}$ in eq 2 is the electronic Hamiltonian, containing the kinetic energy operator $\hat{T}_r$ of the electrons, the interelectronic repulsion V_{rr}, and the electron−nuclear attraction V_{rR}. When adding the internuclear repulsion $V_{RR}(R)$ to $E_i(R)$, I obtain the Born−Oppenheimer PESs $V_i(R)$ on which the nuclei move

$$V_i(R) = E_i(R) + V_{RR}(R) \tag{3}$$

The Born−Oppenheimer surfaces are $3N_A - 6$ dimensional functions. It is clear that for an adsorbate−surface system with a formally infinite number of atoms, most of those need to be treated as frozen or approximated in some other way. Often, the surface is considered rigid, leaving only $3N_{ads}$ degrees of freedom if N_{ads} is the number of adsorbate atoms. As a further restriction, in reduced-dimensionality models, out of these modes, only the most important ones (i.e., those actively participating in the dynamics) are considered. In an extreme but quite common case, as a single coordinate, the "desorption coordinate" is

left. The latter is often simply the distance, Z, of the desorbing species' center-of-mass to the substrate.

In the case of adiabatic dynamics, only the ground-state potential needs to be considered. The two most important adiabatic desorption reactions are IR-induced desorption and phonon-induced desorption, respectively.

2.1.2. Laser-Driven Dynamics in the Ground State: Time-Dependent Schrödinger Equation (TDSE)

On a single potential surface, the IR-photon driven desorption can be described by a TDSE for the nuclei

$$i\hbar\, \frac{\partial \psi(R, t)}{\partial t} = \hat{H}(t)\, \psi(R, t) \tag{4}$$

where ψ is the nuclear wave function and $\hat{H}(t)$ is the nuclear Hamiltonian

$$\hat{H}(t) = \hat{T}_R + V(R) - \mu(R) \cdot E(t) \tag{5}$$

Here, the dipole function is given as

$$\mu(R) = \langle \Psi_0 | \hat{\mu}(r, R) | \Psi_0 \rangle_r \tag{6}$$

where $\hat{\mu}(r, R)$ is the dipole operator and Ψ_0 is the ground-state electronic wave function. The dipole (operator) and the field E are vectors, which I neglect here for notational convenience. Equation 5 assumes the semiclassical dipole approximation, under which the electromagnetic field remains unquantized, and magnetic interactions and the coordinate dependence of the electric field E are neglected. It should be noted that in general, the assumption of coordinate-independent fields at adsorbates at metal surfaces goes beyond the usual long-wavelength approximation for molecular systems, because the metal electrons and the adsorbate modify the optical response. In particular, local-field effects can lead to enhanced photoreaction cross-sections, and differences are found between s- and p-polarized light.[78−82] The TDSE (eq 4) must be solved subject to an initial condition, $\psi(t = 0) = \psi_0$. From the propagated wave function,

$$\psi(t) = e^{-i\hat{H}t/\hbar}\, \psi_0 \tag{7}$$

one obtains expectation values of observables $\hat{A}$ according to

$$\langle \hat{A} \rangle(t) = \langle \psi(t) | \hat{A} | \psi(t) \rangle_R \tag{8}$$

The TDSE can be solved in many different ways and representations.[83,84] Expanding the nuclear wave function on the basis $\phi_\alpha(R)$ of the nuclear, field-free Hamiltonian,

$$[\hat{T}_R + V(R)] \phi_\alpha(R) = E_\alpha \phi_\alpha(R) \tag{9}$$

i.e.,

$$\psi(R, t) = \sum_\alpha C_\alpha(t)\, \phi_\alpha(R) \tag{10}$$

[with $C_\alpha(t) = \langle \phi_\alpha | \psi(t) \rangle$], eq 4 becomes a matrix equation

$$i\hbar \frac{dC_\alpha}{dt} = \sum_\beta [E_\beta\, \delta_{\alpha\beta} - \mu_{\alpha\beta}\, E(t)]\, C_\beta \tag{11}$$

Here, $\mu_{\alpha\beta} = \langle \phi_\alpha | \mu | \phi_\beta \rangle$ are dipole matrix elements connecting

different levels on the "vibrational ladder" toward the desorption continuum. Note that in eq 11, I have neglected diagonal field terms, i.e., $-\mu_{\alpha\alpha}E$, which cause a Stark shift of level $|\alpha\rangle$. Equation 11 has to be solved subject to an initial condition, $C_\alpha(0)$, resulting in time-resolved state populations

$$P_\alpha(t) = |C_\alpha|^2 \qquad (12)$$

A desorption yield can then be defined as

$$Y(t) = 1 - \sum_{\alpha \in N_b} P_\alpha(t) \qquad (13)$$

where N_b is the number of bound states, with an energy $E_\alpha \le D$, and D is the binding energy of the adsorbate. In a one-dimensional (1D) model with the adsorbate−surface bond treated as a Morse potential, D is the Morse well depth

$$V(Z) = D[1 - e^{-\gamma(Z-Z_0)}]^2 \qquad (14)$$

and $\phi_\alpha(Z)$ are the bound ($E_\alpha \le D$) and free ($E_\alpha > D$) Morse eigenfunctions, respectively. The *desorption rate* can be defined as

$$R_{des} = \frac{dY}{dt} \qquad (15)$$

Equations 13 and 14 are sensible definitions only if the desorption is not "delayed" too much, as is sometimes the case in so-called vibrational predesorption. There an internal high-energy vibration with $E_\alpha > D$ may have been excited initially. However, if the coupling of this mode to the desorptive mode is weak, bond breaking may be delayed to an extent that it does not occur at all, within the time scale of relaxation. An example for vibrational predesorption is CO on NaCl(100), where the CO stretch vibration when excited to $v = 1$ is above the adsorption energy[85] (vide infra). For delayed desorption, a more sensible definition of the desorption probability is

$$Y(t) = \int_{Z_{des}}^{\infty} |\psi(Z, Q_1, Q_2, ..., t)|^2 \, dZ \qquad (16)$$

where Z_{des} is some distance far from the surface where a particle can safely be considered "desorbed". In eq 16, the nuclear wave packet is the solution of eq 4. In coordinate representation, it depends on the desorption coordinate Z and other important (internal) modes Q_1, Q_2, etc. The coordinate representation requires solution of the TDSE (eq 4) on a spatial grid. This is anyway the preferred technique when the eigenfunctions ϕ_α are not known, either because $\hat{H}_R$ cannot be diagonalized and/or too many continuum states would have to be considered.[83] Of course, if the desorption is too much delayed, a wave packet propagation becomes numerically prohibitive and alternatives such as master or rate equations are required.

I do not review the numerical methods to solve a TDSE here; for this, the reader is referred to refs 83 and 84. I do mention, however, that with a direct product (grid) basis (the "standard model"), presently, wave functions with up to about six degrees of freedom can be propagated. Using more sophisticated methods such as the multiconfigurational time-dependent Hartree method (MCTDH), higher-dimensional quantum dynamical problems became tractable.[86,87] This is particularly so when some of the more remote modes are treated on a lower (e.g., single configuration) level. To my

knowledge, the highest-dimensional problem in gas−surface dynamics considered so far was a simple atom−surface model, in which a single atom scattered at a surface described by 60 oscillators.[88]

2.1.3. Laser-Driven Dynamics in the Ground State: Density Matrix Description

Instead of solving the TDSE (eq 4), one may resort to a density matrix description and solve a Liouville−von Neumann (LvN) equation

$$\frac{\partial \hat{\rho}}{\partial t} = -\frac{i}{\hbar}[\hat{H}(t), \hat{\rho}] =: \mathscr{L}\hat{\rho} \qquad (17)$$

where $[\hat{H}, \hat{\rho}] = \hat{H}\hat{\rho} - \hat{\rho}\hat{H}$ is the commutator between the nuclear Hamiltonian with field and the density operator $\hat{\rho}$, and $\mathscr{L}$ is the (Hamiltonian) Liouvillian. Equation 17 is solved subject to an initial condition, $\hat{\rho}(t = 0) = \hat{\rho}_0$, formally by

$$\hat{\rho}(t) = e^{\mathscr{L}t}\hat{\rho}_0 \qquad (18)$$

For an initial pure state, for example, the ground state $|\phi_0\rangle$, the density operator is

$$\hat{\rho}_0 = |\phi_0\rangle \langle \phi_0| \qquad (19)$$

Equation 19 can be solved with numerical techniques similar to those employed for wave functions. Again, "standard" methods are known[89,90] as well as methods based on a multiconfigurational expansion.[91] The latter approach allowed, for example, the solution of a LvN equation for CO/Cu(100)—a system with six degrees of freedom, i.e., 12 dynamical variables.[92] Once $\hat{\rho}(t)$ is known, expectation values are calculated from a quantum mechanical trace:

$$\langle \hat{A} \rangle(t) = \text{Tr}\{\hat{A}\hat{\rho}(t)\} \qquad (20)$$

An advantage of the LvN equation over the TDSE is that a thermal ensemble can be treated with a single propagation. On the other hand, solving eq 17 is quadratically more expensive than solving eq 4 because twice as many dynamical variables are involved. The true advantage of a density matrix description emerges for open-quantum systems, i.e., systems that exchange energy and phase with a surrounding "bath"—see section 2.1.6.

In the field-free system eigenstate representation, the LvN equations for an IR-driven process are

$$\frac{d\rho_{\alpha\alpha}}{dt} = \sum_\beta -\frac{i}{\hbar}[V_{\alpha\beta}(t)\rho_{\beta\alpha} - \rho_{\alpha\beta}V_{\beta\alpha}(t)] \qquad (21)$$

for the diagonal elements of the density matrix and

$$\frac{d\rho_{\alpha\beta}}{dt} = -\frac{i}{\hbar}\left\{(E_\alpha - E_\beta) + \sum_\gamma [V_{\alpha\gamma}(t)\rho_{\gamma\beta} - \rho_{\alpha\gamma}V_{\gamma\beta}(t)]\right\} \qquad (22)$$

for the off-diagonals. The latter are also called "coherences", and the former are interpreted as state populations,

$$P_\alpha(t) = \rho_{\alpha\alpha}(t) \qquad (23)$$

Below, I will give theoretical examples, where IR radiation is used to desorb adspecies from surfaces. When using continuous wave (cw) sources for that, however, the problem

arises that during the course of ladder climbing on an anharmonic potential the driving field becomes increasingly off-resonant. This problem may be overcome by using shaped pulses, obtained, for example, by optimal control theory (OCT). The basic idea of OCT is to maximize a target functional, e.g., the population of a target state $|f\rangle$, under the constraints of minimal pulse energy and the quantum equations of motion to hold. This leads to iterative algorithms for the determination of the pulse shape $E(t)$. OCT can be formulated in the wave packet picture[93−95] and in Liouville space.[96] It is also possible in Liouville space when dissipation is present (vide infra).[97,98]

2.1.4. Phonon-Induced Desorption: Arrhenius Expressions

While pure thermal phonon-induced desorption is of no concern here, it is useful to note that, in the simplest possible approximation, the desorption rate will be given by an Arrhenius expression

$$R_{des} = B \exp\left\{-\frac{D}{k_B T_{ads}}\right\} \tag{24}$$

Here B is the "frequency factor", D is the adsorption energy, and T_{ads} is the temperature of the adsorbate bond. The latter is the same as the phonon temperature T_{ph} of the lattice. Note that Arrhenius type theories are always "one dimensional" (1D) by their assumption that a reaction coordinate exists along which the reaction proceeds. They are also classical in the sense that only the Boltzmann factor associated with a barrier height D appears, and tunneling and other quantum mechanical effects are at best considered in an effective way.

Temperature models in connection with Arrhenius type theories are also frequently used for laser-induced desorption and similar reactions. As outlined above, a UV/vis laser pulse penetrates the substrate and heats the electron−hole pairs in the surface region and, by electron−vibration and electron−phonon coupling, also the adsorbate−surface bond and the substrate phonons. As detailed in section 2.2 (see Figure 5 below), the energy flow between the various subsystems is sometimes described by two- and three-temperature models (2TMs and 3TMs), in which the metal electrons, the lattice phonons, and the adsorbate−surface vibrations are treated as coupled reservoirs with time-dependent temperatures $T_{el}(t)$, $T_{ph}(t)$ (for the 2TMs), and $T_{ads}(t)$ (for the 3TMs). Here, it suffices to note that in the case of phonon-mediated desorption, the reaction rate is given by eq 24; however, with a time-dependent adsorbate temperature, $T_{ads}(t)$, which is different from T_{ph}.

It is noted that on top of the Arrhenius type reaction path approximation, in two- and 3TMs, the additional approximation is made that the electrons, phonons, and adsorbate vibrations each carry an individual temperature. As to how good this approximation is will also be discussed below.

2.1.5. Phonon-Induced Desorption: Master Equations

Thermal desorption, outside the topic of surface photochemistry, has been theoretically modeled already some time ago. A particular worthwhile contribution is by Freed, Metiu, and co-workers,[99−101] who use a 1D (Morse) potential for the molecule−surface bond, which is coupled to lattice phonons. A desorption rate can be calculated from populations of the vibrational states of the chemisorptive bond, which are given by the *master equation*

$$\frac{dP_\alpha}{dt} = \sum_\beta W_{\beta\rightarrow\alpha} P_\beta(t) - \sum_\beta W_{\alpha\rightarrow\beta} P_\alpha(t) \tag{25}$$

Here, $W_{\alpha\rightarrow\beta}$ are substrate-induced transition rates between vibrational levels α and β, which depend on the surface (phonon) temperature and a number of other parameters, such as the phonon density of states and polarization, the energy difference $E_\alpha - E_\beta$, and the Morse parameters. These rates were calculated perturbatively, by a Golden Rule treatment (vide infra), and ideally fulfill the principle of detailed balance, i.e.,

$$W_{\alpha\rightarrow\beta} = W_{\beta\rightarrow\alpha} \exp\left\{-\frac{E_\beta - E_\alpha}{k_B T_{ph}}\right\} \tag{26}$$

where T_{ph} is the (constant) surface temperature. The first sum in eq 25 leads to repopulation, the second one to depopulation of state $|\alpha\rangle$. At $T_{ph} = 0$, only downward transitions are possible, while at $T_{ph} > 0$, upward transitions come into play. Once continuum states are reached by upward climbing, the particle is considered desorbed, i.e., retrapping neglected.

The model of Freed, Metiu et al. accounts for anharmonicity of the potential and for multiphonon transitions. No vibrational temperature T_{vib} needs to be assumed. In refs 99−101, it was found that in fact the desorption rate calculated from the master equation deviates over a large temperature range (for Ar on tungsten from about 50 to 1200 K), from the Arrhenius expression. When fitted to Arrhenius in the narrow temperature range where this was possible, the fitted activation energy E_a was always smaller than the Morse well depth D. This is probably due to the fact that the phonon bath couples efficiently to the low-energy vibrational quanta of the Morse oscillator close to dissociation. In passing, I note that the desorption model was later extended to account for relaxation of the excited adsorbate−surface bond due to electron−hole pair excitations.[102]

2.1.6. Open-System Density Matrix Theory

While going beyond Arrhenius, the master eq 25 is still approximate. First of all, it contains no *memory effects*, while in general[103,104] the quantity $W_{\alpha\rightarrow\beta} P_\alpha(t)$ must be replaced by $\int_{-\infty}^t W_{\alpha\rightarrow\beta}(t - t') P_\alpha(t') \, dt'$. In other words, $dP_\alpha(t)/dt$ depends not only on the actual populations $P_\beta(t)$ but also on all previous ones.

Even under this *Markov approximation*, eq 25 is only approximate, because only populations, i.e., diagonal elements of the density matrix $P_\alpha = \rho_{\alpha\alpha}$, are considered, and no off-diagonals are considered. As can be seen from eqs 21 and 22, the latter are mandatory if an external electric field is applied. Furthermore, even without an external field and still within the Markov approximation, the diagonal and off-diagonal elements are in general coupled, as can be seen from the *Redfield equations*,[104−106]

$$\left(\frac{d\rho_{\alpha\beta}}{dt}\right)_{env} = \sum_{\gamma\delta} R_{\alpha\beta,\gamma\delta} \, \rho_{\gamma\delta} \tag{27}$$

Here, $(d\rho_{\alpha\beta}/dt)_{env}$ stands for the environment-induced change of a density matrix element with time, which comes in addition to the Hamiltonian evolution. In the field-free case, therefore, the density matrix elements evolve as

$$\frac{d\rho_{\alpha\beta}}{dt} = -\frac{i}{\hbar}(E_\alpha - E_\beta) + \sum_{\gamma\delta} R_{\alpha\beta,\gamma\delta}\, \rho_{\gamma\delta} \qquad (28)$$

Equations 27 and 28 demonstrate that, apart from coupling diagonal and off-diagonal elements of the density matrix, the *Redfield tensor* accounts for *coherence transfer*; that is, different off-diagonal elements are also coupled.

The Redfield theory is a special variant of what is known as *open-system density matrix theory*. In this approach, one distinguishes a "system" from a "bath" (the environment), and the total Hamiltonian $\hat{H}_{tot}$ is

$$\hat{H}_{tot} = \hat{H}_s + \hat{H}_b + \hat{H}_{sb} \qquad (29)$$

with $\hat{H}_s$, $\hat{H}_b$, and $\hat{H}_{sb}$ denoting the system, bath, and system−bath coupling Hamiltonians, respectively. Defining a reduced (system) density matrix by tracing out the bath degrees of freedom from the total density operator $\hat{\rho}_{tot}$,

$$\hat{\rho} = \mathrm{Tr}_b\, \hat{\rho}_{tot} \qquad (30)$$

one then has to solve an open-system LvN equation of the form

$$\frac{\partial\hat{\rho}}{\partial t} = \mathscr{L}\hat{\rho} + \mathscr{L}_D\hat{\rho} \qquad (31)$$

instead of eq 17. Here, $\mathscr{L}_D$ is the dissipative Liouvillian, which accounts for the coupling of the system to the environment. In eq 31, already the Markov approximation has been assumed to be valid; that is, $(\partial\hat{\rho}/\partial t)$ depends on $\hat{\rho}(t)$ only.

In Redfield theory, one has in (field-free) system eigenstate representation the matrix elements

$$\langle \alpha\, |\mathscr{L}_D\hat{\rho}|\, \beta\rangle = \left(\frac{d\rho_{\alpha\beta}}{dt}\right)_{env} \qquad (32)$$

with $(...)_{env}$ given by eq 27. It is known that Redfield theory can give negative populations $\rho_{\alpha\alpha}$ in certain instances, which is unphysical.[107] Ways to repair this have been suggested.[108]

To avoid this problem a priori, Lindblad showed that in order to have a strictly positive time evolution of the density operator, a dissipative, Markovian Liouvillian must have the form[109−111]

$$\mathscr{L}_D\hat{\rho} = \sum_k \left(\hat{C}_k\, \hat{\rho}\, \hat{C}_k^\dagger - \frac{1}{2}[\hat{C}_k^\dagger\, \hat{C}_k, \hat{\rho}]_+ \right) \qquad (33)$$

Here, $[,]_+$ denotes an anticommutator, k labels various dissipation channels (e.g., energy relaxation, pure dephasing), and $\hat{C}_k$ is a Lindblad operator specifying the nature and strength of this channel.

As an example, *energy relaxation* from state $|\beta\rangle$ to a state $|\alpha\rangle$ with $E_\alpha < E_\beta$, arising from inelastic scattering of system with bath modes, can be described by a Lindblad operator

$$\hat{C}_1 = \sqrt{W_{\beta\rightarrow\alpha}}\, |\alpha\rangle\langle\beta| \qquad (34)$$

At finite bath temperature, T the reverse process is possible, modeled by

$$\hat{C}_2 = \sqrt{W_{\alpha\rightarrow\beta}}\, |\beta\rangle\langle\alpha| \qquad (35)$$

with $W_{\alpha\rightarrow\beta}$ obeying the detailed balance condition (26).

Furthermore, elastic scattering between system and bath modes leads to *pure dephasing* of $|\alpha\rangle$ and $|\beta\rangle$, with a pure dephasing rate $\gamma_{\alpha\beta}^*$, a process for which Lindblad operators exist.[112,113] In the Lindblad approach, the Liouvillian propagator forms a semigroup, i.e., the open-system LvN equation lacks time-reversal symmetry.[111] The theory does not provide any microphysical picture of how to choose the Lindblad operators. Still, the Lindblad equations of motion obey detailed balance, provided the transition rates employed have this property.

Consider an N-level system with direct dipole coupling through elements $V_{\alpha\beta} = \langle\phi_\alpha| - \mu\, E(t)| \phi_\beta\rangle$, which is also coupled to a bath. It is easy to show that the LvN eq 31 takes in field-free system eigenstate representation the form

$$\frac{d\rho_{\alpha\alpha}}{dt} = \sum_\beta -\frac{i}{\hbar}[V_{\alpha\beta}(t)\, \rho_{\beta\alpha} - \rho_{\alpha\beta}\, V_{\beta\alpha}(t)] +$$
$$\sum_\beta W_{\beta\rightarrow\alpha}\, \rho_{\beta\beta} - \sum_\beta W_{\alpha\rightarrow\beta}\, \rho_{\alpha\alpha} \qquad (36)$$

for the diagonal elements of the density matrix and

$$\frac{d\rho_{\alpha\beta}}{dt} = -\frac{i}{\hbar}\Big\{(E_\alpha - E_\beta) + \sum_\gamma [V_{\alpha\gamma}(t)\, \rho_{\gamma\beta} - \rho_{\alpha\gamma}\, V_{\gamma\beta}(t)]\Big\} - \gamma_{\alpha\beta}\, \rho_{\alpha\beta} \qquad (37)$$

for the off-diagonals. In the last equation,

$$\gamma_{\alpha\beta} = \frac{1}{2} W_{\alpha\rightarrow\beta} \qquad (38)$$

is the dephasing rate. Pure dephasing, i.e., additional dephasing independent of energy relaxation, can be included by adding the pure dephasing rate $\gamma_{\alpha\beta}^*$ as introduced above to the right side of eq 38. Equations 36 and 37 show that in the Lindblad model, in the absence of a field, the diagonal and off-diagonal elements are decoupled, and there are no coherence transfer terms. In this limit, therefore, the master eq 25 is correct. In a more general theory, populations and coherences are coupled, coherence terms are present, and memory would have to be considered. Still, eqs 36 and 37 are useful for the direct, IR-induced desorption of an adsorbate from a dissipative surface. Here, the direct molecule−field coupling causes upward (by absorption) and downward transitions (by stimulated emission), and the coupling to the bath causes downward transitions and upward transitions if $T > 0$. This "ladder climbing" is illustrated in Figure 4a. Often, the model is further simplified as the *truncated harmonic oscillator* (THO) model, illustrated in Figure 4b and further described below.

It is often advantageous to define Lindblad operators in configuration rather than eigenstate representation, for the same reasons why this may be practical for wave packet propagations. Here, a number of suggestions were made as to how to choose appropriate Lindblad operators or other dissipative superoperators $\mathscr{L}_D$. Considering energy dissipation in a harmonic oscillator with mass m and frequency ω, the relaxation operator $\hat{C}_1$ of eq 34 is sometimes written in the form

$$\hat{C}_1 = \sqrt{W_{1\rightarrow0}}\, \hat{a} \qquad (39)$$

where $W_{1\rightarrow0}$ is the relaxation rate from $|1\rangle$ to $|0\rangle$. Furthermore,
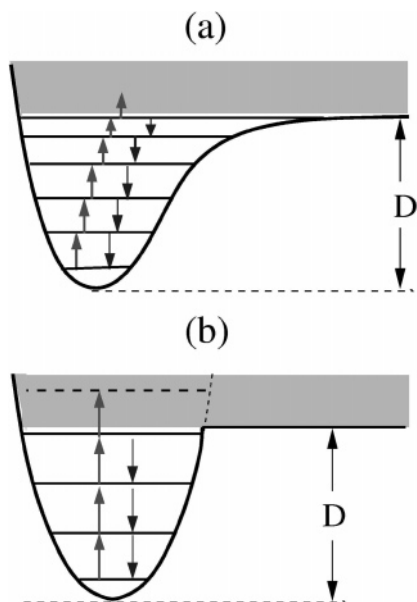
Figure 4. Ladder climbing in an anharmonic potential into the continuum (a). The upward arrows are due to IR excitation (and thermal excitation), and the downward arrows are due to energy relaxation (and stimulated emission). In general, also other than the $\Delta v = \pm 1$ steps shown are possible. The same process in the THO model (b), with N_b harmonic oscillator states below the desorption energy D.

$\hat{a}$ is the standard harmonic annihilation operator,

$$\hat{a} = \frac{1}{\sqrt{2}} \left(\sqrt{\frac{m\omega}{\hbar}} \, q + i \, \sqrt{\frac{1}{m\hbar\omega}} \, \hat{p} \right) \tag{40}$$

where q is the vibrational coordinate and $\hat{p}$ is the momentum operator. When only $\hat{C}_1$ in eq 39 is used in the Lindblad dissipation, then

$$\mathscr{L}_D\hat{\rho} = W_{1\to0} \left(\hat{a} \, \hat{\rho} \, \hat{a}^\dagger - \frac{1}{2}[\hat{a}^\dagger \, \hat{a}, \, \hat{\rho}]_+ \right) \tag{41}$$

with the creation operator (Because $\hat{a}$ and $\hat{a}^\dagger$ are not bounded, they are not Lindblad operators in the strict sense.)

$$\hat{a}^\dagger = \frac{1}{\sqrt{2}} \left(\sqrt{\frac{m\omega}{\hbar}} \, q - i \, \sqrt{\frac{1}{m\hbar\omega}} \, \hat{p} \right) \tag{42}$$

In the harmonic oscillator basis, the diagonal elements $P_\alpha = \rho_{\alpha\alpha}$ evolve as

$$\frac{dP_\alpha}{dt} = W_{1\to0}(\alpha + 1) P_{\alpha+1} - W_{1\to0} \, \alpha \, P_\alpha \tag{43}$$

In deriving eq 43, the equalities $\hat{a}|\alpha\rangle = \sqrt{\alpha}|\alpha - 1\rangle$ and $\hat{a}^\dagger|\alpha\rangle = \sqrt{\alpha+1}|\alpha + 1\rangle$ have been used. Equation 43 states that state $|\alpha\rangle$ gains population from its upper neighbor state $|\alpha + 1\rangle$ with a rate $(\alpha + 1)W_{1\to0}$ and loses population to its lower neighbor state $|\alpha - 1\rangle$ with a rate $\alpha W_{1\to0}$. Therefore, at $T = 0$, when no reexcitations are possible, the strict selection rule $\Delta v = -1$ holds with the choice eq 39, and the relaxation rates are proportional to the quantum number of the decaying level. In this model, only $W_{1\to0}$ needs to be known. It will be shown below that eqs 39 and 43 require not only a harmonic system but also a system–bath coupling $\hat{H}_{sb}$ that is *linear* in the system mode q, i.e.,

$$\hat{H}_{sb} \propto q = \sqrt{\frac{2\hbar}{m\omega}} \, (\hat{a} + \hat{a}^\dagger) \tag{44}$$

The formalism is easily extended to finite bath temperatures. In that case, the dissipative Liouvillian is

$$\mathscr{L}_D\hat{\rho} = W_{1\to0} \left(\hat{a} \, \hat{\rho} \, \hat{a}^\dagger - \frac{1}{2}[\hat{a}^\dagger \, \hat{a}, \, \hat{\rho}]_+ \right) + \\ W_{0\to1} \left(\hat{a}^\dagger \, \hat{\rho} \, \hat{a} - \frac{1}{2}[\hat{a} \, \hat{a}^\dagger, \, \hat{\rho}]_+ \right) \tag{45}$$

where $W_{1\to0}$ and $W_{0\to1}$ are in general both temperature-dependent and have to obey detailed balance. The corresponding master equation for a harmonic system that is linearly coupled to a bath is then given by

$$\frac{dP_\alpha}{dt} = W_{1\to0}(\alpha + 1) P_{\alpha+1} - W_{1\to0} \, \alpha \, P_\alpha + W_{0\to1} \, \alpha \, P_{\alpha-1} \tag{46}$$

that is, transitions from/to level $|\alpha\rangle$ obey the selection rule $\Delta v = \pm 1$.

An attractive feature of the formalism is that it can also be extended to anharmonic, unbound systems and be used in configuration space respresentation. The latter property is immediately obvious from eqs 40 and 42. For anharmonic systems, $\hat{a}$ and $\hat{a}^\dagger$ can be interpreted as lowering and raising operators for (vibrational) levels in an anharmonic potential. In special cases, such as the Morse potential, exact raising and lowering operators are known.[114] In more general cases, approximate raising and lowering operators can be defined[115−117] by using arguments from supersymmetric quantum mechanics (SUSY QM)[118] according to

$$\hat{a} = \frac{1}{\sqrt{2}} \left(\sqrt{\frac{m\omega}{\hbar}} \, f(q) + i \, \sqrt{\frac{1}{m\hbar\omega}} \, \hat{p} \right) \tag{47}$$

$$\hat{a}^\dagger = \frac{1}{\sqrt{2}} \left(\sqrt{\frac{m\omega}{\hbar}} \, f(q) - i \, \sqrt{\frac{1}{m\hbar\omega}} \, \hat{p} \right) \tag{48}$$

Here,

$$f(q) = -\frac{\hbar}{m\omega} \frac{d\phi_0/dq}{\phi_0} \tag{49}$$

where ϕ_0 is the ground-state wave function and $\omega = (E_1 - E_0)/\hbar$. Equation 47 goes over into eq 40 in the harmonic case. The approximate ladder operators violate the strict selection rules outlined above, and transitions other than $\Delta v = -1$ (and $\Delta v = +1$ at $T > 0$) become possible. To treat dissipation, only ϕ_0, its derivative, the energy difference $E_1 - E_0$, and the relaxation rate $W_{1\to0}$ need to be known.

Equation 47 has a clear advantage over eq 40. In the harmonic oscillator case, the linear system–bath coupling $\hat{H}_{sb} \propto (\hat{a} + \hat{a}^\dagger)$ increases with increasing q according to eq 44. If q is the adsorbate–surface distance, Z, the system–bath coupling becomes infinite for $Z \to \infty$. This is unphysical for a dissociative potential. In contrast, $f(q)$ approaches a *constant* c,[116] and with $\hat{H}_{sb} \propto (\hat{a} + \hat{a}^\dagger) \propto f(q) = c$, the dissipative transition rate goes smoothly to zero far from the surface since the coupling matrix elements $\langle \alpha |c| \beta \rangle$ vanish.

Other dissipative Liouvillians $\mathscr{L}_D$ have been suggested, which can also be used in a configuration space representation. Caldeira and Leggett derived as a Liouvillian for the

microscopic model of a harmonic oscillator linearly coupled to an Ohmic bath, in the high-temperature (classical) limit[119]

$$\mathscr{L}_D \hat{\rho} = -W_{1\to 0}\left(\frac{2mk_BT}{\hbar^2}\{q,[q,\hat{\rho}]\} + \frac{i}{\hbar}\{q,[\hat{p},\hat{\rho}]\}\right) \quad (50)$$

Gao developed from this starting point a dissipative Liouvillian with a Lindblad operator valid for all temperatures. At $T = 0$, his Lindblad operator reads[120-122]

$$\hat{C}_1 = \sqrt{W_{1\to 0}}\,\frac{1}{\sqrt{2}}\left(\sqrt{\frac{m\omega}{\hbar}}f(q) + i\,\sqrt{\frac{1}{m\hbar\omega}}\frac{df(q)}{dq}\hat{p}\right) \quad (51)$$

For higher temperatures, see refs 120−122. For $f(q) = q$, eq 51 is again identical to the Lindblad operator for a harmonic oscillator with linear system−bath coupling (eqs 39 and 40). For anharmonic systems, Gao chose empirical forms for $f(q)$ such as $f(q) = (1 − \exp\{-bq\})/b$,[122] thus sharing similarities with the formalism based on the generalized raising and lowering operators.

While numerics is of no concern here, it should be noted that density matrix propagations can be time-consuming. If many basis functions/grid points, say N, are needed, it becomes also impossible to keep the $N \times N$ density matrix in memory. A way out here are the *stochastic wave packet* methods, by which the LvN equation can be unravelled exactly, in the limit $M \to \infty$, by propagating a set of M "quantum trajectories" $\psi_n(t)$, $n = 1, ..., M$. In the so-called Monte Carlo wave packet (MCWP) method,[123-125] when applied to a Liouvillian of Lindblad form, the propagation is under the influence of a non-Hermitean Hamiltonian, in which the Lindblad operators appear in a negative, imaginary potential $-(i/2\hbar) \sum_k \hat{C}_k^\dagger \hat{C}_k$. A wave packet also undergoes discontinuous "jumps" triggered by a random-number-generated algorithm. Such a jump involves application of a Lindblad operator on the wave function

$$|\psi_n(t + \Delta t)\rangle = \hat{C}_k |\psi_n(t)\rangle \quad (52)$$

and subsequent renormalization. The MCWP method also offers a possible treatment of the fundamental "measuring process" or "reduction of the wave packet" problem in quantum mechanics. Namely, by application of $\hat{C}_k$, the wave packet is projected on a particular eigenstate. This can be seen from eq 52 as follows: In a two-state model, the wave function $|\psi_n(t)\rangle$ is a vector $\psi = (\psi_1, \psi_2)$, with ψ_1 and ψ_2 being the components of $|\psi\rangle$ in states $|1\rangle$ and $|2\rangle$. The Lindblad operator $\hat{C}_1 = \sqrt{W}|1\rangle\langle 2|$ becomes a matrix

$$\underline{C}_1 = \sqrt{W}\begin{pmatrix} 0 & 1 \\ 0 & 0 \end{pmatrix}$$

Hence, the operation $\underline{C}_1\,\psi$ gives, after renormalization, (1, 0)−The wave packet is reduced to state $|1\rangle$.

In the MCWP method, expectation values of operators are computed as

$$\langle\hat{A}\rangle(t) = \sum_{n=1}^{M} \langle\psi_n(t)|\hat{A}|\psi_n(t)\rangle \quad (53)$$

A drawback of the method is the slow statistical convergence

of the sum (eq 53). Improved sampling techniques have been suggested.[126-128]

2.2. Weakly Nonadiabatic Processes

2.2.1. Hot-Electron-Mediated Ladder Climbing

The substrate-mediated laser desorption from metal surfaces is frequently described by models similar to those used for phonon-induced desorption, i.e., by "ladder climbing" in the electronic ground state up to the desorption continuum, albeit under participation of electronically excited states. This is why I denote these dynamics as "weakly adiabatic".

Arrhenius Type Models. In particular, Arrhenius type theories are popular for fitting experimental desorption yields in FLD. The starting points here are two- or 3TMs, associated with two or three "reservoirs": the electrons of the metal, the substrate (lattice) phonons, and, in 3TMs, also the adsorbate. As illustrated in Figure 5a for the 3TM, the three
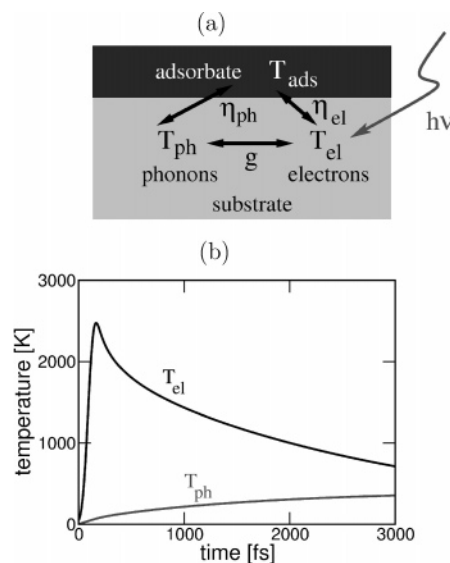
Figure 5. (a) Illustration of 2TMs and 3TMs. (b) $T_{el}(t)$ and T_{ph} curves according to the 2TM, for a Pt surface when a Gaussian pulse of width fwhm = 80 fs, fluence F = 6 mJ/cm^2, and wavelength λ = 619 nm was applied, at t = 0. The initial temperature was 85 K.[117]

subsystems are coupled by characteristic coupling constants: electrons and phonons in the metal by the electron−phonon coupling constant g, metal electrons and the adsorbate by a vibration−electron constant η_{el}, and phonons and adsorbate by a vibration−phonon coupling constant η_{ph}.

A typical FLD experiment then proceeds as follows. The laser pulse penetrates the uppermost surface layers and excites electrons in the substrate. Provided the deposited energy density is high enough, a large number of excited electrons is created, which thermalizes quickly by electron−electron scattering, giving rise to an electronic temperature, $T_{el}(t)$. The latter is time-dependent as a result of the time dependence of the exciting pulse but also because the hot electrons relax by heat diffusion and by coupling to the lattice phonons. As a consequence, also phonons are heated and eventually cooled again, modeled by a phonon temperature $T_{ph}(t)$. Without an adsorbate, this scenario constitutes the well-known 2TM of the response of a metal surface to an ultrashort intense laser pulse.[129-131]

Quantitatively, the electron and phonon temperatures in 2TM are calculated from the two coupled equations

$$C_{\text{el}}\frac{\partial T_{\text{el}}}{\partial t} = \frac{\partial}{\partial z} K \frac{\partial}{\partial z} T_{\text{el}} - g(T_{\text{el}} - T_{\text{ph}}) + S(z, t) \quad (54)$$

$$C_{\text{ph}}\frac{\partial T_{\text{ph}}}{\partial t} = g(T_{\text{el}} - T_{\text{ph}}) \quad (55)$$

In eq 54, C_{el} and C_{ph} are the electron- and lattice-specific heat constants. Equation 54 describes how the electron temperature changes due to thermal diffusion (first term on the right with K = thermal conductivity of the electrons), electron–phonon coupling (second term), and the external laser pulse (third term). The source term can be calculated, for a metal film of thickness d, from[131]

$$S(z, t) = \frac{AI(t) \exp(-\alpha z)}{1 - \exp(-\alpha d)} \quad (56)$$

where $AI(t)$ is the absorbed fraction of the intensity I of a laser pulse and α^{-1} is the optical penetration depth. The latter can be taken from tabulated[132] values of the complex refractive index. In eq 55, which describes the phonons, the heat conductivity of the lattice has been neglected because for metals it is orders of magnitude smaller than that of the electrons.

By solving eqs 54 and 55, one obtains $T_{\text{el}}(t)$ at different z. As an example, I show in Figure 5b the phonon and electron temperatures at a Pt surface ($d \rightarrow \infty$), after a Gaussian laser pulse with fwhm 80 fs was applied. Note that the electron temperature rises on a sub-picosecond time scale to its maximal value $T_{\text{el}}^{\text{max}}$ of a few 1000 K, while the phonon temperature is delayed and never reaches temperatures that high.

For desorption, electron and phonon heat baths need to be coupled to the adsorbate "reservoir", giving rise to an adsorbate temperature $T_{\text{ads}}(t)$. The adsorbate–surface bond can be heated by the electrons, through the coupling constant η_{el} or by the phonons through η_{ph}.

If the electronic channel dominates, it was shown in ref 133 from a Langevin model for the electron heat bath that, after various simplifications, a classical differential equation is obtained for the adsorbate temperature:

$$\frac{\partial T_{\text{ads}}}{\partial t} = \eta_{\text{el}}(T_{\text{el}} - T_{\text{ads}}) \quad (57)$$

Equation 57 has to be solved in addition to the 2TM eqs 54 and 55, leading to a 3TM. In the classical limit used in ref 133, the desorption rate is now given as

$$R_{\text{des}} = \frac{D\eta_{\text{el}}}{k_{\text{B}}T_{\text{ads}}(t)} \exp\left\{-\frac{D}{k_{\text{B}}T_{\text{ads}}(t)}\right\} \quad (58)$$

The quantities D and η_{el} are often used as model parameters to fit experimental data. Physically, D can be interpreted as an effective activation energy, while η_{el} is the rate for energy transfer from the adsorbate–surface bond to the surface, caused by electron–vibration coupling. At $T_{\text{el}} = 0$, η_{el} is the corresponding relaxation rate $W_{1\rightarrow 0}$ of a surface oscillator. Ways to calculate η_{el} (or $W_{1\rightarrow 0}$) from microscopic models will be outlined below.

If also a phononic mechanism via the coupling parameter η_{ph} is important, an alternative model is useful. Namely, the energy content U_{ads} of the adsorbate may be calculated from[24,26,30]

$$\frac{dU_{\text{ads}}}{dt} = \eta_{\text{el}}(U_{\text{el}} - U_{\text{ads}}) + \eta_{\text{ph}}(U_{\text{ph}} - U_{\text{ads}}) \quad (59)$$

Assuming a single, harmonic system mode, one can define an adsorbate vibrational temperature from the energy content of a harmonic oscillator at temperature T_{ads},

$$U_{\text{ads}} = \hbar\omega\left[\exp\left\{\frac{\hbar\omega}{k_{\text{B}}T_{\text{ads}}}\right\} - 1\right]^{-1} \quad (60)$$

with U_{ads} and T_{ads} being both time-dependent. The calculated $T_{\text{ads}}(t)$ can be used in the Arrhenius equation eq 24 to obtain the desorption rate R_{des}.

Through eq 59, the adsorbate temperature depends on η_{el} and also on η_{ph}, the latter being a measure for the inverse time scale of adsorbate–phonon coupling. According to this treatment, a laser-driven, substrate-mediated desorption process is dominantly electronic, if the first term in eq 59 dominates, and phononic if the second one does. For metal surfaces, η_{el}^{-1} is often in the order of picoseconds, and η_{ph}^{-1} is in the order of nanoseconds (vide infra). As a consequence, the electronic mechanism frequently dominates FLD from metals. This, however, depends on the particular adsorbate mode responsible for desorption. Because the smallest η_i^{-1} (i = el, ph) determines the time scale on which $T_{\text{ads}}(t)$ rises, it also determines through the Arrhenius expression the rate of reaction and hence the yield. In 2PC experiments, the yield is measured as a function of delay time $\Delta\tau$ between two subsequent pulses, and the various mechanisms can be discriminated.

While the Arrhenius models allow for beautiful physical interpretation and analysis, it must be kept in mind that they are approximate in many ways. In particular, they are inherently classical and 1D. Apart from this, the concept of an electron temperature $T_{\text{el}}(t)$ is questionable at least within the first few 100 fs after the pulse according to experimental[134] and theoretical investigations.[135−138] Therefore, the applicability of the concept of an electron temperature is not always valid, in particular if short FLs are employed. Also, the validity of an adsorbate temperature $T_{\text{ads}}(t)$ is questionable in general:[117,139] Only in the long-time limit, often several picoseconds, the level distribution becomes Boltzmann.

Classical Trajectories with Electronic Friction. Some of the above restrictions can be overcome by MD, which includes electronic friction. This approach was popularized by Tully and co-workers.[140] In this method, the (multidimensional) nuclear motion is treated classically, whereas the electronic degrees of freedom are hidden in a generalized Langevin formalism, in the form of friction and fluctuating forces. If q is the only degree of freedom considered (e.g., the molecule–surface distance Z), then the equation of motion is

$$m_q\frac{d^2q}{dt^2} = -\frac{dV}{dq} - \eta_{qq}\frac{dq}{dt} + R_q(t) \quad (61)$$

Here, V is the ground-state potential, and η_{qq} is related to the electronic friction coefficient of above through $\eta_{qq} = m_q\eta_{\text{el}}$. $R_q(t)$ is a fluctuating force that obeys a fluctuation–dissipation theorem,

$$\langle R_q(t)| R_q(t')\rangle = 2k_{\text{B}}T_{\text{el}}\,\eta_{qq}\,\delta(t - t') \quad (62)$$

and depends on the electronic temperature. In practice, the fluctuating forces are Gaussian white noise with $\langle R_q(t)\rangle =$

0, which can be obtained from the so-called Box−Müller algorithm,[141]

$$R_q(t) = \left(\frac{2k_B T_{el} \gamma_{qq}}{\Delta t}\right)^{1/2} (-2\ln b)^{1/2} \cos(2bc) \quad (63)$$

with random numbers b and c drawn from the interval [0, 1] at each time step (Δt is the time step).

For more than one degree of freedom, eq 61 generalizes to

$$m_q \frac{d^2 q}{dt^2} = -\frac{\partial V}{\partial q} - \sum_s^F \eta_{qs} \frac{ds}{dt} + R_q(t) \quad (64)$$

with a friction matrix $\underline{\underline{\eta}}$ that accounts for nonadiabatic energy transfer to electron−hole pairs. If F is the number of degrees of freedom considered, $\underline{\underline{\eta}}$ is an $F \times F$ matrix, and each element depends on the coordinates. Ways to calculate the friction matrix will be outlined in section 4. The formalism can also be extended to account not only for electron−hole pairs but also for phonons.[140,142]

The above formalism has been used to treat relaxation of vibrationally excited molecules at metal surfaces, e.g., of CO at Cu(100).[140] The approach was also used for the dissociative sticking of diatomics (H_2, N_2) on metal surfaces (Ru, Cu) and for the reverse process, (thermal) associative desorption.[142,143] Of particular relevance for this review are applications to FLD, again of CO from Cu surfaces, by Head-Gordon and co-workers.[144,145] As we have seen, in this case, the electronic temperature in eq 62 is large and time-dependent, according to the 2TM; hence, the fluctuating forces are large. A molecule, kicked by the random forces, can be considered desorbed when its energy is larger than the binding energy, D, and if it was for a sufficiently long time, at a distance larger than Z_{des} from the surface.

Master Equations and Model Hamiltonians. A further step forward, which also accounts for quantum effects, is to use a master eq 25 for the ground-state populations $P_\alpha = \rho_{\alpha\alpha}$, or generalized master equations derived from Redfield or Lindblad theories. While methods to calculate transition rates $W_{\alpha \to \beta}$ will be outlined in greater detail in section 4, it is useful to introduce already here model Hamiltonians often used for relaxation and excitation of adsorbate−surface bonds due to "hot electrons".

In particular, for negative ion resonance-mediated processes, a frequently used Hamiltonian is

$$\hat{H} = \hat{H}_s + \hat{H}_e + \hat{H}_{es} \quad (65)$$

Here, the system Hamiltonian $\hat{H}_s$ describes, in 1D idealization, the adsorbate−surface vibration, $\hat{H}_s = -(\hbar^2/2m_q)(d^2/dq^2) + V(q)$. $\hat{H}_e$ is an electron Hamiltonian modeling the electron bath, and $\hat{H}_{es}$ is the coupling between the two. For $\hat{H}_e$, the Newns−Anderson Hamiltonian[146,147]

$$\hat{H}_e = \sum_k \epsilon_k c_k^\dagger c_k + \epsilon_a c_a^\dagger c_a + \sum_k V_{ak}(c_a^\dagger c_k + c.c.) \quad (66)$$

is useful. Here, $|k\rangle$ are the metal band states, and $|a\rangle$ is a single affinity level (the adsorbate resonance). The terms $c_k^\dagger$ and $c_a^\dagger$ are creation, and c_k and c_a are the annihilation operators for these levels. Furthermore, ϵ_k and ϵ_a denote one-electron energies, and the electronic adsorbate−surface coupling operators are V_{ak}. The acceptor level ϵ_a and the coupling operators V_{ak} are functions of q. Furthermore, the vibration−electron coupling $\hat{H}_{es}$ is often assumed to be linear in the system coordinate,

$$\hat{H}_{es} = \lambda\, c_a^\dagger c_a\, q \quad (67)$$

where $n_a = c_a^\dagger c_a$ is the temporal population of the resonance level and λ is a coupling constant. Equations 65−67 constitute what is sometimes also called the local polaron model.[148]

Within this linear coupling model, a Redfield type equation of motion (eq 28) can be derived, as shown in ref 149, for example. Following this reference, one notes that by making in the (field-free) Redfield equation (eq 28) the diagonal approximation $\rho_{\alpha\beta} = \rho_{\alpha\alpha} \delta_{\alpha\beta}$, one arrives at the master eq 25 with[139,149−152]

$$W_{\alpha \to \beta} = |\langle\alpha |q| \beta\rangle|^2 \chi(\omega_{\alpha\beta}) \quad (68)$$

with $\hbar\omega_{\alpha\beta} = E_\alpha - E_\beta$. Equation 68 describes, when used in eq 25, hot-electron-mediated interlevel transitions between system levels $|\alpha\rangle$ and $|\beta\rangle$. Within a Golden Rule treatment, the function $\chi(\omega_{\alpha\beta})$ can be approximated by[149]

$$\chi(\omega_{\alpha\beta}) \approx 4\pi \lambda^2 \rho_a(\epsilon_F)^2 \omega_{\alpha\beta}\{1 + n_B[T_{el}(t), \hbar\omega_{\alpha\beta}]\} \quad (69)$$

Here, λ is the coupling constant from eq 67, $\rho_a(\epsilon_F)$ is the local density of adsorbate states at the Fermi level ϵ_F, and

$$n_B[T_{el}(t), \hbar\omega] = \left[\exp\left\{\frac{\hbar\omega}{k_B T_{el}}\right\} - 1\right]^{-1} \quad (70)$$

the Bose−Einstein distribution function for electron−hole pairs, at electronic temperature $T_{el}(t)$ and energy $\hbar\omega$. Note that in the last equation a thermalized electron gas has been assumed.

The perturbative expression (eqs 68 and 69), when used in the master eq 25, can be further simplified by assuming that the adsorbate−surface bond is a harmonic oscillator with frequency ω_0.[149] This leads to a master equation with precisely the form of eq 46, i.e., transitions between nearest neighbors only, with

$$W_{1 \to 0} = [1 + n_B(T_{el}, \hbar\omega_0)]\, \eta_{el} \quad (71)$$

Here, η_{el} is again the rate $W_{1 \to 0}$ at zero temperature. It can be calculated from eqs 68 and 69 when the local density of states is approximated as a Lorentzian centered at the excitation energy $\epsilon_a + \Lambda_a - \epsilon_F$ of the adsorbate,

$$\rho_a(\epsilon_F) = \frac{\Delta_a}{\pi[(\epsilon_a + \Lambda_a - \epsilon_F)^2 + \Delta_a^2]} \quad (72)$$

With the equality $\langle 0 |q| 1\rangle = \sqrt{\hbar/2m\omega_0}$ for the harmonic oscillator, one has

$$\eta_{el} = \frac{2\pi\hbar}{m} \lambda^2 \rho_a^2(\epsilon_F) \quad (73)$$

In the equations above, Λ_a is the shift and Δ_a is the broadening of the resonance level $|a\rangle$. Both are due to the coupling of $|a\rangle$ to metal states $|k\rangle$ and can be calculated from the couplings V_{ak}. For example, the resonance width is

$$\Delta_a = \sum_k \pi|V_{ak}|^2 \delta(E - \epsilon_k) \quad (74)$$

Note that Δ_a (and Λ_a) are generally energy-dependent, which is often neglected. (The energy shift Λ_a is often neglected as a whole.)

Because a harmonic oscillator is bound, the formalism cannot account for hot-electron-mediated desorption. Desorption is sometimes modeled within the THO model of Figure 4b. Accordingly, the particle is considered desorbed when it reaches the level with quantum number $N_b + 1$, where N_b is the vibrational quantum number just below the desorption energy D. When solving eq 46, one can calculate a mean population of the vibrational levels as

$$n(t) = \sum_\alpha \alpha \, P_\alpha(t) \qquad (75)$$

where α is the vibrational quantum number. From there, an adsorbate vibrational temperature may be defined from the Bose−Einstein distribution

$$n(t) = \left[\exp\left\{ \frac{\hbar\omega_0}{k_B T_{ads}(t)} \right\} - 1 \right]^{-1} \qquad (76)$$

It can be shown that in the classical limit ($\hbar \rightarrow 0$), $T_{ads}(t)$ can be obtained from the differential eq 57 instead. In this limit, it also turns out, in the THO model, that the desorption rate is given by

$$R_{des} = (N_b + 1) \, \eta_{el} \, n_B(T_{el}, \hbar\omega_0) \exp\left\{ -\frac{D}{k_B T_{ads}(t)} \right\} \quad (77)$$

with an Arrhenius form similar to eq 58. The factor $\eta_{el} \, n_B(T_{el}, \hbar\omega_0)$ is the upward rate $W_{0 \rightarrow 1}$, at electron temperature T_{el}.

In refs 139, 149, and 152, the formalism was applied to vibrational heating of the CO stretch mode of CO/Cu(100). The excited-state resonance was assumed to arise from temporary population of the $2\pi^*$ orbital of CO (see below).

2.2.2. STM-Induced Processes: Inelastic Electron Tunneling (IET)

The formalism just outlined is, with appropriate modifications, applicable also for inelastic electron (or hole) tunneling (IET) in STM experiments. As an example, the STM-induced desorption of H atoms from H-covered Si(100)2 × 1 surfaces in the "below threshold regime",[36] was modeled[37] within a ladder climbing scheme, by master equations analogous to eq 46. Now, however, the transition rates account for IET and for dissipation. In ref 37, the relevant vibrational transition rates within a harmonic, 1D model (with the Si−H distance r being the only coordinate considered), are

$$W_{1 \rightarrow 0} = W_{1 \rightarrow 0}^{IET} + W_{1 \rightarrow 0}^{diss} \qquad (78)$$

$$W_{0 \rightarrow 1} = W_{0 \rightarrow 1}^{IET} + W_{1 \rightarrow 0}^{diss} \, e^{-\hbar\omega_0/k_B T} \qquad (79)$$

Here, $W_{\alpha \rightarrow \beta}^{diss}$ are dissipative transition rates, for which in the upward term (eq 79) the detailed balance condition has been used. $W_{0 \rightarrow 1}^{IET} = W_{1 \rightarrow 0}^{IET}$ is the IET rate connecting levels $|0\rangle$ and $|1\rangle$. The latter consists of a dipole[153] and a resonance term,[154] both proportional to the tunnel current I:

$$W_{0 \rightarrow 1}^{IET} = \frac{I}{e}(f_{0 \rightarrow 1}^{dip} + f_{0 \rightarrow 1}^{res}) \qquad (80)$$

Here, $f_{0 \rightarrow 1}^{dip}$ is the probability for excitation due to the direct

coupling of the field of the tunnel electron to the dipole moment μ of the adsorbate−surface bond. Furthermore, $f_{0 \rightarrow 1}^{res}$ is the probability for excitation due to temporary population of a negative ion resonance state. For both the dipole and the resonance terms, Golden Rule expressions similar to those of above have been given.[37] Without going into details, I note that the transition rates $W_{0 \rightarrow 1}^{res}$ depend not only on the tunneling current but also on the STM voltage, V. This is mainly because the energy Δ for excitation from the neutral to the resonance state depends on V, according to $\Delta = \Delta_0 - eV$. For H/Si, it was argued that the resonance term dominates, and the total inelastic tunneling fraction $f_{in} = f_{0 \rightarrow 1}^{res} + f_{0 \rightarrow 1}^{dip}$ was estimated to be in the order of 10^{-4} to 10^{-2} at voltages of about 2 and 4 V, respectively.[37] Within the truncated oscillator model, again, a simple rate expression can be derived, by which it was possible to fit experimental observations.[37]

At this point, a word about time scales is in order. Assuming an inelastic tunneling fraction of 10^{-3} and a typical tunnel current I of about 3 nA, eq 80 gives $W_{0 \rightarrow 1}^{IET} \approx 1.9 \times 10^7 \, s^{-1}$. This suggests typical transition times in the order of 10^{-7} s with the following implications: (i) The desorption in the IET regime is not "ultrafast". (ii) Vibrational relaxation cannot be neglected even when it proceeds, as for the H−Si stretch mode of H:Si(100)2 × 1, on the nanosecond time scale (see below). In contrast, in the "above threshold" regime where $|eV| > \Delta$, STM-induced desorption can be as fast as DIET and vibrational relaxation is not an issue.

The theory just outlined has been refined in many ways. Still, in most cases, these extended models are based on model Hamiltonians similar to those of eqs 65−67, which are used in perturbation theory to calculate transition and desorption rates. Some newer theory makes use of first principles information, e.g., from density functional theory (DFT). Because STM manipulation of adsorbates, in particular in the IET regime, is not my main concern here, the reader is referred to some of the rich literature.[41,62,155−171]

2.3. Strongly Nonadiabatic Processes

2.3.1. Photodesorption from Insulating Surfaces

Photodesorption of adspecies from insulating surfaces by UV/vis light is an example for a "strongly nonadiabatic" process. The reaction is largely analogous to gas-phase photodissociation[172,173] in the sense that (i) the laser excitation is *direct* and (ii) the electronically excited states are *stationary* on the time scale of nuclear motion. The surface "merely" modifies interaction and excited-state potentials and orients the molecules, thus leading to "surface aligned photochemistry".[174] While the direct mechanism is very probable for insulators, indirect, substrate-mediated pathways cannot always be ruled out.

For photodesorption from or photodissociation at insulating surfaces, one frequently uses two-state models, with a ground state $V_g(R)$ and an excited state $V_a(R)$. The corresponding time-dependent nuclear Schrödinger equation is

$$i\hbar \frac{\partial}{\partial t} \begin{pmatrix} \psi_a \\ \psi_g \end{pmatrix} = \begin{pmatrix} \hat{H}_a & \tilde{V}_{ag} \\ \tilde{V}_{ga} & \hat{H}_g \end{pmatrix} \begin{pmatrix} \psi_a \\ \psi_g \end{pmatrix} \qquad (81)$$

for the nuclear wave functions $\psi_n(R)$ with $n = g, a$. Here,

$$\tilde{V}_{ag}(R, t) = V_{ag}(R) - \langle \Psi_a(r, R) \, |\hat{\mu} E(t)| \, \Psi_g(r, R) \rangle_r \quad (82)$$

is an electronic coupling matrix element connecting states $|g\rangle$ and $|a\rangle$. It consists of a direct field coupling term, and a nonadiabatic coupling term $V_{ag}(R)$. The latter accounts for radiationless transitions due to non-Born−Oppenheimer or spin−orbit effects and is expressed here in a diabatic representation. Details of "diabatic" and "adiabatic" pictures will be given below. The radiationless coupling terms are often neglected in two-state models. Note that also the diagonal elements $\tilde{V}_{nn}$ are neglected here, i.e.,

$$\hat{H}_n = \hat{T}_R + V_n(R) \tag{83}$$

because I assume that the laser field $E(t)$ in the UV/vis regime will not induce any transitions among the vibrational levels ϕ_α^n on surface V_n.

On insulators, where both vibrational relaxation and electronic quenching can be neglected, the solution of eq 81 gives all one needs to calculate properties of interest. One such property is the absorption cross-section $\sigma(\omega)$ as a function of the exciting laser frequency, ω. If a cw light source is used, the absorption cross-section (at $T = 0$) can, in the perturbative limit, be calculated as[172,173]

$$\sigma(\omega) = K\omega \int_{-\infty}^{\infty} C(t) \exp\left\{i\left(\omega + \frac{E_0^g}{\hbar}\right)t\right\} dt \tag{84}$$

from the Fourier-transformed correlation function

$$C(t) = \langle\phi(0)|\phi(t)\rangle \tag{85}$$

$$\phi(t) = e^{-i\hat{H}_a t/\hbar} \mu_{ag} \phi_0^g \tag{86}$$

(K is a constant.) That is, $\sigma(\omega)$ is obtained from multiplying the initial ground-state vibrational wave function $\phi_0^g(R)$ with energy E_0^g, with the transition dipole moment $\mu_{ag}(R)$, promoting it to the excited state and propagating it there.

2.3.2. DIET from Semiconductor and Metal Surfaces

In contrast, molecules adsorbed on metal surfaces have photoactive final states that are typically embedded in a continuum of substrate electronic excitations. This is even so for semiconductors, if the final states are not located within a band gap.

Multistate Models. The coupling of an excited, photoactive adsorbate state, $|a\rangle$, to substrate continuum states $|k\rangle$, can be modeled by a generalization of eq 81 as

$$i\hbar\frac{\partial}{\partial t}\begin{pmatrix}\psi_a\\\psi_g\\\psi_{k_1}\\\psi_{k_2}\\\vdots\end{pmatrix} = \begin{pmatrix}\hat{H}_a & \tilde{V}_{ag} & \tilde{V}_{ak_1} & \tilde{V}_{ak_2} & \cdots\\\tilde{V}_{ga} & \hat{H}_g & \tilde{V}_{gk_1} & \tilde{V}_{gk_2} & \cdots\\\tilde{V}_{k_1a} & \tilde{V}_{k_1g} & \hat{H}_{k_1} & \tilde{V}_{k_1k_2} & \tilde{V}_{k_1k_3} & \cdots\\\tilde{V}_{k_2a} & \tilde{V}_{k_2g} & \tilde{V}_{k_2k_1} & \hat{H}_{k2} & \tilde{V}_{k_2k_1} & \cdots\\\vdots & \vdots & \vdots & \vdots & \vdots & \ddots\end{pmatrix}\begin{pmatrix}\psi_a\\\psi_g\\\psi_{k_1}\\\psi_{k_2}\\\vdots\end{pmatrix} \tag{87}$$

Here, $\psi_n(R)$ is the nuclear wave function on state $|n\rangle$. Note that in this model energy is conserved. Once again, $\tilde{V}_{nm}(t)$ accounts for non-Born−Oppenheimer and optical couplings in general, $\tilde{V}_{nm}(t) = V_{nm}(R) - \mu_{nm}E(t)$, and the diagonal terms $\tilde{V}_{nn}$ have been neglected. The neglect of direct excitation $|g\rangle \rightarrow |a\rangle$ corresponds to the setting $\mu_{ag} = 0$. I have assumed that only one resonance state $|a\rangle$ exists, a restriction that can easily be removed. The non-Born−Oppenheimer couplings between the $|a\rangle$ and the metal continuum states $|k\rangle$ is by coupling functions V_{ak}, similar to those appearing in the

Newns−Anderson model. The situation that I have in mind is illustrated in Figure 6a.
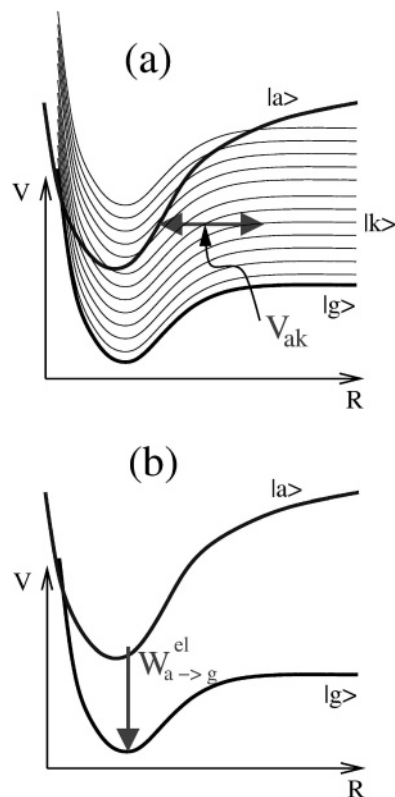

Figure 6. (a) 1D illustration of the coupled multistate model, with ground state $|g\rangle$, a photoactive excited state $|a\rangle$, and a continuum of states $|k\rangle$ above and a specific coupling element V_{ak} indicated by the double arrow. (b) Illustration of an effective two-state model, with a transition rate $W_{a\rightarrow g}^{el} = \Delta_a/\hbar$.

Optical Potential Models. For a (quasi-) continuum of states, eq 87 is too hard to solve, from both the quantum chemical and the quantum dynamical points of view. To simplify the quantum chemical problem, model assumptions for the coupling matrix elements V_{nm} and the potential surfaces V_n can be made. For example, the metal excitations can be approximated by vertically displaced potentials $V_k(R) = V_g(R) + k\delta$, where δ is an elementary excitation energy.[175−178]

Alternatively, one may absorb the continuum, within a projector operator formalism, in a complex potential felt by a wave packet in the excited adsorbate state. In this case, the excited-state Hamiltonian becomes[175,179]

$$\hat{H}_a = \hat{T}_R + V_a(R) - \frac{i}{2}\Delta_a(R) \tag{88}$$

and no continuum states are explicitly considered anymore. Here, Δ_a is the resonance width that can be calculated from the Newns−Anderson model as outlined above. In this formalism, originally suggested for dissociative electron attachment to gas-phase molecules,[179] energy is *not* conserved, since the complex potential resembles the decay of the resonance state $|a\rangle$. For a coordinate-independent resonance width Δ_a, this decay is exponential with an electronic lifetime

$$\tau_{el} = \frac{\hbar}{\Delta_a} \tag{89}$$

Open-System Density Matrix Theory. This approach is conceptually similar to open-system density matrix theory, within an effective, dissipative, two-state model. Accordingly, one has to solve, in the Markov approximation, a LvN equation of the form[180,181]

$$\frac{\partial}{\partial t}\begin{pmatrix} \hat{\rho}_a & \hat{\rho}_{ag} \\ \hat{\rho}_{ga} & \hat{\rho}_g \end{pmatrix} = -\frac{i}{\hbar}\left[\begin{pmatrix} \hat{H}_a & \tilde{V}_{ag} \\ \tilde{V}_{ga} & \hat{H}_g \end{pmatrix}, \begin{pmatrix} \hat{\rho}_a & \hat{\rho}_{ag} \\ \hat{\rho}_{ga} & \hat{\rho}_g \end{pmatrix}\right] + \frac{\partial}{\partial t}\begin{pmatrix} \hat{\rho}_a & \hat{\rho}_{ag} \\ \hat{\rho}_{ga} & \hat{\rho}_g \end{pmatrix}_{\text{env}} \quad (90)$$

for the density matrix. In eq 90, the $\hat{\rho}_i$ and $\hat{\rho}_{ij}$ are operators in the vibrational space, i.e., matrix blocks in the representation of ground- and excited-state vibrational functions $|\phi_\alpha^g\rangle$ and $|\phi_\alpha^a\rangle$. The off-diagonal blocks are electronic coherences, while from the diagonal ones electronic populations can be gained as $\text{Tr}\hat{\rho}_a$ and $\text{Tr}\hat{\rho}_g$. The last term in eq 90 accounts again for energy and phase relaxation but also for substrate-mediated excitation. Within the Lindblad approach, energy relaxation of the excited state $|a\rangle$ with a rate

$$W_{a\to g}^{\text{el}} = \frac{\Delta_a}{\hbar} \quad (91)$$

gives rise to

$$\frac{\partial}{\partial t}\begin{pmatrix} \hat{\rho}_a & \hat{\rho}_{ag} \\ \hat{\rho}_{ga} & \rho_g \end{pmatrix}_{\text{env},1} = -W_{a\to g}^{\text{el}}\begin{pmatrix} \hat{\rho}_a & \dfrac{\hat{\rho}_{ag}}{2} \\ \dfrac{\hat{\rho}_{ga}}{2} & -\hat{\rho}_a \end{pmatrix} \quad (92)$$

DIET, typically enforced with nanosecond lasers, is modeled by a single, Franck–Condon excitation of the ground-state wave function ϕ_0^g to the excited state, i.e., $\hat{\rho}_0 = |a\rangle\langle a| \otimes |\phi_0^g\rangle\langle\phi_0^g|$. Furthermore, eq 92 is then the only "dissipative" term entering eq 90. This corresponds to an electronic Liouvillian $\mathscr{L}_D^{\text{el}}$ with Lindblad operator

$$\hat{C}_1^{\text{el}} = \sqrt{W_{a\to g}^{\text{el}}}\,|g\rangle\langle a| \quad (93)$$

The resonance width Δ_a (and the rate $W_{a\to g}^{\text{el}}$) depends in general on R. If this dependence is neglected, the resonance decays again strictly exponential according to ref 89, and $\tau_{\text{el}} = (1/W_{a\to g}^{\text{el}})$. Additional vibrational relaxation can be included via a total Liouvillian $\mathscr{L}_D^{\text{vib}} + \mathscr{L}_D^{\text{el}}$, with $\mathscr{L}_D^{\text{vib}}$ derived by the formalism of sections 2.1 and 2.2. The effective two-state model with a decaying upper state, as an alternative to a nondissipative multistate model, is illustrated in Figure 6b.

A special variant of this theory has been introduced by Gadzuk within his "jumping wave packet" model. Accordingly, the DIET (at $T = 0$) is treated in two steps. In step one, the ground-state wave function ϕ_0^g is projected on the excited state $|a\rangle$, propagated there for some reference time τ_R, damped then to the ground state $|g\rangle$, and propagated to a final time, t:

$$|\psi(t;\tau_R)\rangle =$$
$$\exp\left\{-\frac{i\hat{H}_g(t-\tau_R)}{\hbar}\right\}|g\rangle\langle a|\exp\left\{-\frac{i\hat{H}_a\tau_R}{\hbar}\right\}|a\rangle\langle g|\phi_0^g\rangle \quad (94)$$

From this, expectation values $A(t;\tau_R) = \langle\psi(t;\tau_R)\,|\,\hat{A}|\,\psi(t;\tau_R)\rangle$

are determined. To compute observables, in a second step, an incoherent averaging scheme is adopted. Assuming a coordinate-independent resonance width Δ_a, the excited state decays exponentially and observables are given by

$$\langle\hat{A}\rangle(t) = \frac{1}{\tau_{\text{el}}}\int_0^\infty e^{-\tau_R/\tau_{\text{el}}}A(t;\tau_R)\,\mathrm{d}\tau_R = \int_0^\infty w(\tau_R)\,A(t;\tau_R)\,\mathrm{d}\tau_R \quad (95)$$

where $w(\tau_R)$ is an exponential weight function. In practice, eq 95 is evaluated as a sum over M' residence times τ_{R_i}, chosen from an appropriate interval.

For coordinate-independent electronic quenching, Gadzuk's algorithm is rigorously equivalent to the open-system density matrix approach, because it turns out to be a special variant of the MCWP method with the averaging (eq 53). A numerical proof of this statement was given in ref 182, and an analytical one was given in refs 183 and 184. In refs 183 and 184, it was also shown how to generalize the algorithm to coordinate-dependent quenching. This is useful, because the jumping wave packet method is much more efficient than the ordinary MCWP scheme, i.e., $M' \ll M$. In the coordinate-dependent case, the modified Gadzuk scheme involves propagation of wave packets under the influence of the non-Hermitean Hamiltonian (eq 88) to obtain weights w_i, which replace the exponential weights in a discrete version of eq 95.

Semiclassical Surface Hopping. The same effective excited-state potential and jumps are also characteristic of a semiclassical surface hopping method, which was recently suggested by Gross and co-workers for DIET.[185–187] In general, surface hopping is an approximate method to treat multidimensional, nonadiabatic dynamics,[188–190] where nuclei are treated classically and electrons are treated quantum mechanically. It was also used for nonadiabatic molecule–surface scattering,[191,192] and it has been generalized to situations with continua.[193]

In the application to DIET, the total *electronic* wave function Φ is expanded as[185,193]

$$\Phi(r, R, t) = \sum_n c_n(t)\,\Psi_n(r, R) + \varphi(r, R, t) \quad (96)$$

where $|n\rangle = \Psi_n$ is the explicitly considered excited state that depends, as usual, on electron and, parametrically, on the nuclear coordinates. φ is a collective wave function for the molecular ground state $|g\rangle$ plus the continuum of substrate excitations $|k\rangle$. The equation of motion for the electrons is

$$i\hbar\frac{\partial\Phi(r, R, t)}{\partial t} = \hat{H}_r[r, R(t)]\,\Phi(r, R, t) \quad (97)$$

where $\hat{H}_r = \hat{T}_r + V_{rr} + V_{rR}$ is the electronic Hamiltonian in which nuclei are treated classically; that is, $R = R(t)$. The classical trajectories are obtained from Ehrenfest forces according to

$$m\frac{\mathrm{d}^2 R}{\mathrm{d}t^2} = -\nabla_R\left[V_{RR} + \frac{\langle\psi_{occ}\,|\,\hat{H}_r|\,\psi_{occ}\rangle}{\langle\psi_{occ}|\psi_{occ}\rangle}\right] \quad (98)$$

where ψ_{occ} is the currently populated electronic state. On which surface the nuclei are currently travelling is regulated by the fewest switching algorithm.[190,193] To avoid the explicit inclusion of continuum states, Gross and co-workers introduced an effective, non-Hermitian Hamiltonian.[194] The

quantum mechanical treatment of electrons involves, in a diabatic representation (see below), solution of a time-dependent Schrödinger equation,

$$ i\hbar \frac{dc_n(t)}{dt} = \sum_m c_m \left(V_{nm} - \frac{i}{2}\Delta_{nm} \right) \quad (99) $$

for the coefficients, which give through $P_n(t) = |c_n(t)|^2$ the occupation probability of state $|n\rangle$ at time t. The coupling terms in eq 99 are matrix elements in the electronic basis,

$$ V_{nm}[R(t)] = \langle \Psi_n | \hat{T}_r + V_{\text{eff}} | \Psi_m \rangle_r \quad (100) $$

$$ \Delta_{nm}[R(t)] = \langle \Psi_n | \Delta | \Psi_m \rangle_r \quad (101) $$

Here, $V_{\text{eff}}(r, R)$ is an effective potential (also containing the internuclear repulsion V_{RR},[185−187] and $\Delta(r, R)$ accounts for the coupling to the continuum. The diagonal elements $V_{nn}(R) = V_n(R)$ correspond to potential curves of excited states $|n\rangle$, and $\Delta_{nn}(R) = \Delta_n$ is the corresponding resonance width. In the Newns−Anderson model, it would be calculated from eq 74. All of these matrix elements depend on time through the classical trajectories $R(t)$ of the nuclei. With only one excited state, $|a\rangle$, explicitly considered the force in eq 98, is just the derivative of potential curve V_a. In the dissipative surface hopping method,[185] it is also assumed that after a jump the system loses all of its energy; that is, only a single jump (to the ground state) occurs per trajectory. Averaging over many trajectories gives, if $\Delta_a = $ const., an exponential decay of the population of $|a\rangle$ with a lifetime $\tau_{\text{el}} = \hbar/\Delta_a$. In essence, this corresponds to the Gadzuk hopping scheme, however, with classical nuclei. While multidimensional DIET is difficult to treat with quantum nuclei, this restriction does not apply to the semiclassical surface hopping method.

Coupled Electron−Nuclear Models. If the restriction of classically moving nuclei is relaxed, one ends up with fully quantum mechanical, coupled electron−nuclear models. Holloway and co-workers[195] have introduced such a model for DIET some time ago. In their approach, one solves a time-dependent Schrödinger equation

$$ i\hbar \frac{\partial \Psi_{\text{tot}}(r, R, t)}{\partial t} = [\hat{T}_R + \hat{T}_r + V(r, R)]\Psi_{\text{tot}}(r, R, t) \quad (102) $$

for the *total*, electron−nuclear wave function $\Psi_{\text{tot}}(r, R, t)$. $\hat{T}_r$ and $\hat{T}_R$ are again kinetic energy operators for electrons and nuclei, and $V(r, R) = V_{rr} + V_{rR} + V_{RR}$ contains all potential terms. In ref 195, the model was applied to photodesorption of NO from a Pt surface, with one electronic ($r = x$) and one nuclear ($R = Z$) degree of freedom. $V(x, Z)$ was chosen as a suitable model potential. As initial states, $\Psi_{\text{tot}}(x, Z, 0) = g(x) \phi_n(Z)$ products made of a Gaussian electronic wave packet moving toward the surface and a bound NO vibrational state $\phi_n(Z)$ were taken. The solution of eq 102 then gives desorption probabilities, for example, with all non-Born−Oppenheimer couplings accounted for.

Apart from the fact that it is not clear how to construct $V(x, Z)$, the method is also numerically costly since both the light electrons and the heavy nuclei have to be propagated on a grid. Furthermore, the laser-excitation step was neglected. Some of these drawbacks can be overcome by expanding the total wave function as

$$ \Psi_{\text{tot}}(r, R, t) = \sum_n \Psi_n(r, R) \, \psi_n(R, t) \quad (103) $$

Here, the Ψ_n are again the electronic wave functions depending parametrically on R, and $\psi_n(R, t)$ is the nuclear wave function on state $|n\rangle$. There are various possibilities of how to choose the electronic basis functions $\Psi_n(r, R)$. In an *adiabatic* representation, $\Psi_n = \Psi_n^a$ is evaluated from the eigenvalue equation

$$ [\hat{T}_r + V(r, R)]\Psi_n^a(r, R) = V_n^a(R) \, \Psi_n^a(r, R) \quad (104) $$

for each parameter value R. This results in a coupled time-dependent Schrödinger equation for the nuclei, which is written in the form

$$ i\hbar \frac{\partial \psi_n^a(r, t)}{\partial t} = \sum_m [\hat{K}_{nm}^a + V_{nm}^a - \mu_{nm}^a E(t)] \, \psi_m^a(r, t) \quad (105) $$

Here, the superscript "a" stands for "adiabatic". The adiabatic potential matrix $\underline{\underline{V}}^a$ is diagonal with elements $V_{nm}^a(R) = \langle \Psi_n | V(r, R) | \Psi_m \rangle_r = \delta_{nm} V_n^a(R)$, where V_n^a are adiabatic potential curves. The kinetic coupling matrix elements $\hat{K}_{nm}^a$ contain the well-known first- and second-order derivative couplings, in a 1D model ($R = q$), given by

$$ \hat{K}_{nm}^a = -\frac{\hbar^2}{2m_q} \left[\left\langle \Psi_n^a \left| \frac{d^2\Psi_m^a}{dq^2} \right. \right\rangle + 2\left\langle \Psi_n^a \left| \frac{d\Psi_m^a}{dq} \right. \right\rangle \frac{d}{dq} \right] \quad (106) $$

In eq 105, dipole coupling to an external field is included through dipole matrix elements $\mu_{nm}^a = \langle \Psi_n^a | \hat{\mu}(r, R) | \Psi_m^a \rangle_r$ in adiabatic representation.

Another representation, which avoids singular behavior of the K_{nm}^a at avoided crossings of potential curves, is the *diabatic* representation. Here, a reference geometry R_0 for the nuclei is chosen and the eigenvalue equation

$$ [\hat{T}_r + V(r; R_0)] \, \Psi_n(r; R_0) = V_n(R_0) \, \Psi_n(r; R_0) \quad (107) $$

is solved. This results in a coupled time-dependent Schrödinger equation for the nuclei in diabatic representation (for which I use no superscript)

$$ i\hbar \frac{\partial \psi_n(r, t)}{\partial t} = \sum_m [\hat{K}_{nm} + V_{nm} - \mu_{nm} E(t)] \, \psi_m(r, t) \quad (108) $$

Now, the potential matrix, with elements $V_{nm} = \langle \Psi_n | V(r, R) | \Psi_m \rangle_r$ is full, while $\hat{K}_{nm} = \hat{T}_R \delta_{nm}$ is diagonal. Furthermore, the dipole matrix is different in the diabatic representation from the adiabatic one. Different choices of the reference geometry R_0 constitute different diabatic representations.

In quantum chemistry, one first solves the electronic Schrödinger eq 107 to obtain adiabatic potentials and electronic wave functions. If in addition the kinetic coupling operators are known, it is straightforward to transform to the diabatic picture.[196−198]

I mention that the diabatization scheme of above with a specific choice R_0 is only one of many other, more sophisticated possibilities. The reader is referred to ref 199 for an overview.

The diabatic Schrödinger eq 108 is equivalent to the multistate model of eq 87, where, however, a few additional approximations had been made. It is also equivalent to eq

102. Finally, close connections to the surface hopping method exist. As emphasized above, however, eq 87 cannot be solved efficiently because too many metal states $|k\rangle$ would be needed to converge the expansion eq 103. To improve on this, in ref 200, a special diabatic representation has been suggested, called the "extended close coupling" scheme. In this scheme, diabatic states are generated from a set of various reference points R_{0i}, rather than from as single one, and orthogonalized to each other. In this way, rather thick metal films representing a Pt surface could be treated efficiently, with a converged number of metal electronic states. In this work also, the substrate-mediated excitation was considered, however, as "regular" dipole transitions between metal states, which are then non-Born–Oppenheimer coupled to a resonance state, $|a\rangle$.

The just mentioned coupled wave packet model (in diabatic representation) combines various pictures that have been used in the literature for DIET from metals. In Figure 7, I illustrate these pictures, for the example of NO desorbing
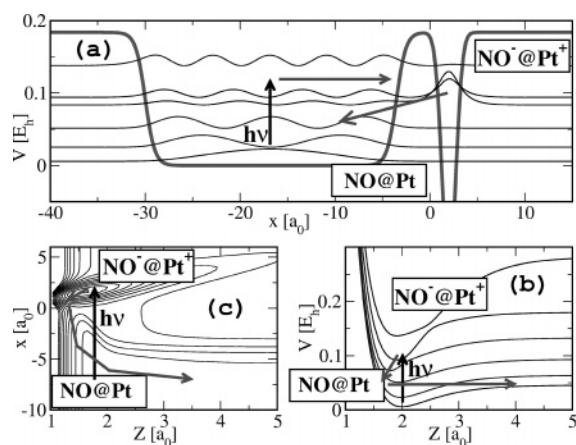

Figure 7. DIET of a NO molecule from a Pt metal film, about 30 a_0 thick. Illustrated are the three "pictures" referred to in the text, derived from the model potential $V(x, Z)$ of ref 195, which is shown in panel c (in the surface region as a contour plot, with the lowest contour at $-0.2\ E_h$, and an increment of $0.05\ E_h$). Panel b gives a 1D potential cut along the electron coordinate x for a fixed value of $Z = Z_0$, where Z_0 is the equilibrium distance of NO from Pt. Also indicated are the electron densities $|\Psi_i(x; Z_0)|^2$ of the six bound, diabatic electronic wave functions. In panel c, I show the corresponding six potential energy curves (in this case, in the adiabatic representation), i.e., $V_i^a(Z)$. The laser-driven coupled nuclear and electron dynamics is indicated by arrows; according to ref 200.

from a Pt film.[200] The three panels correspond to the coupled multistate model (panel b), which emphasizes nuclear motion, to what one might call the "effective electron potential" model (panel a), where the electron motion is central, and—as a synthesis of the two—the combined electron–nuclear model of Holloway et al. (panel c).

2.3.3. Processes Related to DIET

As mentioned earlier, other processes involving "sudden" transitions to excited states can be handled with the same formalism as DIET. In particular, the wave packet hopping scheme of Gadzuk was used for STM-induced desorption in the "above threshold" regime[39,40,201–203] and for ESD.[204–206] I will return to some of these later.

Furthermore, reduced density matrices in a vibrational state representation were propagated to describe nonadiabatic, STM-induced isomerizations in double-well situations, where

both electronic and vibrational relaxation were considered by a dissipative Liouvillian $\mathscr{L}_D^{vib} + \mathscr{L}_D^{el}$ of Lindblad form.[207,208]

2.3.4. DIMET from Metal Surfaces

Nonadiabatic Density Matrix Models. When intense FLs are used for photodesorption, the singular excitation–deexcitation model is no longer adequate due to possible reexcitations—This is the DIMET limit. In the two-state density matrix theory, the hot-electron, substrate-mediated excitation can be modeled with an additional term in eq 90:[180,181]

$$\frac{\partial}{\partial t}\begin{pmatrix}\hat{\rho}_a & \hat{\rho}_{ag} \\ \hat{\rho}_{ga} & \hat{\rho}_g\end{pmatrix}_{env,2} = W_{g\to a}^{el}(t)\begin{pmatrix}\hat{\rho}_g & -\dfrac{\hat{\rho}_{ag}}{2} \\ -\dfrac{\hat{\rho}_{ga}}{2} & -\hat{\rho}_g\end{pmatrix} \quad (109)$$

In DIMET, the initial condition is $\hat{\rho}_0 = |g\rangle\langle g| \otimes |\phi_0^g\rangle\langle\phi_0^g|$ for $T = 0$ initially. Furthermore,

$$W_{g\to a}^{el}(t) = W_{a\to g}^{el}\exp\left\{-\frac{V_a - V_g}{k_B T_{el}(t)}\right\} \quad (110)$$

is an explicitly time-dependent upward rate that obeys detailed balance. Equation 109 corresponds to a Lindblad operator

$$\hat{C}_2^{el} = W_{g\to a}^{el}(t)|a\rangle\langle g| \quad (111)$$

In the case of purely substrate-mediated photoexcitation, eq 109 is the only way to transfer population from $|g\rangle$ to $|a\rangle$. Direct excitation can enter the Hamiltonian matrix $\underline{\underline{H}}$ through dipole-coupling terms. Again, vibrational relaxation can be included.[117]

From a numerical point of view, the direct propagation of density matrices on a grid is costly and therefore limited to one or two system degrees of freedom when "standard methods" are used.[89,209,210] With MCWP methods and its special variant, the jumping wave packet method, DIET processes with up to four dimensions were treated so far—See below. The MCWP or related methods can also be used for DIMET, as demonstrated in refs 182, 184, and 211. For DIMET, however, these methods are much more involved and have not been used in more than two dimensions so far. Nevertheless, stochastic wave packet methods are potentially suited to treat multidimensional DIMET and so are multi-configurational approaches.[91,212]

Other Excitation–Deexcitation Models. This promise holds also true for other excitation–deexcitation algorithms, e.g., semiclassical surface hopping,[185] and for jumping wave packet methods based on time-dependent perturbation theory.[213] The latter has been used for DIMET and related nonadiabatic processes, in more than one dimension.[213]

Comparison of Friction and Excitation–Deexcitation Models. Note that the "strongly nonadiabatic" excitation–deexcitation models of this section are somewhat different from the "weakly nonadiabatic" electronic friction models of section 2.2. In particular, there is no desorption according to the latter if there is no vibrational relaxation of the molecule–surface bond by coupling to electron–hole pairs. This arises from the basic and sensible assumption that the very same physical mechanism is responsible for relaxation and hot-electron-induced vibrational heating and desorption.

As a consequence, the time scale of desorption is determined by the electronic friction coefficient, $t_{des} \sim \eta_{el}^{-1} \sim$ several picoseconds.

In the excitation−deexcitation models, on the other hand, FLD is a result of repeated excitation−deexcitation cycles between ground and excited electronic states.[23,180,181,214] Now, the time scale for desorption is determined by the rise time of $T_{el}(t)$, i.e., typically a few hundred femtoseconds (see Figure 5b). This is shorter than suggested by the electronic friction scenarios. The predicted, faster desorption is the reason that at least in single-pulse DIMET, vibrational relaxation is considered (and found) less important when excitation−deexcitation models are used.[117] For FLD of CO from copper, a time scale of <325 fs has been found by SHG pump−probe experiments.[28] This is shorter than predicted by the frictional models, a shortcoming of the latter that had been realized some time ago.[28,145]

Furthermore, for a system like NO/Pt where a negative ion resonance is believed to be the relevant excited state $|a\rangle$, the adsorbate is expected accelerate toward the surface after excitation, due to image charge attraction (see below). This model would also explain, through the temporary elongation of the NO bond in the anion state, the observed, relatively high vibrational excitation of the desorbing molecules.[21,22] These and other dynamical details follow from the topology of the excited state potential and are nicely reproduced by the excitation−deexcitation models. In contrast, friction models reflect the ground-state topology only, at least in their present form.

3. Potential Energy Surfaces (PESs)

3.1. First-Principle Calculations

The first-principle calculation of ground- and excited-state potentials is a formidable task. This is particularly so for metal surfaces, where it is safe to say that not even reliable methods exist for accurate excited-state calculations.

Without going into details, and also leaving problematic cases aside, I note that ground state PESs for single atoms and for diatomic molecules interacting with ideal, low-index metal surfaces can now be calculated with reasonable accuracy. The most frequently adopted methodology here is periodic DFT[215,216] in two-dimensional (2D) slab[217] or three-dimensional (3D) supercell geometries,[218] employing plane wave bases, (ultrasoft) pseudopotentials, and gradient-corrected exchange−correlation functionals.[219,220] Still there are not so many examples where full-dimensional PESs have been generated in this way, fitted to analytic forms, and used for dynamics. In this context, "full-dimensional" means that the solid is still considered rigid; that is, an atom experiences a 3D and a diatomic molecule a six-dimensional (6D) PES. For atoms (hydrogen), an incomplete list of examples is H on Ni(111), Ni(100), Ni(110),[221] Pd(111),[222,223] Pd(100), Pd(110),[223] NiAl(110),[224] and Cu(111).[225] If surface motion is to be included, semiempirical potentials based on DFT such as EMT (effective medium theory)[226,227] and EAM (embedded atom method)[228] are useful. For diatomic molecules, an analogous list is H_2/Pd(100),[229,230] H_2/Cu-(100),[231,232] H_2/Pt(111),[233,234] H_2/Pd(111),[235] H_2/Ru(0001),[236] N_2/Ru(0001),[237] and O_2/Al(111).[238]

There are fewer investigations of global PES of small molecules interacting with insulator and semiconductor surfaces. One additional complication here is that surface reconstruction is the rule rather than the exception. For these

surfaces, one often uses a local approach, i.e., a cluster instead of a periodic model. The cluster model has the advantage of being suitable also for excited-state calculations, since all of the powerful techniques of quantum chemistry designed for this purpose can be used.[199,239−241] On the other hand, the results do depend on the size and the shape of the chosen cluster. For ionic species, care must be taken to properly embed the cluster in a point charge field and/or polarizable environment. Semiconductor clusters should be covered at their boundaries with hydrogens to saturate artificial dangling bonds. For metals, the cluster ansatz is very problematic,[217,242] unless special embedding schemes are adopted.[243−248]

The situation is even more difficult for *excited* states. Configuration interaction (CI) and multiconfiguration self-consistent field (MCSCF) techniques[239,249−254] can be used for adsorbates on ionic and semiconductor surfaces. Meanwhile, also TD-DFT methods[255] are being used for the same purpose.[254] Even for oxide surfaces, the density of excited states can be very large,[249] and a multitude of different types of excitations may be located in the relevant energy region, e.g., metal-to-ligand, metal-to-oxygen, ligand-to-ligand excitations, etc. Furthermore, the energetic location of excited states is sensitive to details of the embedding scheme. The complexity of the problem results in high computational cost, which is why, to the best of my knowledge, no full-dimensional excited-state potential for a molecule on a surface has been presented to date. Reduced-dimensionality models, however, do exist. Apart from several 1D examples, which will be described below, up to four-dimensional (4D) PESs for selected excited states of diatomic molecules on oxide surfaces were computed ab initio. Example systems are NO/NiO(100)[249,256] and CO/Cr_2O_3(0001),[257,258] which will also be considered below.

The calculation of molecular excited states on metal surfaces is especially tricky because of the continuum of metal excitations, into which they are embedded. A brute-force way is to employ clusters, which are then treated with standard quantum chemistry methods. An early example is the calculation of excited states of CO and NO at Pt(111) along the desorption coordinate, Z in ref 259 (and for NO−Pt also ref 260), where small clusters were employed. In particular, SDCI (CI with singles and doubles excitations included) was used for "clusters" Pt−NO and Pt−CO. The photochemistry of Pt/CO was also studied in ref 261 with Pt_2−CO clusters and similar methods.

Presently, the CI techniques for calculation of excited states are being extended to much larger clusters and to the multireference regime. In refs 262−264, CI and MRCI schemes were applied to N_2/Pt_{64}, CO/Pt_{97}, and H_2CO/Ag_{97}. Various adsorbate excited states, among them electron attachment states, were determined. This was achieved by using a "shell type" model. Only for the metal atoms closest to the adsorbate, a good basis (with d functions) was used, while more distant metal atoms were treated on a lower level, for example, as one-electron atoms. By a localization procedure, the atomic orbitals were transformed to a localized MO basis and classified as "confined to the adsorption site" or "remote". Only the adsorbate-like localized MOs were selected for the CI calculations. In this way, one finds, for example, for N_2/Pt_{64}, a negative ion state about 4.2 eV vertically above the ground state, which corresponds to an electron transferred from the metal to a $2\pi^*$ orbital of N_2.[262] This excited state is bound and shifted toward the surface,

in qualitative agreement with the Antoniewicz model to be discussed below.

Time-dependent DFT is another method for excited states of large systems. The method was recently applied to CO adsorbed on Ni(111)[265] and Pt(111).[266] Cluster models were used for this, in ref 266 with up to 22 Pt atoms, and the excitation space was reduced to single excitations.

Also, for metals, embedded cluster calculations for *excited* adsorbate states have been suggested. For example, a small adsorbate–substrate complex can be treated with the machinery of excited-state quantum chemistry, and the metallic environment can be treated by periodic DFT.[267] In ref 267, the vertical excitation energy for an internal $5\sigma \rightarrow 2\pi^*$ excitation with CO adsorbed on a Pd(111) surface was accurately determined by CASSCF and CI type calculations "embedded in periodic DFT". Generally, there is a great many possibilities of how this metallic embedding can be done.[243] A take-home message is that the embedding is hardly ever free of unambiguities. Furthermore, in all models above, excited states are treated as stationary states, rather than resonances.

Finally, when it comes to larger, e.g., organic molecules on surfaces, little is known from the first principles world, in particular about excited states. Molecules as large as benzene,[40] or even bigger,[268,269] on Si surfaces have been studied with the help of cluster models and DFT. Typically, hybrid functionals popular in quantum chemistry such as B3LYP[270] are used, together with atomic orbital bases, and PESs are only computed along selected modes. Presently, several groups are studying the adsorption of even larger molecules on metal surfaces with periodic DFT codes;[271,272] however, they are not aiming at global PESs. Excited states have hardly ever been determined for these systems. Often, a first guess for the relevant excited state is obtained by attaching an electron (or hole) to the molecule, thus mimicking a negative (positive) ion resonance.[40]

3.2. Model Potentials

Given the complexity of the electronic structure problem, the use of model PESs has a rich tradition in theoretical surface photochemistry. In particular, low-dimensional two-state models are popular.

The two most prominent examples are the celebrated Menzel–Gomer–Redhead (MGR),[273,274] and Antoniewicz[275] models, respectively. In the first, an adsorbate resides in a bound potential, e.g., a Morse potential $V_g(Z)$, before being transferred to a repulsive excited state $V_a(Z)$, for example, of anti-Morse form. As a result, the desorbing particle will initially move *outward* in the MGR model.

In the second case, the excitation is to a bound excited state, arising, for example, from the transfer of an electron from the metal to a low-lying acceptor level of the adsorbate. A protoypical example is NO/Pt, for which in a 1D model an excited-state model[214,276]

$$V_a(Z) = V_g(Z) + \Phi - \text{EA} - \frac{e^2}{4Z} \qquad (112)$$

has been suggested. Asymptotically, for $Z \rightarrow \infty$, this potential accounts for the energy difference between ionic and neutral (ground) state, through a cost factor Φ (the work function of the metal) and a gain factor EA (the electron affinity of the molecule). Closer to the metal surface, the ionic state is stabilized by image charge attraction, the last term in eq 112.

As a consequence, a photoexcited adsorbate moves initially *inward* in the Antoniewicz model.

The negative ion state (eq 112) is a good candidate also for an active resonance in STM experiments with positive sample bias, where the lowest unoccupied molecular orbital (LUMO) is temporarily populated and where Φ is the work function of the tip. In contrast, at negative sample bias, the highest occupied molecular orbital (HOMO) is depopulated and a positive ion resonance may dominate in IET.[157] Of course, "hole resonances" may also be operative in photodesorption. A model potential corresponding to eq 113 for the positive resonance state would be

$$V_p(Z) = V_g(Z) - \Phi + \text{IP} - \frac{e^2}{4Z} \qquad (113)$$

where $\text{IP} - \Phi$ is the energy needed to transfer an electron from the molecule to the surface.

The two potential models, MGR and Antoniewicz, are schematically illustrated in Figure 2b,c, respectively. Note that in both models desorption will proceed in the ground state if the excited state is short-lived. The situation in Figure 2b with the adsorbate desorbing in the excited state holds only for long-lived excited states (vide infra).

The 1D MGR and Antoniewicz models have been extended in the dimensionality, the number, the character, and the topology of the participating excited states. In particular, for systems containing molecular oxygen, neutral O_2, O_2^-, and O_2^{2-} species are possible adspecies, and for each of them (diabatic), PESs and model couplings have been suggested. An example is O_2/Pt(111).[277] Similar models were developed for other systems and processes (e.g., molecule–surface scattering), for example, for O_2/Al(111),[278,279] and NO/Cs/Ru.[280] In these models, more than one degree of freedom was considered, for example, r, the interatomic distance within the diatomic molecule, and Z, the desorption coordinate.

Also, the topology of the excited states was modeled in various ways. Examples are 2D two-state models for NO/Pt(111),[281] two-mode two-state models for NH_3/Pt(111)[282–284] and NH_3/Cu(111),[285–289] three-mode two-state models for NH_3/Cu(111) and Cu(100),[290] and up to seven-dimensional PES for NO on NiO[185] (six for the NO molecule in front of the surface and one for a phonon mode). The parameters and shape of these potentials were based either on limited ab initio information or, as in most cases, on empirical data and "educated guesses".

4. Energy Transfer to the Substrate

The energy transfer from an adsorbate to the surface and *vice versa* is central to photodesorption and similar processes. In particular, the vibrational damping and the quenching of electronically excited adsorbate states are important.

4.1. Vibrational Relaxation

4.1.1. Mechanisms

The vibrational damping coefficient η, or energy relaxation rate, of an adsorbate vibration is defined as in ref 291

$$\eta = W_{1 \rightarrow 0} - W_{0 \rightarrow 1} = \tau_{\text{vib}}^{-1} \qquad (114)$$

where τ_{vib} is the vibrational lifetime. The $W_{\alpha \rightarrow \beta}$ are temper-

ature-dependent. This rate can experimentally be probed by pump−probe spectroscopy and IR line width measurements. It must be noted, however, that the line width is not solely determined by energy relaxation but also by pure dephasing and inhomogeneous broadening, which sometimes dominate.

The two most prominent mechanisms for vibrational energy (and phase) relaxation at surfaces are vibration−phonon and vibration−electron coupling, giving rise to individual contributions to η

$$\eta = \eta_{ph} + \eta_{el} = \tau_{vib}^{ph-1} + \tau_{vib}^{el-1} \quad (115)$$

Note that in a FL experiment the phonon and electron rates will generally depend on different temperatures, T_{ph} and T_{el}.

Vibrational lifetimes were measured for a variety of modes and substrates. An interesting case is the internal stretch mode of adsorbed CO, where vibrational lifetimes of ∼4.3 ms, ∼2.3 ns, and ∼3 ps were reported for NaCl(100),[292,293] Si(100),[294] and Cu(100)[295] surfaces, respectively—see Table 1.

Table 1. Experimental Vibrational Lifetimes τ_{vib} for the CO ($v = 1$) Stretch Mode on Various Surfaces[a]

surface	NaCl(100)	Si(100)	Cu(100)
CO frequency (cm^{-1})	2107	2081	2086
Debye frequency (cm^{-1})	220	520	240
lifetime τ_{vib}	4.3 ms	2.3 ± 0.5 ns	3 ± 1 ps
comments	^{13}C^{16}O, 22 K	100 K	300 K
refs	292, 296	294	295, 296

[a] The vibrational frequency of CO and the Debye frequencies are also given.
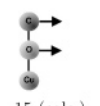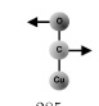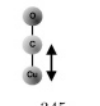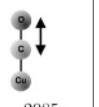
For both the insulator and the semiconductor surface, relaxation by vibration−electron hole pair coupling is inefficient, because the fundamental energy gap between valence and conduction band is much larger than the vibrational quantum $\hbar\omega_0$ of about 2100 cm^{-1}. On the other hand, this frequency is much higher than the Debye frequency of a typical substrate of a few hundred cm^{-1}.[296] This makes also the direct energy transfer from the CO vibration to the substrate phonons slow, resulting in comparatively long vibrational lifetimes. Long lifetimes are also found for other high-frequency adsorbate modes on nonmetallic surfaces. An example is the Si−H stretch vibration of the already mentioned H:Si(100)2 × 1 surface, with a lifetime in the nanosecond range.[297] For CO/Cu(100), the phononic decay channel is also inefficient. Nevertheless, a short lifetime in the picosecond range is observed as a result of the coupling of the CO mode to electron−hole pairs of the metal.

In comparison to high-energy modes, low-frequency adsorbate modes can behave quite differently. At metal surfaces, vibration−electron coupling still often dominates. However, if ω_0 is smaller or only moderately larger than the Debye frequency, one- and two-phonon relaxation can become substantial in addition.[298] An example is shown in Table 2, listing theoretical electron and phonon contributions to the lifetimes of all six CO modes of CO/Cu(100).[140,299,300] In the following, some theory to treat vibrational relaxation by vibration−phonon and by vibration−electron coupling will be reviewed separately.

4.1.2. Vibration–Phonon Coupling

Vibrational relaxation of adsorbates by coupling to substrate phonons is the dominant damping channel for insulator

Table 2. Theoretical Vibrational Lifetimes τ_{vib} (in ps) for Various (Schematically Sketched) Modes of CO/Cu(100) at $T = 0$ K[300] and $T = 300$ K[140] [a]

mode	frustr. transl. (degenerate)	frustr. rotation (degenerate)	Cu-CO stretch	CO stretch
ω_0 (exp.)	15 (calc.)	285	345	2085
τ_{vib} ($T = 0$K)				
electrons (the.)	108	2.3	82	3.3
(exp. [300])	40	>1	>10	3
τ_{vib} ($T = 300$ K)				
electrons	9.7	0.7	5.6	1.6
phonons	4.9	3.8	6.6	> 1000
both	2.3	0.7	2.8	1.6

[a] Also, some experimental values are given as cited in ref 300.

and semiconductor surfaces and, in some cases, also of low-frequency adsorbate modes at metal surfaces.[298]

Formalism. Conceptually, the most straightforward way to treat vibrational energy relaxation by vibration−phonon coupling is to excite the mode locally and follow its subsequent fate with MD. This can be done by explicit cluster or periodic models for the vibrating surface or within a system−bath concept by using a Redfield type relaxation theory[301] or a generalized Langevin model.[302] MD requires multidimensional force fields. "On the fly" first principle MD such as Car Parrinello[303] avoid this problem but are costly, and quantum effects are still missing. A full quantum simulation, on the other hand, is limited to low-dimensional models. Even MCTDH, when applied to favorable "system plus harmonic bath" problems, is restricted presently to about 100 surface oscillators.[88] Semiclassical methods of various kinds are promising.[304−307] Finally, if the lifetimes are long, real-time dynamics is impractical.

On the other hand, vibration−phonon coupling is often weak, which makes this problem ideal for perturbation theory. One then typically starts with a system−bath Hamiltonian of the form of eq 29, where $\hat{H}_s$ describes the adsorbate (the system), $\hat{H}_b$ the substrate phonons, mostly treated harmonic, and $\hat{H}_{sb}$ is the mechanical coupling between the two. If only a single adsorbate mode, q, is of interest, a suitable Hamiltonian is, with Q_k denoting normal mode coordinates of the substrate,

$$\hat{H} = \hat{H}_s(q) + \sum_{k=1}^{N} \hbar\omega_k b_k^{\dagger} b_k + \sum_k^{N} f_k(q)\, Q_k +$$
$$\sum_{k,l}^{N} g_{kl}(q)\, Q_k Q_l + \sum_{k,l,m}^{N} h_{klm}(q)\, Q_k Q_l Q_m + \cdots \quad (116)$$

Here, b_k and $b_k^{\dagger}$ are annihilation and creation operators of the N harmonic bath vibrations with frequencies ω_k. The third and later terms in eq 116 are system−bath couplings, which account for one-, two-, three-, etc. "phonon" processes, and $f_k(q)$, $g_{kl}(q)$, $h_{klm}(q)$, etc. are the corresponding coupling functions. In eq 116, the frequencies ω_k and normal modes Q_k may be obtained from normal-mode analysis of a large cluster. The coupling functions can be obtained from the total potential, by Taylor expansion, from derivatives of V with respect to the normal coordinates, at the equilibrium positions

$Q_{10}, ..., Q_{N0}$. Still, eq 116 is a model Hamiltonian that neglects, for example, frequency shifts in the bath as a function of q. It also treats the bath modes as local vibrations, rather than real phonons with wavevector and polarization. This feature, however, can easily be implemented.[298]

In an even simpler variant of eq 116, (i) only one-phonon processes are considered, (ii) the system is also treated harmonic (with system frequency ω_0), and (iii) the coupling functions $f_k(q)$ are linearized. This is the harmonic–linear model mentioned in section 2.1.6, with Hamiltonian

$$\hat{H} = \hbar\omega_0\, a^\dagger a + \sum_{k=1}^{N} \hbar\omega_k\, b_k^\dagger b_k + \sum_k \lambda_k\, q\, Q_k \quad (117)$$

Here, $a^\dagger$ and a are the harmonic creation and annihilation operators $a^\dagger$ and a of eqs 42 and 40. Equation 117 is of the linear coupling form of eq 44. If the coupling constants λ_k are not known, one frequently uses a single coupling constant, λ, instead, which empirically accounts for an average system–bath coupling strength.

According to Fermi's Golden Rule, transition rates between $\nu = 1$ and $\nu = 0$ of the adsorbate vibration are calculated generally from

$$W_{1\to 0} = \frac{2\pi}{\hbar} \sum_i \sum_f w_i(T)\, [1 - w_f(T)]\, |\langle 0, f\,|\hat{H}_{sb}|\, 1, i\rangle|^2 \times$$
$$\delta(\epsilon_f - \epsilon_i - \hbar\omega_0) \quad (118)$$

where $|i\rangle$ and $|f\rangle$ are initial and final bath states and ϵ_i and ϵ_f are the corresponding energies. Furthermore, $w_i(T)$ and $1 - w_f(T)$ are the probabilities that these states are occupied and empty, respectively, at temperature T.

Specializing to vibration–phonon coupling, at $T = 0$, the transition rates between $\nu = 1$ and $\nu = 0$ for one- and two-phonon processes are

$$W_{1\to 0}^{(1)} = \frac{2\pi}{\hbar^2} \sum_k |\langle 0, 1_k\, |f_k(q)Q_k|\, 1, 0_k\rangle|^2\, \delta(\omega_0 - \omega_k)$$

$$W_{1\to 0}^{(2)} = \frac{2\pi}{\hbar^2} \sum_{k,l} |\langle 0, 1_k, 1_l\, |g_{kl}(q)\, Q_k Q_l|\, 1, 0_k, 0_l\rangle|^2 \times$$
$$\delta(\omega_0 - \omega_k - \omega_l) \quad (119)$$

with 0_k and 1_k denoting bath oscillator k in its ground or first excited state, respectively. Extensions to three- and higher-phonon contributions are straightforward. From the above expressions, it is an easy matter to integrate out the harmonic bath. The δ functions can be approximated, for example, by Lorentzians. Alternatively, one can rewrite them as phonon densities of states[298] or as spectral densities.[308,309] For the density of states, if not calculated, common models such as the Debye model are frequently adopted. At finite temperature, upward rates come into play and upward and downward rates are related by detailed balance, as in eq 26.

In the harmonic, bilinear coupling model eq 117, one obtains for general $\alpha \to \beta$ vibrational transitions at $T = 0$, the rates

$$W_{\alpha\to\beta} = \delta_{\alpha,\beta+1}\, \alpha\, W_{1\to 0} \quad (120)$$

This is, as mentioned earlier, the strict selection rule $\Delta\nu = -1$ with a relaxation rate proportional to the quantum number α of the decaying state. The rate $W_{1\to 0}$, equivalent to η_{ph} at $T = 0$, is given with the model eqs 117 and 119 by

$$W_{1\to 0} = \frac{\pi}{2m\omega_0} \sum_k \frac{\lambda_k^2}{M_k\, \omega_k}\, \delta(\omega_0 - \omega_k) \quad (121)$$

Here, M_k is the mass of the lattice normal mode k. Note that eq 121 predicts a clear isotope effect, with larger m causing shorter lifetimes. At finite temperature, the same modifications apply as above.

Applications. The above and related formalisms have been applied to a variety of systems. In a number of papers, the decay of the Si–H stretch mode at hydrogen-covered silicon surfaces was investigated by perturbation theory. The experimental lifetime of the first excited Si–H stretch vibration of H:Si(100)2 × 1 at $T = 300$ K is $\tau_{vib} \sim 1.2$ ns[297] and increases with decreasing temperature to several ns. For D:Si(100)2 × 1, the lifetime is much shorter, $\tau_{vib}(D) \sim 250$ ps at room temperature. The H:Si(111)1 × 1 surface behaves similarly, with $\tau_{vib}(H) \sim 950$ ps at room temperature.

In refs 36 and 37, the relaxation of the Si–H vibration was treated within a 1D harmonic-oscillator model, with the lifetime at $T = 0$ entering as an empirical parameter. The only coordinate explicitly considered was the Si–H distance, r. Because the Si–H stretching mode has a frequency of about 2100 cm^{-1} while the Debye frequency is ~ 520 cm^{-1}, a multiphonon mechanism must be at work. In refs 37 and 297, a relaxation by emission of three Si–H bending vibrations (with about 630 cm^{-1} each), plus one bulk Si phonon, was proposed. For this four-"phonon" process, a fourth-order, temperature-dependent variant of the equations above was used, leading to

$$W_{1\to 0} =$$
$$\sum_{k,l,m,n} A_{klmn}(n_{B,k} + 1)\, (n_{B,l} + 1)\, (n_{B,m} + 1)\, (n_{B,n} + 1) \times$$
$$\delta(\omega_0 - \omega_k - \omega_l - \omega_m - \omega_n) \quad (122)$$

where $n_{B,k} := n_B(T, \hbar\omega_k)$ is the Bose–Einstein occupation for bath mode k as defined in eq 70 and A_{klmn} contains, formally, the transition matrix elements. Because of the four temperature factors, a strong temperature dependence of the decay rate was predicted; accordingly, the vibrational lifetime would decrease from $T = 300$ K to $T = 100$ K by a factor of about 2, in agreement with experiment.[297] The shorter lifetime of the D–Si stretch mode is due to the smaller mismatch of the Si–D frequency with the bulk frequencies.

Sun et al. had earlier calculated the vibrational lifetime of the Si–H stretch mode for H-covered Si(111) and Si(110) surfaces using Bloch–Redfield relaxation theory.[301,310] In their model, the vibration–phonon coupling was again assumed to be linear, and the relaxation rate evaluated as

$$\tau_{vib}^{-1} \propto |\langle 0\, |r|\, 1\rangle|^2 \int_{-\infty}^{+\infty} e^{-i\omega_0 t}\, \langle \delta F(0)|\delta F(t)\rangle_{class}\, dt \quad (123)$$

The force–force correlation function appearing under the integral was evaluated classically, using a parametrized force field. This approach thus utilizes aspects from perturbation theory and from classical MD. For hydrogen-covered Si(111), a vibrational lifetime of $\tau_{vib}(H) \sim 1.7$ ns was found in this way.

Similarly, in refs 311 and 312, a semiempirical bond-order potential[313–315] was used to provide "absolute" rates for H:Si(100)2 × 1. As a new aspect, two modes were treated

nonperturbatively, namely, the r mode and the Si−Si−H bending along the bending angle, ϕ. The system modes were treated as anharmonic and nonlinearly (in the system coordinates) coupled to harmonic surface oscillators. The latter were obtained from a normal-mode analysis of medium-sized clusters. Because the bending was treated nonperturbatively, a lower-order description could be used for the phonon bath: So far, one- and two-phonon contributions were considered.

A lifetime for the stretching mode of H:Si(100) of about 1.5 ns was found at room temperature,[311,312] which increases with decreasing temperature, both findings in reasonable agreement with experiment. Also, higher excited vibrations $v > 1$ and the vibrational relaxation of the bending mode were considered. It was found that, in particular for the bending mode, the decay rates increase approximately according to the simple scaling law (eq 120) with vibrational quantum number. In Figure 8, I show a representative cluster
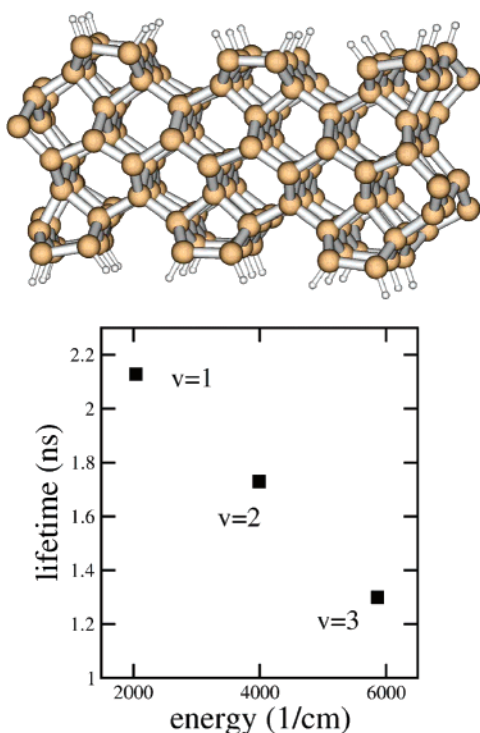

Figure 8. Vibrational relaxation of the Si−H stretch mode of H:Si-(100)2 × 1. Top: Cluster model comprised of 180 atoms. Bottom: $\tau_{\text{vib}}(v)$ at $T = 0$ K, as a function of excitation energy. v is the vibrational quantum number of the Si−H stretch. See ref 312 for details.

used for normal-mode analysis, along with the lifetimes of the first three excited levels of the Si−H stretch mode. It was also predicted that the Si−H bending mode decays on a picosecond time scale, i.e., by 3 orders of magnitude faster than the stretching modes. Because $\omega_\phi \sim 630$ cm^{-1}, two phonons are required to achieve this.

Similar short lifetimes were found for the C−H stretching modes of H-terminated diamond surfaces.[316,317] For example, for H:C(100), a vibrational lifetime as short as 0.8 ps was predicted, which is due to a 1:2 resonance.[317]

Efficient vibration−phonon coupling should also be able to compete with electronic damping, for low-frequency adsorbates modes, even at metal surfaces. For example, Persson suggested[298] that the Ni−CO vibration of CO/Ni(100) decays dominantly by such a mechanism.

Accordingly, the vibration of $\hbar\omega_0 \sim 400$ cm^{-1} emits two phonons (the Debye frequency of Ni is $\sim$300 cm^{-1}), thereby decaying on a sub-picosecond time scale. This finding is in accord with experimental IR absorption line widths.[318]

If few-phonon decay is not possible, the vibrational lifetime can become very long. This is the case for CO/NaCl(100), where, to relax the CO stretch quantum of 2100 cm^{-1}, at least seven phonons are needed.[308,309] Tully and co-workers modeled these high-order phonon processes by perturbation theory. They employed an overall coupling constant λ to reproduce the 4.3 ms decay of the fluorescence signal obtained in experiment.[292] Moreover, vibrational energy pooling was modeled in refs 308 and 309 for this system; that is, the occurrence of CO molecules excited up to as high as $v = 15$ after the CO bond had been pumped with IR photons. The energy pooling is due to lateral vibrational energy exchange of the type CO(1) + CO(1) → CO(2) + CO(0).

In this context, it should be noted that also in other systems lateral energy transfer can become very efficient in comparison to vertical energy loss. An example is the possible Förster transfer of a localized Si−H vibrational quantum to a laterally propagating band of Si−H phonons in H:Si(111).[37]

4.1.3. Vibration−Electron Coupling

Formalism. Vibrational damping due to coupling to electron−hole pairs can also be treated perturbatively. The key is again eq 118, where $|i\rangle$ and $|f\rangle$ are now initial and final *electronic* states, with energies ϵ_i and ϵ_f. Furthermore,

$$w(\epsilon_i) = f(\epsilon_i - \mu) = \left[1 + \exp\left\{\frac{\epsilon_i - \mu}{k_B T}\right\}\right]^{-1} \quad (124)$$

is the probability, according to a Fermi−Dirac distribution, that $|i\rangle$ is occupied at temperature T, with $\mu \approx E_F$ being the chemical potential. Similarly, $1 - w(\epsilon_f) = 1 - f(\epsilon_f - \mu)$ is the probability that $|f\rangle$ is empty.

Using an electron−vibration Hamiltonian eq 65, and for the electronic part a Newns−Anderson Hamiltonian analogous to eq 66, the electronic states entering eq 118 are $|a\rangle$ and $|k\rangle$. Furthermore, for the coupling operator, one may take $\hat{H}_{\text{sb}} = \hat{H}_{\text{es}}$, where $\hat{H}_{\text{es}}$ is a linear coupling operator of the form eq 67.

Precisely within this model, Persson and Persson[319] derived approximate expressions for the vibrational damping rate. If an adsorbate vibrates along q around $q = 0$, the adsorbate resonance close to the Fermi energy, $|a\rangle$ in eq 66, will move up and down energetically and therefore be temporarily occupied. For low-amplitude motion, the adsorbate level can be expanded as

$$\epsilon_a(q) \approx \epsilon_a(0) + \left.\frac{d\epsilon_a}{dq}\right|_0 q \quad (125)$$

around $q = 0$. Using this and several further approximations, Persson and Persson[319] have shown that the Golden Rule gives, at $T = 0$, a vibrational damping rate

$$\eta_{\text{el}} = \tau_{\text{vib}}^{-1} \approx \frac{4\pi\hbar}{m}\left(\left.\frac{d\epsilon}{dq}\right|_0\right)^2 \rho_a^2(\epsilon_F) \quad (126)$$

Here, $\rho_a(\epsilon_F)$ is the local density of states at the Fermi level, which can be approximated by a Lorentzian, analogous to eq 72. Comparing eqs 126 with 73, one notes that both

equations are identical if the coupling constant λ defined in eq 67 is $\propto (d\epsilon_a/dq)|_0$.

Equation 126 can, under the further assumption that in eq 72 Λ_a and Δ_a depend only weakly on energy, be written as[319]

$$\eta_{el} = 2\pi\omega_0 (\delta n_a)^2 \qquad (127)$$

where δn_a is the fluctuation of the occupation of acceptor level $|a\rangle$ during one vibration. By estimating[319] or calculating[320] this charge fluctuation, therefore, one obtains a first guess for the electronic friction coefficient. By this procedure in ref 319, $\tau_{vib} = 1.8$ ps has been determined for the CO stretch mode of CO/Cu(100), already in close agreement with the experimental value of $\sim$3 ps.[295]

This theory gives insight, but for reliable predictions, one would like to have more quantitative expressions. In this context, the theory of Tully and Head-Gordon is worthwhile to mention, which is based on an ab initio quantum chemical cluster model.[140,299,300] The starting point is again Fermi's Golden Rule (eq 118). The electronic initial and final bath states $|i\rangle$ and $|f\rangle$ states are Born−Oppenheimer (i.e., adiabatic) electronic wave functions $\Psi_i(r;R)$ and $\Psi_f(r;R)$. Furthermore, the coupling operator $\hat{H}_{sb}$ is the kinetic energy operator of the nuclei, $\hat{H}_{sb} = \hat{T}_R$. The matrix elements for the $|1_i, i\rangle \to |0_f, f\rangle$ vibronic transition, at $T = 0$, are

$$\langle 1_i, i |\hat{H}_{sb}| 0_f, f\rangle = \langle\phi_1^i|\langle\Psi_i| \hat{T}_R| \Psi_f\rangle_r |\phi_0^f\rangle_R \quad (128)$$

Here, ϕ_1^i is the first excited vibrational state in electronic state i and ϕ_0^f is the vibrational ground state in electronic state f. For a single nuclear mode $R = q$ and $\hat{T}_q = -(\hbar^2/2m_q) (d^2/dq^2)$, one obtains

$$\langle 1_i, i |\hat{T}_R| 0_f, f\rangle =$$
$$\langle\phi_1^i |T^{(2)}(q)| \phi_0^f\rangle_q + 2\left\langle\phi_1^i\left|T^{(1)}(q)\right| \frac{d\phi_0^f}{dq}\right\rangle_q \quad (129)$$

The $T_{if}^{(1)}(q)$ and $T_{if}^{(2)}(q)$ are the first- and second-order derivative couplings, which appeared in eq 106:

$$T_{if}^{(1)}(q) = -\frac{\hbar^2}{2m_q}\left\langle\Psi_i \left|\frac{d\Psi_f}{dq}\right.\right\rangle_r \qquad (130)$$

$$T_{if}^{(2)}(q) = -\frac{\hbar^2}{2m_q}\left\langle\Psi_i \left|\frac{d^2\Psi_f}{dq^2}\right.\right\rangle_r \qquad (131)$$

Now, one neglects eq 131 and approximates $T_{if}^{(1)}(q) \approx T_{if}^{(1)}(0)$. Furthermore, I assume that the molecular vibration is harmonic and that all PESs are parallel, i.e., $\langle\phi_\alpha^i| \phi_\beta^f\rangle_q = \delta_{\alpha\beta}$. Finally, one approximates the ground-state electronic wave function Ψ_0 as a single Slater determinant, generated from a Hartree−Fock cluster calculation, and the electronically excited states Ψ_n as singly excited determinants derived thereof. The electronic excitation energies are (further) approximated as $\epsilon_r - \epsilon_n$, where ϵ_n is the energy of an occupied, and ϵ_r of an empty ("virtual") orbital (The ϵ_i values are orbitals, not state energies now.) By this procedure, one obtains a rate for transition from $v = 1$ to $v = 0$ in the ground state, by simultaneously exciting electrons from below the
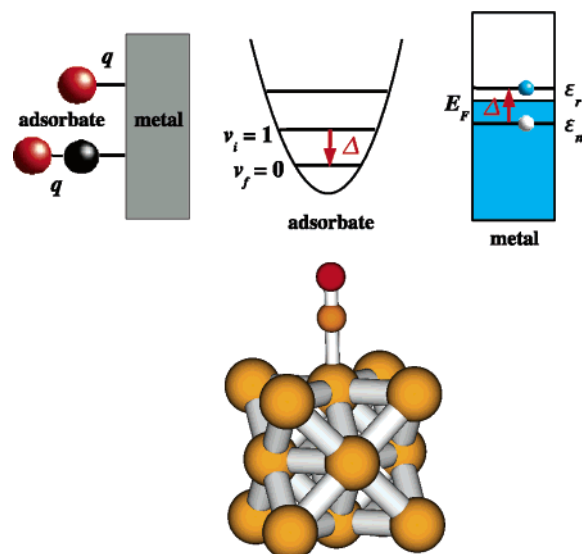

Figure 9. Vibrational relaxation by vibration−electron coupling. Top three panels: Schematic illustration of possible adsorbate modes, q, and deexcitation/excitation processes. $\Delta = \hbar\omega_0$ is the energy of one vibrational quantum. Bottom: Largest cluster CO/Cu$_{14}$ used in ref 299.

Fermi level to levels above it—see Figure 9. The corresponding rate is[299]

$$\eta_{el} = W_{1\to0} =$$
$$\pi\hbar \frac{\hbar\omega_0}{m_q} \sum_{n\in occ} \sum_{r\in virt} \left|\left\langle\chi_r\left|\frac{d\chi_n}{dq}\right|_0\right\rangle\right|^2 \delta(\epsilon_n - \epsilon_r + \hbar\omega_0) \quad (132)$$

where χ_i denotes a Hartree−Fock orbital. Furthermore, the matrix element is a one-electron integral with $(d\chi_i/dq)|_0$ denoting the derivative of orbital χ_i at $q = 0$. Head-Gordon and Tully rewrote eq 132 in an LCAO-MO frame, ending up, after a few additional approximations, with a trace formula

$$\eta_{el} = \frac{\pi\hbar}{m_q} \text{Tr}\{\underline{\underline{P}}(E_F^-) \underline{\underline{G}}^q \underline{\underline{P}}(E_F^+)\underline{\underline{G}}^q\} \qquad (133)$$

Here,

$$\underline{\underline{G}}^q = \underline{\underline{H}}^q - E_F \underline{\underline{S}}^q \qquad (134)$$

where $\underline{\underline{H}}^q$ is the first derivative of the Fock matrix with respect to normal mode q, at $q = 0$. $\underline{\underline{S}}^q$ is the same for the overlap matrix. E_F is again the Fermi energy, and $\underline{\underline{P}}(E_F^\pm)$ is the local density of states just above (E_F^+) and below (E_F^-) of the Fermi level, respectively. The latter can be calculated from the coefficients $C_{\mu p}$ of AO μ in MO p as

$$\underline{\underline{P}}(E) = \sum_p \underline{C}_p \underline{C}_p^\dagger \delta(E - \epsilon_p) \qquad (135)$$

A few points are worth mentioning. (i) The formalism can be extended to finite temperature as indicated above. The transition rates obey then detailed balance. (ii) The $v = 1$ vibrational lifetime is the inverse of η_{el} and, according to eq 133, is proportional to the vibrational mass m_q. (iii) If only

a single acceptor orbital of the adsorbate is important (e.g., the $2\pi^*$ orbital of NO, CO, or N_2), eq 133 reduces to[299]

$$\eta_{el} \propto \omega_0 \, (\delta n_a)^2 \qquad (136)$$

in analogy to the Newns−Anderson form (eq 127). (iv) Within the harmonic model, at $T = 0$, the same scaling as in eq 120 holds. (v) The same formalism can be applied for an entire friction matrix $\underline{\underline{\eta}}$ as needed, for example, for MD with electronic friction (see eq 64), according to

$$\eta_{el;qs} = \pi\hbar \, \mathrm{Tr}\{\underline{\underline{P}}(E_F^-) \, \underline{\underline{\tilde{G}}}^s \, \underline{\underline{P}}(E_F^+) \, \underline{\underline{\tilde{G}}}^q\} \qquad (137)$$

where $\underline{\underline{\tilde{G}}}^q$ and $\underline{\underline{\tilde{G}}}^s$ contain now derivatives of energy and overlap matrices with respect to *mass-weighted* normal mode coordinates, e.g., $\tilde{q} = q\sqrt{m_q}$.

A similar approach, albeit in the framework of periodic DFT, had earlier been taken by Hellsing and Persson.[321] Accordingly, the electronic damping for an adsorbate mode q can be derived, after additional approximations, from TD-DFT,[255] resulting in a Golden Rule type expression

$$\eta_{el} = \frac{2\pi\hbar}{m_q} \sum_\mu \sum_\nu \left| \left\langle \psi_\mu \left| \frac{\partial v}{\partial q} \right| \psi_\nu \right\rangle \right|^2 \delta(\epsilon_\mu - E_F) \, \delta(\epsilon_\nu - E_F) \qquad (138)$$

The "additional approximations" consist mostly of the quasi-static limit, i.e., the assumption of a slowly vibrating adsorbate. In eq 138, the ψ_μ and ϵ_μ are one-electron wave functions and energies, derived from periodic DFT, and $(\partial v/\partial q)$ is the derivative of Kohn−Sham potential with respect to q.

Applications. The cluster approach of Tully and Head-Gordon has been applied, within Hartree−Fock theory, to vibrational damping of CO/Cu(100).[140,299,300] Typical cluster sizes were CO/Cu_6, CO/Cu_{10}, and CO/Cu_{14}—see Figure 9.

As can be seen from Table 2, the vibrational lifetimes for the various modes range (at $T = 0$) from 2 ps (frustrated rotation) to about 100 ps (frustrated translation). In that table, also considered are temperature effects and the fact that vibration−phonon coupling will contribute to the total lifetime. The latter was determined in ref 140 from MD with electronic friction.

The periodic DFT approach of Persson and co-workers was in first applications, used for atomic and molecular vibrations relaxing at jellium metal surfaces.[321] In more modern applications, slab calculations were performed with plane-wave basis sets, ultrasoft pseudopotentials, and GGAs. Examples are refs 322−324, where the friction coefficient η_{el} was calculated as a function of atom−surface distance Z for hydrogen and deuterium atoms at Cu(111).

The friction coefficients are useful for photodesorption but, more generally, also for vibrational relaxation and for sticking of adsorbates in gas−surface scattering.[325,326] They can also be used for a first principles theory of "chemicurrents",[322] i.e., currents induced after electron−hole pair excitation by atoms or molecules interacting with metal surfaces.[327]

In ref 143, the method was applied to calculate, in a two-mode model, the friction matrix for associative desorption of N_2 from Ru(0001) surface. The experimental observation here is that the desorbing molecules are vibrationally surprisingly "cold", which was speculated to be due to energy loss by coupling of the NN vibrational mode, to electron−hole pairs of the metal. Corresponding MD with electronic

friction calculations were carried out to test this hypothesis. The two modes considered were r, the N−N distance, and Z, the N_2−surface distance in parallel orientation. While electronic friction does account for some vibrational cooling, the experiment could not fully be explained.

4.2. Electronic Relaxation

The relaxation of electronically excited adsorbates has a strong influence on the desorption dynamics. The resonance width Δ_a plays a central role in all models of above. Again, at $T = 0$, the electronic lifetime of state $|a\rangle$ is given by $\tau_{el} = \hbar/\Delta_a = 1/W_{a \to g}^{el}$, whereas at finite electronic temperature one has

$$\tau_{el}^{-1} = W_{a \to g}^{el} - W_{g \to a}^{el} \qquad (139)$$

In most of the recent studies of laser-/electron-induced desorption and similar surface reactions, the lifetimes of adsorbate excited states are used as empirical parameters, sometimes chosen to fit experimental data such as desorption yields. In particular, for metal surfaces, for which the adsorbate lifetimes are as short as femtoseconds, both time-resolved measurements and quantum mechanical calculations are still rare.

4.2.1. Excited Metal Bulk and Surface States (SSs)

In some contrast, the longer-lived excited electronic states of bulk, "hot electrons", or of excited electrons trapped in SSs are relatively well-studied, both experimentally and theoretically. The experimental method of choice here is time-resolved two-photon-photoemission (TR-2PPE).[328−331] In this two-pulse experiment, a first pulse excites an electron from below E_F to an empty bulk or SS, and the second pulse probes the transient dynamics in this state by exciting it above the vacuum level, where it can be detected. Other experimental methods giving information about quasiparticle lifetimes are angle-resolved photoemission (PES) and STS.[332]

According to so-called Fermi liquid theory, and also according to more quantitative scattering theory when applied to free-electron gaslike situations, the lifetime of electrons excited into Bloch states with an energy $E - E_F$ above the Fermi level is in the limit of a high density of electronic states given as[333]

$$\tau_{el} = B\left(\frac{1}{E - E_F}\right)^2 \qquad (140)$$

where B is proportional to $\rho^{5/6}$, with ρ being the average electron density. More sophisticated theories are based on the calculation of self-energies from first principles, which takes the band structure of a real metal, calculated by DFT, into account.[334−337] The lifetime can be determined from the imaginary part of the self-energy, which in most applications to date is calculated in the so-called GW approximation.[338]

Free-electron like metals such as Al not only follow eq 140 nicely, but there is also agreement between the free-electron models and the first principles theory as far as the energy dependence of τ_{el} is concerned. This agreement does not hold, however, for the prefactor B in eq 140, which is different in free-electron and from band structure models.[339,340] For Al, the first-principles lifetimes are in the order of 100 fs for $E - E_F \approx 0.5$ eV, decreasing to about 5 fs at $E - E_F \approx 4$ eV.

The quadratic scaling (eq 140) does not apply anymore for main group metals with a more complicated band structure, such as Be, for d-band metals such as Cu,[339] Ag,[341] and Au,[342,343] and for certain other metals[344-346] and nonmetals.[347] In these cases, τ_{el} can behave even nonmonotonic as a function of excitation energy. The first-principle formalism based on DFT and the GW approximation can also be used to determine the lifetimes of holes.[348,349] The holes have, at the same energy, typically a longer lifetime than the electrons.[348]

Electronic excitations localized at metal surfaces, such as excited electrons in image potential, quantum well, or other SSs, have lifetimes ranging from femtoseconds far into the picosecond range. For example, the lifetimes of the lowest image potential states of Cu(100) were determined by TR-2PPE to be in the order of a few tens to hundreds of femtoseconds.[330] Image potential states arise from the Coulomb-like image potential, which behaves asymptotically like

$$\lim_{z \to \infty} V(z) = -\frac{e^2}{4z} \tag{141}$$

where z is the coordinate of the electron along the surface normal. Image states are located in front of the surface forming a hydrogen-like Rydberg series in analogy to atomic physics. The energy of an electron trapped in an image state with quantum number n ($n = 1, 2, ...$), is in 1D idealization given by[350]

$$E_n = -\frac{A}{(n + a)^2} \tag{142}$$

where $A = R_H/16 = 0.85$ eV and R_H is Rydberg's constant for hydrogen and $a \leq 0.5$ is a quantum defect. The corresponding image state wave functions are hydrogen-like wave functions. They penetrate, however, into the bulk, giving rise to inelastic electron–electron scattering and therefore to a finite lifetime, τ_n, of image potential state n.

In a simple, hydrogen-like picture, the lifetimes scale according to[350]

$$\tau_n \propto n^3 \tag{143}$$

In a slightly more sophisticated approach, one may introduce a more realistic interaction potential for electrons in contact with a surface. Chulkov et al. have developed such an effective one-electron potential $V(z)$ for various metals, which is periodic inside the solid and has the correct asymptotics of eq 141.[340] This potential can be used to determine more realistic eigenenergies E_n and wave functions $\psi_n(z)$ of the image potential states numerically. The lifetimes of image potential states can then be estimated from a simple overlap criterion as[340]

$$\tau_n = \frac{\hbar}{b(E_n - E_F)p_n} \tag{144}$$

Here, $p_n = \int_{bulk}|\psi_n(z)|^2 \, dz$ is the penetration of image state n into the bulk region and thus a measure for electron–electron scattering and $b = 0.13$ (for Cu and Ag) is an empirical constant. Equation 144 has been used not only for bare metal surfaces[351] (see below) but also for variants of it to calculate lifetimes for overlayer systems such as N$_2$/Xe/Cu(111)[352] or Ar/Cu(100).[353] In these systems, the overlayers

"isolate" SSs from the substrate, which leads to smaller penetration of the corresponding wave functions into the bulk and, therefore, to longer lifetimes.

A more sophisticated theory, which goes beyond the simple overlap formula and a one-electron approach, treats the electron–electron scattering process explicitly. Using model potentials of the type above and the resultant wave functions, the contributions of inelastic electron–electron scattering to the lifetime can be calculated again from the electronic self-energy in GW approximation.[340] This approach was successfully applied to image potential and other SSs of many materials.[354-359]

As an example, let us consider again the image states of Cu(100). For the lowest three image states, the lifetimes according to eq 144 and the self-energy calculations of ref 354 are given in Table 3 and are compared to experiment.[330]

Table 3. Lifetimes of the First Three Image States of Cu(100) (in fs), According to Various Theoretical Methods and Experiment

image state n	1	2	3
eq 144[351]	22	112	337
self energy[354]	30	132	367
exp.[330]	40 ± 6	110 ± 10	300 ± 15

The lifetimes for Cu(100) are comparatively long, which is a consequence of the fact that at $k_{||} = 0$, the Cu(100) band structure supports an energy gap several electronvolts wide around the vacuum level, in which the image states are embedded—see Figure 10a below. Their penetration into the bulk is therefore small. The Cu(111) surface supports also a gap at $k_{||} = 0$; however, in this case, the $n = 1$ is energetically closer to the band edge, and therefore, the wave function penetrates much further into the bulk. As a consequence, the $n = 1$ lifetime of Cu(111) is only 17.5 fs according to theory[354,355] and 18 ± 5 fs according to experiment.[360] It should be noted that lifetimes, and more generally the spectroscopic line widths, are in general also to some extent determined by electron–phonon coupling[359] and other broadening mechanisms.[331]

4.2.2. Adsorbate Excited States

A big challenge is the measurement (and calculation) of lifetimes of electronically excited adsorbates, because they can be ultrashort. An example where this lifetime, even on a metal surface, is still comparatively long and therefore accessible are alkali atoms adsorbed on Cu surfaces. Here, because of the electropositivity of alkalis such as Cs, the ground state is Cs$^+$/Cu$^-$, and a photochemically relevant excitation is to an antibonding Cs^0/Cu^0 state (A state). In the case of Cu(111), the photoexcitation is from a SS to the A state and direct (see below). The observed, unusual long lifetime of the antibonding state for Cs/Cu(111) is about $\tau_{el} \approx 15 \pm 6$ fs[361] ($T = 300$K) or $\tau_{el} \approx 50$ fs according to ref 362 ($T = 50$ K).

In refs 363, 364, and 371, one- and multielectron contributions to the resonance width, Δ_a, were computed. The one-electron contributions, which are due to resonant charge transfer (RCT), were estimated from an electronic wave packet approach. Accordingly, a 3D electron wave packet, modeling the valence electron of Cs, is placed in front of a Cu surface, and the charge transfer into the substrate followed in time. The multielectron contribution, on the other hand, is due to inelastic electron–electron scattering (see above)
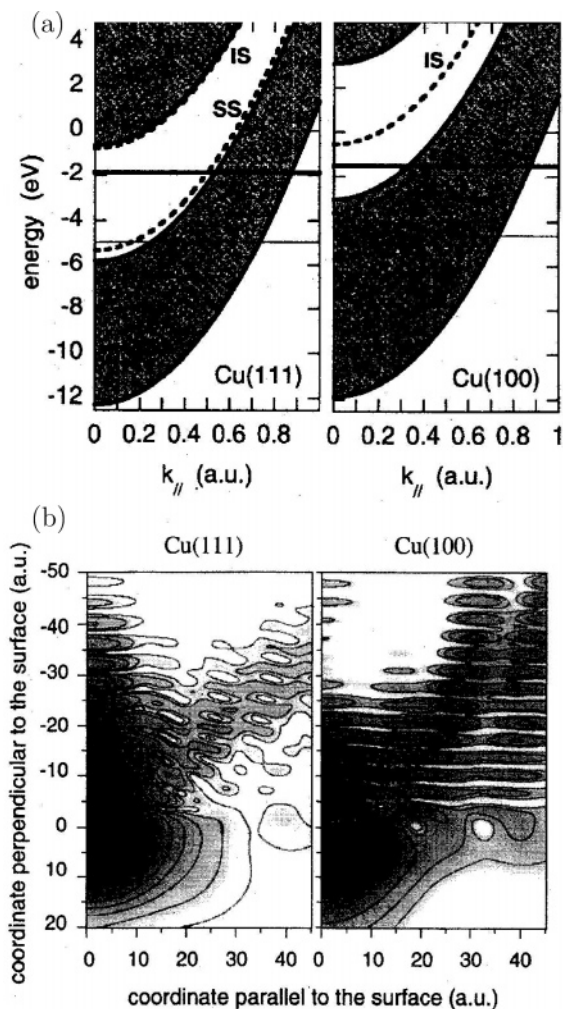
Figure 10. (a) Band structure of Cu(111) and Cu(100), as a function of electron momentum parallel to the surface, $k_{||}$. SS is the SS ($n = 0$), and IS is the $n = 1$ image state. Thick horizontal lines indicate the energetic position of the Cs A state for Cs/Cu (see the text). (b) Snapshots of wave packets for the transient A state of Cs/Cu, as a $\log(|\psi|^2)$ plot, in cylindrical coordinates. Reprinted with permission from ref 363. Copyright 2001 American Physical Society.

and was again determined from the self-energy evaluated in GW approximation. The total computed resonance width

$$\Delta_a = \Delta_{RCT} + \Delta_{ee} \qquad (145)$$

of 23.5 meV for Cs/Cu(111) gives a lifetime $\tau_{el} = \hbar/\Delta_a \approx$ 28 fs in good agreement with experiment. For this system, Δ_a is dominated by $\Delta_{ee} = 16.5$ meV, whereas RCT is blocked, and $\Delta_{RCT} = 7$ meV. This blocking is again due to the large projected band gap of Cu(111), in which the A state is located, as illustrated in Figure 10a. As shown in Figure 10b, the electron has to enter the bulk under an angle.

Because the A state is repulsive (see below), an influence of nuclear motion on the TR-2PPE spectra is found. First attempts to model this have been presented within a quantum–classical scheme for the combined nuclear/electron dynamics.[365] A quantum treatment was published recently.[366]

For Cs/Cu(100), the A state is also located in the band gap but energetically closer to bulk electronic states. As a consequence, a wave packet in front of the surface takes a less pronounced lateral detour, the charge transfer is faster, and $\Delta_{RCT} = 112$ meV is bigger. The inelastic

electron–electron contribution is $\Delta_{ee} = 20$ meV, similar to Cs/Cu(111), resulting in a total resonance width $\Delta_a = 132$ meV and $\tau_{el} = 5$ fs. The corresponding band structure and electron wave packet dynamics are also illustrated in Figure 10. The experimental lifetime of the A state of Cs/Cu(100) is difficult to determine, but a value of 6 ± 4 fs has been suggested. Similar behavior has been found for other alkali/Cu(111) systems.[367]

The methodology of using one-electron model potentials in conjunction with wave packet propagation had earlier been developed for the H^-/Cu(111) system.[368] Again, the band structure of Cu(111) blocks the transfer of the electron to the surface, leading to relatively long lifetimes. In ref 368, Gauyacq and co-workers studied the dependence of the "negative ion resonance" width Δ_a (and τ_{el}), as a function of atom–surface distance, Z. A near-exponential decay of $\Delta_a(Z)$ was found. In the wave packet model,[368,369] resonance widths Δ_a are determined by first computing the wave packet autocorrelation function,

$$C(t) = \langle \psi(0) \mid \psi(t) \rangle \qquad (146)$$

and then fitting to an expression

$$C(t) = \sum_a^L A_a \exp\left\{ -i\left(E_a - i\frac{\Delta_a}{2} \right)t \right\} \qquad (147)$$

where L is a small number. Here, $\psi(t) = e^{-i\hat{H}t/\hbar} \psi(0)$ is the propagated 3D electron wave packet and $\hat{H}$ is a one-electron Hamiltonian containing an appropriate one-electron pseudopotential.

This Z-dependent resonance width $\Delta_a(Z)$ can then be used, by treating the motion of the projectile classically, to estimate the amount of RCT during H^-/surface scattering.[368,370] Similar approaches were used for nonadiabatic ion–surface scattering in other systems.[371,372] See also the related papers.[373–375] Quite generally, the theory of nonadiabatic atom and molecule/surface collisions including RCT has many facets and a long history.[376,377] As an alternative to the explicit propagation of electronic wave packets, the coupled angular mode (CAM) approach, possibly in a multistate version with nonadiabatic couplings between the individual states,[75,378–380] was adopted. The CAM method[381] gives the positions and widths of excited states, in particular of negative-ion resonances, as a function of projectile–substrate distance.[378] The CAM method is similar to so-called R-matrix theory,[382,383] and also to projection operator techniques,[384] for electron–molecule scattering. Accordingly, the interaction of an electron is treated as a scattering problem, with "inner" and "outer" regions of interaction space, which are treated at different levels. The scattering wave function has to be matched at a point separating both regions. In the inner region, different angular modes are mixed by the anisotropic electron–adsorbate/surface potential, which justifies the name of the method. While useful for molecules, most applications of the CAM method were for atom/surface scattering. Among several molecular examples are N_2,[75] H_2^+,[379] or H_2.[385] The nuclear dynamics was treated either classically, by rate equations, or by time-independent scattering theory.

One-electron pseudopotentials similar to those used for electron wave packets were also adopted to calculate, by the complex scaling method, the widths and energies of excited atoms (e.g., Rydberg atoms) or ions interacting with surfaces; see refs 386–390. In the complex scaling method, the time-

independent Schrödinger is solved with a complex scaled coordinate, giving complex eigenvalues whose real part gives the energetic position and the imaginary part the width of the resonance.

All of the methods above are based on the one-electron picture and one-electron model potentials. Multielectron effects, such as inelastic electron–electron scattering, can later be computed via self-energies in the GW approximation as described above or by a nonequilibrium Green's function approach.[391,392]

The calculation of lifetimes of excited adsorbates near metal surfaces from more established electronic structure theory, ideally from first principles, is only in its beginnings. In ref 393, a tight-binding Green's function method was proposed, in which a Dyson equation

$$\underline{\underline{G}}(E) = (\underline{\underline{1}} - \underline{\underline{G}}^0(E)\,\underline{\underline{V}})^{-1}\,\underline{\underline{G}}^0(E) \qquad (148)$$

is solved. Here, $\underline{\underline{G}}^0 = (E\underline{\underline{1}} - \underline{\underline{H}}^0)^{-1}$ is an unperturbed, block diagonal Green's matrix for an isolated adsorbate interacting with an infinite surface, derived from the interaction-free Hamiltonian $\underline{\underline{H}}^0$. $\underline{\underline{V}}$ is the coupling between molecule and surface at finite distance, and $\underline{\underline{G}}$ is the corresponding perturbed Green's matrix. Solving eq 148 at energy $E^+ = \lim_{\eta\to 0}(E + i\eta)$ gives the density of states according to

$$\rho(E) = -\frac{1}{\pi}\mathrm{Tr}\{\mathrm{Im}[\underline{G}(E^+)]\} \qquad (149)$$

Projecting the latter on the adsorbate level(s) of interest gives the local, or projected, density of states ρ_a. In the noncoupling situation, ρ_a is a δ function that broadens when the molecule interacts with the surface. The fwhm of ρ_a is the resonance width, Δ_a. The method was used to estimate the lifetime of the negative ion resonance of a diatomic molecule on a metal surface. With "typical" tight-binding parameters representing an Antoniewicz type situation, a lifetime in the femtosecond range is found around the equilibrium bond length, which increases exponentially with molecule–surface distance, Z; see Figure 11. The method should be extendable to the ab initio world.
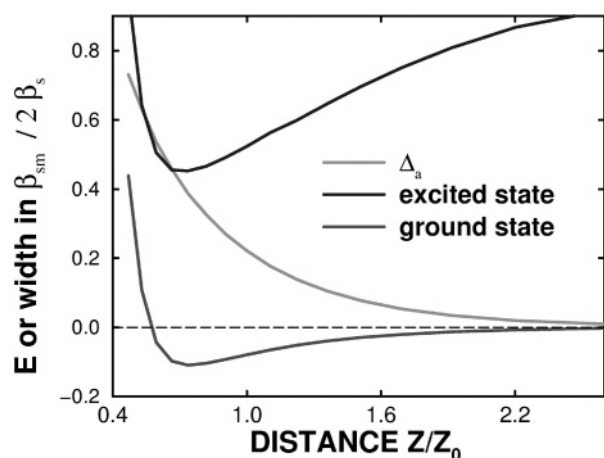

Figure 11. Results from a tight-binding Dyson equation approach.[393] Shown are the computed potential energy curves for the ground state and a (negative ion resonance) excited state of a diatomic molecule adsorbed on a surface, and the resonance width Δ_a, as a function of molecule–surface distance. Units are in $2|\beta_s|$ for energies and $|\beta_{sm}|$ for the width, where β_s and β_{sm} are the tight-binding parameters for the metal–metal and metal–molecule (at $Z = Z_0$) interaction, respectively. Z_0 is a reference distance defined in ref 393.

Also in ref 394, a tight-binding LCAO method has been used to estimate lifetimes, in this case for He^+ at Al(100). Similarly, Taylor and Nordlander use a cluster model within DFT to obtain a projected density of states ρ_a for an atom in front of a cluster,[395]

$$\rho_a(E) = \sum_m |\langle \psi_m | \phi_a \rangle|^2\,\delta(E - E_m) \qquad (150)$$

Here, ψ_m denotes Kohn–Sham orbitals of the combined system, and ϕ_a denotes the Kohn–Sham orbital in question of the isolated atom. By broadening the δ functions by Lorentzians, it is possible to determine the width of ρ_a around $E = E_a$ and define a lifetime.

While the Dyson equation considers an isolated adsorbate on an infinite substrate, the cluster approach is local and therefore plagued with the same shortcomings as the Tully/Head–Gordon cluster model. In ref 396, therefore, the Taylor–Nordlander model was used in conjunction with periodic DFT, using a slab geometry. As a first example, the width of the Li 2s level in front of an Al(100) surface was calculated. In the periodic approach, also the adsorbates are in a periodic arrangement; hence, the lifetime depends on coverage. It was found that at low coverage, the Li 2s resonance width is around 1 eV, when the Li atom is $\sim 4\ a_0$ away from the surface. This suggests again a femtosecond lifetime.

Even shorter lifetimes are possible for core-excited species.[397] An example is core-excited sulfur atoms on Ru(0001).[398] Here, a S 2s electron was excited to the $3p_z$ level. The "core–hole clock" method was used to measure the excited-state lifetime, in this case dominated by the tunneling of the excited electron into the bulk. The electron tunnels on the ultrashort time scale of 320 as = 0.32 fs. The measured transfer time was also supported theoretically by electron wave packet propagation.[398]

Excited-state lifetimes could also be determined, in principle, by solving eq 87 from coupled nuclear wave packets or, equivalently, by solving the electron–nuclear Schrödinger eq 102. The decay of an initial wave packet in front of the surface by nonadiabatic couplings is in general nonexponential, and because the model is energy-conserving, a "lifetime" cannot be strictly defined. Such approaches have in fact been used in refs 195, 198, and 200, giving lifetimes in the order of several femtoseconds for NO/Pt.

A related wave packet approach is the "surrogate Hamiltonian" method of Kosloff and co-workers. Their method will be applied below for FLD, but it can also be used for lifetime calculations, which was done for NO/NiO(100).[399,400] In the surrogate Hamiltonian method, one considers a system coupled to a set of N environmental modes, treated as two-level systems.[399,400] For NO/NiO(100), the two-level systems were electron–hole pairs. The model leads to 2^N coupled Schrödinger equations and is therefore conceptually similar to multistate treatments like eq 87. The theory accounts for the decay of the resonance state within a given system–bath coupling model. A dipolar coupling mechanism was assumed to be operative for NO/Ni(100), and an excited-state lifetime of a few femtoseconds to several tens of femtoseconds was estimated,[399] depending on the charge of the bath dipoles used.

5. Adiabatic Dynamics: Photodesorption in the Ground State

IR light can act in various ways to desorb adspecies from surfaces. First, the radiation may be absorbed by the substrate, leading to thermal desorption by surface heating. Second, the field may couple directly to the dipole of the adsorbate−surface bond, leading to ladder climbing into the desorption continuum. Third, a high-frequency internal adsorbate vibration may be excited by the IR photons, leading to (pre-) desorption.

5.1. Direct Resonant Excitation of the Adsorbate−Surface Bond

Direct, resonant IR desorption has, for chemically bound species, so far not been achieved experimentally. This is due to the fact that dipole-driven vibrational ladder climbing in the ground state with monochromatic IR light is hampered by the decreasing level spacing in the anharmonic potential. Also, for metal surfaces, vibrational quenching is fast, which disfavors excitation.

On the other hand, with intense pulses, it is possible to excite overtones of adsorbate vibrations. This was demonstrated experimentally for CO/Ru(0001), by Wolf and co-workers.[401] They used 120 fs pulses with a carrier frequency close to the CO stretch mode and fluences up to about 17 mJ/cm^2. At low fluences (a few mJ/cm^2), only the $|0\rangle \rightarrow |1\rangle$ transition was observed; at higher fluences also, $|1\rangle \rightarrow |2\rangle$ absorption sets in.

The experimental observation was corroborated by a three-state density matrix model, where the three states indicate the $|0\rangle$, $|1\rangle$, and $|2\rangle$ CO vibrational levels. Energy and phase relaxation as well as direct excitation by the laser pulse were taken into account. The energy relaxation was assumed to proceed on a picosecond time scale, and dephasing rates were estimated from IR line widths. Within that model it was found that, at a fluence of 11 mJ/cm^2, for example, the $|1\rangle$ level can be populated with about a 15% probability and $|2\rangle$ to about 5%—See Figure 12.
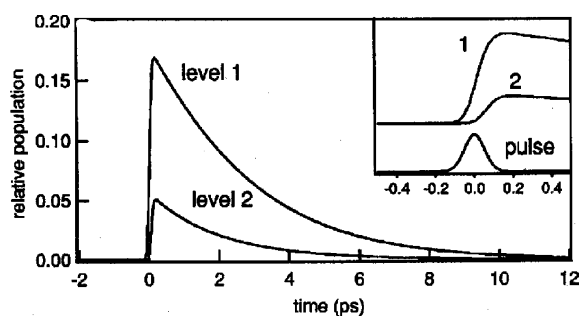

Figure 12. Result of a three-level open-system density matrix simulation of the fs laser-induced IR excitation of CO/Ru(0001).[401] The populations of levels $|1\rangle$ and $|2\rangle$ are shown as a function of time. The inset shows the short-time behavior and the pulse envelope. Reprinted with permission from ref 401. Copyright 2001 American Institute of Physics.

In ref 401, it was also found that at higher coverage lateral energy loss, by Förster transfer due to CO−CO dipole coupling, becomes very efficient. At low coverage, where Förster transfer plays no role, it was argued that the population of $|2\rangle$ could be enhanced by using negatively chirped pulses. The negative chirp accounts for the smaller level spacing $E_2 - E_1$ in comparison to $E_1 - E_0$.

Recently, the possibility to use optimal IR pulses for state-selective excitation of various CO modes was theoretically investigated, for a three-mode model of CO/Cu(100).[402] In the model, the CO stretch (r), the CO−surface mode (Z), and a (dark) lateral mode was taken into account. Energy relaxation for all three modes was included, with rates taken from the work of Head−Gordon and Tully. The pulses were optimized using OCT for open quantum systems, treated in the Markov approximation.[97,98] The result was that even at ambient temperatures, a substantial population of higher levels should be accessible with optimized pulses.

As an alternative to using single chirped, or optimal control pulses, a *sequence* of N pulses

$$E(t) = \sum_{i=1}^{N} E_{0i}\, s_i(t - t_{0i}) \cos(\omega_i t) \qquad (151)$$

should work well for ladder climbing. In eq 151, the individual field amplitudes E_{0i} and frequencies ω_i, as well as shape function s_i (which peak at t_{0i}), may be adjusted to optimize the target state population. This was suggested in earlier works on IR excitation of overtones of adsorbate modes, where the shape functions were chosen either as sin^2 or Gaussian functions.

An example is NH$_3$ on Cu(111). The molecule sits upright on top of a Cu atom with N pointing down, H$_3$ up, and bound by $D \approx 0.7$ eV. Along the umbrella mode of the molecule, the dipole moment changes appreciably,[403] suggesting that overtones of this mode could be excited by IR photons. This possibility was investigated by nuclear wave packet propagation in refs 403 and 404. A two-mode model with umbrella mode, r, and molecule−surface distance, Z, was adopted. Assuming that the radiation does not penetrate the surface, it was found[404] that it should indeed be possible to selectively excite the umbrella mode with a frequency of about 1200 cm^{-1}, at least up to its first overtone ($v_r = 2$). For that, as sequence of two IR pulses, each 1 ps long, with a fluence of about 30 mJ/cm^2, was used. In ref 405, this model was generalized to account for energy relaxation. For that purpose, a model was developed in which the molecular dipole couples to the substrate electrons, leading to vibrational lifetimes on a picosecond scale. Using open-system density matrix theory and the two-mode model, it was found that temporary IR excitation of the umbrella mode by the "old" picosecond pulses is still possible but less effective.[405] Reoptimizing the pulses gave higher target yields.[405] The IR preparation of an adsorbate can also enhance the cross-section for photodesorption with UV/vis light. A few examples of this "IR + UV strategy" will be given below in section 9.2.

The same, dissipative two-mode model was adopted in ref 406 to laser-isomerize the NH$_3$ molecule on the surface from the N down to an inverted, less bound configuration. The most promising strategy to achieve isomerization from the "left" well of the asymmetric, dissipative double-minimum potential to the other well, is by exciting the molecule to vibrational levels above the barrier, from where it relaxes with a 1:1 probability into the "left" and "right" wells. By repeating the excitation out of the "left" well, with either a pulse train or a long pulse, population accumulates in the right (target) configuration.

Finally, in ref 403, sequences of IR pulses were constructed that lead to the desorption of the molecule. However, the corresponding field parameters are somewhat unrealistic when simple Gaussian pulses are used. In principle, the

desorption by a static electric field, under an STM tip for example, should also be possible. In refs 403 and 407, it was found that for an ammonia molecule, bound by 0.7 eV, a critical field strength of about 1 V/Å would be needed. This is unfeasible for an STM experiment on a metal surface, but in the case of semiconductors and/or for less strongly bound adsorbates, static field desorption may be possible.

In fact, direct desorption of adsorbates by electromagnetic (radiation) in the ground state is easier for physisorbed systems.[408] For example, a combined experimental/theoretical study[18] of ^{4}He and ^{3}He physisorbed on Pt(111) showed that the atoms can be removed from the surface already by the blackbody radiation at room temperature. This is possible because the He atom is bound by only 9 meV, and a single photon suffices to desorb it.

The same mechanism had earlier been suggested for the desorption of H_2 molecules physisorbed on a Cu(510) surface.[19] Accordingly, the desorption rate can be calculated from

$$R_{des} = A \int_D^\infty n_B(T,\hbar\omega)\, \omega^3\, C(\omega)\, d\omega \qquad (152)$$

where A is a constant and $C(\omega)$ is a dipole−dipole correlation function. The latter is (for $T = 0$) given as

$$C(\omega) = \sum_\alpha |\mu_{0\alpha}|^2\, \delta(\omega - \omega_{\alpha 0}) \qquad (153)$$

In eq 152, D is again the adsorption energy and n_B is the Bose−Einstein factor, eq 70. In eq 153, $\mu_{0\alpha}$ is the transition dipole moment connecting vibrational levels $|0\rangle$ and $|\alpha\rangle$, and $\omega_{\alpha 0}$ is the corresponding transition frequency. Using this theory, the desorption rates in Table 4 were obtained, which

Table 4. Desorption Rates for H_2 from Terraces of Cu(510) According to Ref 19

temperature (K)	210	296	370
R_{des} (theor.) (s^{-1})	4×10^{-4}	8×10^{-4}	12×10^{-4}
R_{des} (exp.) (s^{-1})	5×10^{-4}	8×10^{-4}	15×10^{-4}

are in good agreement with the experimental data.

5.2. Intramolecular Resonant Excitation and Predesorption

Quite some time ago, IR-laser-induced photodesorption of NH_3 from Cu(100) was observed experimentally, however, with frequencies that excite the N−H stretching mode of about 3400 cm^{-1}.[17] Using a master equation, which took phonon and electronic damping and molecular dipole coupling into account, it was argued[17] that the desorption mechanism is a thermal process arising from "resonant heating". Accordingly, the N−H bond serves as an "antenna" that directs radiation energy, via surface phonons, to the molecule−surface bond, to break it. Unfortunately, the process is nonselective in the sense that also coadsorbed ND_3 desorbs when NH_3 acts as an antenna. [Only recently, the goal was achieved to *selectively* excite and break an adsorbate−surface bond by IR photons without thermalization, for the example of H/Si(111).[409,410]]

That intramolecular, high-energy vibrations can efficiently be excited by radiation, which by subsequent coupling to other modes leads to desorption, is well-known from "predesorption" of molecules from insulators. Examples are CH_3F physisorbed on NaCl[411,412] and, as mentioned, CO

adsorbed on NaCl(100).[85,292,293,413−417] In contrast to NH_3/Cu(100),[17] (i) the coupling of the intramolecular and the desorptive mode is not substrate-mediated and (ii) the excitation energy is larger than the binding energy, D. For CO/NaCl(100), for example, the binding energy is about 1100 cm^{-1} as compared to the vibrational quantum of CO of about 2100 cm^{-1} (for $^{13}C^{16}O$).

When vibrationally exciting the CO bond by IR radiation, it couples into other modes such as the molecule−surface vibration, and desorption will occur. Because the potential is strongly bound along the CO distance, r, and because the coupling between r and the molecule−surface bond, Z, is weak, the molecule is trapped at the surface for a long time, before desorption occurs. Experimentally, the desorption rate after IR radiation has been measured to be $R_{des} \leq 10^{-4}$ s^{-1}.[293]

In refs 416 and 417, the predesorption rate for CO/NaCl-(100) was calculated, using a Golden Rule type theory and a master equation approach. In ref 416, a system was considered consisting of the r and Z modes (perpendicular orientation of the molecule), while in ref 417, this model was extended by a rotational degree of freedom. In the 2D model, the experimental desorption rate could be reproduced with the initial state $|v_r = 0, v_Z = 1\rangle$. The desorption rate increases when v_r and/or v_Z increase. In the 3D model of ref 417, it was found that also rotational predesorption is substantial. It was also observed that the predesorption rate could be considerably enhanced by temperature, through phonon assistance, and by laser control.

6. UV/vis Photodesorption from Insulating Surfaces

In this chapter, I review recent theory on photodesorption and similar reactions of atoms and molecules at insulating surfaces. Here, I consider "direct" excitation by UV/vis light sources, and lifetime effects can be neglected.

A first example concerns the photodissociation of a HCl molecule at an ice surface, which was studied in ref 418. The hydrogen atom leaves the surface, while Cl remains adsorbed. This study is in line with earlier theoretical[419−423] and experimental work[424,425] on the photodissociation of hydrogen halides on (ionic) insulators. It aims at a better understanding of surface-aligned chemistry, on the unravelling of differences to the well-studied dissociation of HCl in the gas phase, van der Waals complexes (e.g., Ar−HCl[426,427] or Ar_2−HBr[428]), and in matrices (e.g., in solid Ar),[429] and on practical aspects of pollution chemistry.

The time-dependent MCTDH method was used to calculate the cw absorption spectrum according to eq 84, after sudden excitation of the molecule from the ground state $|g\rangle = |X^1\Sigma^+\rangle$, to the repulsive, excited state $|a\rangle = |A^1\Pi\rangle$. (The notation applies to the free molecule.) A 2D model in which the Cl atom remains in its fixed position on the surface and where H can move laterally and vertically in the (x, z) plane was used. Initially, the H atom resides halfway between the Cl atom and a nearby O atom of the ice surface; that is, H points toward the surface. Model potentials based on earlier work were used.[430] The main findings were as follows: (i) The H wave packet splits into many fractions after photo-excitation, with desorbed, adsorbed, and subsurface parts. (ii) The angular distribution of the emitted H atom shows structures characteristic for a rainbow effect. (iii) Most importantly, the calculated absorption spectrum exhibits structures that are related to the temporary trapping and oscillation of the H wave packet after excitation, between

the Cl atom and the ice surface. In contrast, the absorption spectrum of free HCl is structureless. As to whether these structures survive under a multidimensional treatment is subject to current investigation. Also, surface atom motion will tend to wash out this "cage effect".[429] Effects of atom motion on photodesorption cross-sections $\sigma(\omega)$ were also studied in ref 431, for nonadiabatically coupled model systems, by a Gaussian wave packet/path integral method.

As another recent example for surface photochemistry at insulators within a two-state model, the ground- and excited-state potential energy curves $V_g(Z)$ and $V_a(Z)$ along the adsorbate−surface distance Z were calculated for alkali atom (Na and K) desorption from SiO$_2$.[254] Cluster models in conjunction with ab initio methods were used for this purpose. Here, the ground state at equilibrium geometry was the charge transfer state $S^-−A^+$ and the excited-state $S−A$ (with S = surface and A = adsorbate).

In ref 254, also, the lifetime of the excited state was estimated based on the assumption that energy transfer to the solid can be neglected and τ_{el} is solely determined by spontaneous emission. In this case, τ_{el} is the inverse of the Einstein A_{if} coefficient for emission from the initial (excited) to the final (ground) state, i.e.,

$$\tau_{el} = A_{if}^{-1} = \left(\frac{2}{c^3} \omega_{fi}^{2} f_{fi} \right)^{-1} \quad (154)$$

in atomic units. Here, f_{fi} is the oscillator strength, and $\hbar\omega_{fi}$ is the energy difference for the transition. With an energy difference of 7.3 eV and an oscillator strength at equilibrium distance of 1.5×10^{-2}, both calculated from TD-DFT, a lifetime $\tau_{el} \sim 28$ ns was estimated. Hence, the relaxation during desorption of the alkali atom can indeed be entirely neglected. Dynamics calculations, on the other hand, were not carried out.

A similar energetic ordering, i.e., "ionic" below "neutral" potential is characteristic also for molecular oxygen adsorbed on a reduced TiO$_2$(110) rutile surface, which was studied in refs 251−253. In this case, clusters were saturated at the boundaries with hydrogen, rather than embedding them in a point charge field. The chosen cluster is Ti$_2$O$_9$H$_{11}$, with O$_2$ sitting upright halfway between two Ti ions, as indicated in the sketch below. The adsorption of O$_2$ in the ground state was also examined with the help of periodic Hartree−Fock calculations, using a slab model. As far as adsorption energies, bond lengths, and other properties are concerned, quite good agreement between periodic and cluster models was found.
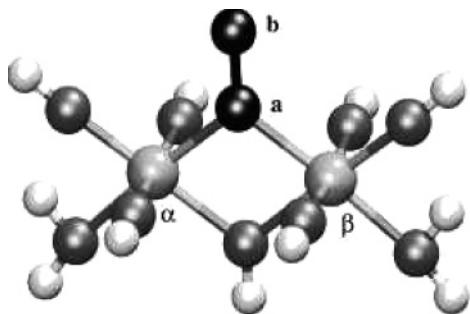

Figure 13. Cluster model Ti$_2$O$_9$H$_{11}$ as used in ref 252. Reprinted with permission from ref 252. Copyright 2003 American Institute of Physics.

Excited- and ground-state potentials were subsequently calculated, within the cluster model, from MCSCF and MRCI

(multireference configuration interaction) wave functions. With this methodology, the ground state $|g\rangle$ was found to be S−O$_2^-$, and the lowest excited-state was S$^-$−O$_2$, around the ground-state equilibrium geometry. For increasing O$_2$− surface distance, Z, however, this order reverses; that is, the molecule desorbs as a neutral species. The crossing (in the diabatic picture) of the two potential curves occurs at around 3 Å.

For O$_2$/TiO$_2$, the desorption after direct photon excitation was modeled by means of the coupled wave packet method according to the two-state TDSE of eq 81. The full coupling element $\tilde{V}_{ga}(Z)$ comprising dipole and non-Born−Oppenheimer terms was calculated in a diabatic representation. In certain areas along Z, in particular close to the crossing point of the potentials, the non-Born−Oppenheimer coupling was found to be larger than 10 meV, suggesting nonnegligible transition probabilities.

The photodesorption yields were estimated from the TDSE by assuming that molecules that are excited will automatically also desorb. With this assumption, reasonable agreement with experimental data[432] was found up to a photon energy of about 3.8 eV. Above that, the calculated desorption yields deviate substantially from experiment, which was interpreted as indicative for additional, so far neglected, substrate-mediated channels.

7. UV/vis Photodesorption from Semiconductor and Metal Surfaces

7.1. Direct DIET

In this subsection, desorption of adsorbates by direct excitation, mostly with nanosecond lasers, will be reviewed. Direct excitation is typically realized for nonmetallic substrates, however, with exceptions. A few specific examples will be given below.

7.1.1. H:Si(100)2 × 1

The desorption of H and D from hydrogen-covered Si-(100)2 × 1 is not only possible with an STM but also with UV photons. This was demonstrated in ref 20. By the process, a direct $\sigma \rightarrow \sigma^*$ transition is enforced.[20] Here, $V_\sigma = V_g$ refers to a ground state, which is bound by about 3.4 eV along the H−Si distance r, and $V_{\sigma^*} = V_a$ to an excited, repulsive state. On the basis of MCSCF cluster calculations, Avouris and co-workers constructed potential curves $V_g(r)$ and $V_a(r)$, which they used to explain their "above threshold" STM experiments at sample bias voltages of > 7 V.[35] In particular, a semiclassical variant of Gadzuk's jumping wave packet algorithm was used to rationalize the unusual large isotope effect in the yields,

$$R = \frac{Y(H)}{Y(D)} \quad (155)$$

of about 50. To do so, an ultrashort lifetime of the excited state of $\tau_{el} \sim 0.5$ fs had to be assumed. This short lifetime is a consequence of the fact that the $\sigma \rightarrow \sigma^*$ excitation lies in the conduction band of the Si surface, with plenty opportunity to couple to empty substrate states. As a result of the short lifetime, desorption probabilities are very small. For H, the yield is about 10^{-3} per excitation event, and for the heavier correspondingly smaller, causing the large isotope effect.

The same model and method was adopted by Vondrak and Zhu to explain their UV desorption experiment, showing a similarly large isotope effect.[20] In refs 201 and 202, effects of an (exponential) coordinate dependence of the quenching rate $W^{el}_{a \to g}(Z)$ were considered in addition. Furthermore, because the excitation is direct, it can be speculated that shaped laser pulses could be useful to control the reaction.[202] In fact, in ref 202, it was argued that ultrashort pulses would enhance the cw DIET desorption probability dramatically. Further "control strategies" will be considered in section 9.2.

As soon as with an STM (single) hydrogen atoms have been desorbed from H:Si(100)2 × 1,[35,43] a Si dimer with one H and one "dangling" bond is left. It was also shown[44,45] that with an STM operating at negative sample bias, the remaining H atom can laterally and reversibly be switched back and forth between the dangling bond Si site and its original position. Also here, a large isotope effect was found for the switching probabilities, $P_{sw}(H)/P_{sw}(D) \sim 7$. In most previously known atom switches, the atom is only weakly bound to a metal surface. The reversible transfer of Xe atoms from a Ni surface to an STM tip is, meanwhile, the classic example.[49,207] In contrast, in the present example, the H atom is bound by more than 1 eV.

Because of this large barrier, it was argued in refs 44 and 45 that H switching on Si(100) requires electronic excitation. A 1D two-state model for the STM hydrogen switch was devised,[44,45] with ground- and excited-state potentials $V_g(x)$ and $V_a(x)$ along a "switching coordinate", x, constructed from periodic DFT calculations. Both potentials are double-minima, with "left" and "right" wells corresponding to stable positions of a single H atom on a Si dimer. The excited state, about 2.7 eV above the ground state, is a short-lived "resonance" with a diffusion barrier much shallower than in the ground state. The lifetime of the resonance was estimated as $\tau_{el} \sim 2$ fs.

In ref 208, this two-state model was adopted within open-system density matrix theory. The "above threshold" STM excitations were treated as in STM-DIET, by a singular Franck−Condon transition. Different from refs 44 and 45, it was argued that the switching occurs in the ground state, not in the excited state, however, much closer to the barrier top after electronic quenching. In contrast to photodesorption, the vibrational relaxation in the ground state cannot be neglected and both τ_{el} and τ_{vib} must be included. Otherwise, in a double-minimum situation, a rate cannot be properly defined, because the population oscillates between left and right wells forever. The time scale for switching, i.e., the time after which the H atom has "decided" which well to choose, is determined by the vibrational lifetime, τ_{vib} in this case. The situation is illustrated in Figure 14.

In ref 208 also, the possibility was investigated to directly excite the H−Si−Si dimer with 2.7 eV photons. For that purpose, FL pulses with $\sin^2$ shape were considered, with fwhm values ranging from 20 to 120 fs. As a result, switching seems possible with higher efficiency than with an STM. For a fixed pulse width of 20 fs, the switching probability increases approximately linear with laser fluence, up to a fluence of about 8 mJ/cm². For even higher fluences, the switching probability drops again, probably due to stimulated emission. A large influence of the switching probability on the pulse length was found.

7.1.2. Cs/Cu(111)

Another system where direct excitation leads to subsequent nuclear motion is Cs/Cu(111). The excitation from the SS
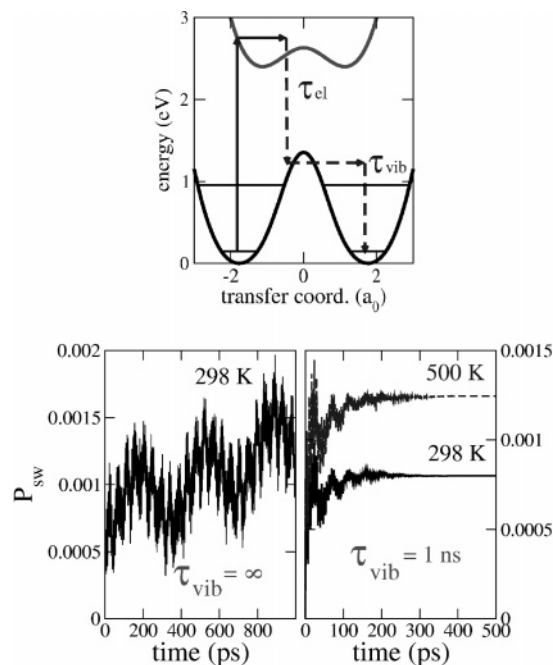

Figure 14. Switching of a H atom on a Si_2 dimer of Si(100). Top: Model. Bottom: Time-resolved switching probability, with and without vibrational relaxation included; after ref 320.

to the antibonding resonance state, A, is direct, and the A state is long-lived, as we have seen. Petek and co-workers achieved the SS → A transition experimentally with a FL pulse with an energy of about 3.1 eV, at a coverage of $\theta \sim 0.1$.[329] By time-resolved two-photon photoemission (TR-2PPE), the nuclear motion of the adatom on the excited-state surface was monitored in real time.[433] It was found that the atom moves outward, within 50 fs by ~ 0.06 Å. First attempts to model the influence of nuclear motion, i.e., possibly of desorption, on the TR-2PPE spectra have been mentioned above.[365,366]

7.1.3. Other Examples

Another system with a comparatively long, but not infinitely long, excited state lifetime (several tens to a few hundred of femtoseconds), is Xe adsorbed on an oxidized Si surface. Photodesorption of Xe from this surface, after direct photoexcitation, was studied experimentally in ref 435 and theoretically in ref 250. In the latter paper, excited states were determined along the desorption coordinate by CASSCF cluster calculations and subsequently used in classical surface hopping.

All examples so far in this chapter were for 1D nuclear motion, and other degrees of freedom were neglected. This is unsatisfactory, in particular for molecules. Here, in a series of papers, Klüner and co-workers fill a gap by considering multidimensional quantum dynamics of diatomic molecules desorbing from transition metal oxide surfaces.[436] The goal is to treat the problem as high-dimensional as possible.

7.1.4. CO/Cr₂O₃(0001)

While $Cr_2O_3(0001)$ is a large-gap material, I refer to photodesorption of CO from this surface in this chapter, since the lifetime of the excited state is assumed to be comparatively short. The photodesorption of CO from $Cr_2O_3(0001)$ in the DIET limit after direct excitation was experimentally studied in ref 437. In their theoretical work, Klüner et al. assumed a Franck−Condon excitation of the ground-state

wave function to a "representative" excited state in the right energy window. Specifically, the excitation was to an $^3\Pi$ state, corresponding to a CO $5\sigma \rightarrow 2\pi^*$ transition.[257,258,438−440] Up to 4D PESs (including Z, the azimuthal and polar angles θ and ϕ, and a lateral mode, X[258]) were determined, using a cluster Cr_4O_6CO embedded in a point charge field and the ab initio CASSCF method. The PESs were fitted to an analytic form. As an example, in Figure 15, a 2D contour
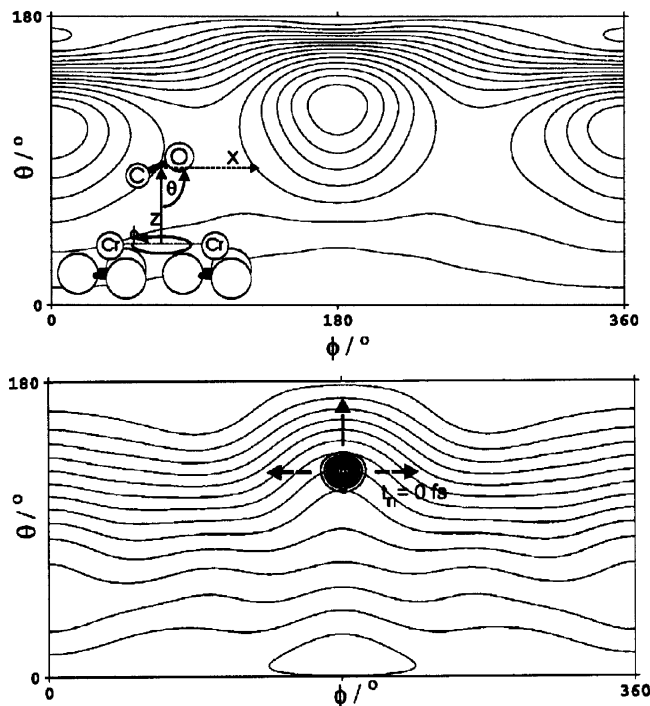
Figure 15. 2D contour plots of the ground (upper panel) and excited-state potentials (lower panel) for Cr_2O_3.[438] On the lower figure, the ground-state wave function is projected, i.e., the initial state after Franck−Condon excitation. Reprinted with permission from ref 438. Copyright 2002 American Institute of Physics.

plot along the angular coordinates is shown for the ground and excited states.

As can be seen from the inset of the upper panel of Figure 15, the CO molecule resides, in ground-state configuration, halfway between two Cr ions, in tilted polar orientation at $\theta = 120°$. In the excited state (lower panel), this is no longer the equilibrium geometry and so the excited wave packet feels forces along both angles (arrows in Figure 15). The desorbing molecules are therefore rotationally "hot". Experimentally, it was found that at low total angular momentum J, the molecules desorb preferentially in helicopter like orientation, while at high J cartwheel rotation dominates.[437]

To understand this behavior, the LvN eq 90 with energy relaxation eq 92, and a constant resonance width Δ_a obtained from an "educated guess", was solved by the jumping wave packet scheme.[214,276] A lifetime τ_{el} of 10 fs was able to reproduce the experimentally estimated desorption probability of between 10^{-1} and 10^{-2}. The calculations were done in refs 257 and 438 in a 3D model (Z, θ, ϕ), and in ref 440 in a 4D model (Z, θ, ϕ, X).

In both references, the "rotational alignment" of desorbing CO at low and high J was investigated but could not be fully explained. It may well be that a 6D quantum simulation[441] is needed and/or that a two-state model or the coordinate-independent resonance width assumption are not realistic.

On the other hand, the simulations nicely reproduce the observed lateral velocity distribution of desorbing CO.[440]

7.1.5. NO/NiO(100)

Klüner et al. also developed ab initio models for DIET of NO from NiO(100).[249,256,443−445] So far, up to 4D two-state models were considered.[445] In the 3D model of ref 256, for example, the two center-of-mass coordinates Z and X and the angle θ are included. In earlier 2D studies, the Z and θ and the Z and r modes had been considered, respectively. Again, a "representative" two-state model was used. The excited state was the lowest sextet, with a NiO^+-NO^- like charge transfer configuration. Adopting only a single "representative" excited state, on top one which is optically forbidden, was justified by the observation that many excited states in the relevant energy region exist, all with similar topology.[249,256] The same argument applies to CO/Cr_2O_3. Again, Gadzuk's averaging scheme was used, with a lifetime of ∼25 fs for the 2D model of ref 443, and a longer $\tau_{el} \sim$ 50 fs in the 3D case,[256] to fit experimental desorption yields.

Experimentally, the most striking feature of the NO/NiO-(100) system is a distinct bimodal velocity distribution.[442] This was explained for the 2D case in ref 443 by the topology of the potential $V_a(Z,\theta)$ of the negative-ion resonance, causing the Franck−Condon excited wave packet to bifurcate. Bifurcation in the excited state was also found to be central in the 3D case; however, now the topology of $V_a(Z, \theta, X)$ along X and hence motion along that coordinate seem decisive.

The semiclassical surface hopping method of Gross et al. was applied for the same system.[185−187] Because nuclear motion was treated classically in this work, the photodesorption of NO from NiO could be treated with up to seven nuclear degrees of freedom, using model potentials. It was found that DIET proceeds through two "channels", an "early" and a "late" one. The origin of the above-mentioned bimodal velocity distribution could not be fully explained.

Another experimental feature for NO/NiO(100) is the pronounced, superthermal vibrational excitation of desorbing NO molecules. One finds for the ratios of populations of vibrational levels, $P_1/P_0 = 0.17$ and $P_2/P_0 = 0.06$.[442] This corresponds to a vibrational temperature (if any exists) of around 2000 K. This was explained in ref 444 in accord with earlier findings for similar systems,[1,183] by the assumption that an intermediate anion NO^-, being stretched, returns vibrationally excited to the ground state from where it desorbs.

7.2. Substrate-Mediated DIET

For all examples of section 7.1, the excitation is direct. For metal surfaces, the excitation is hardly ever direct but substrate-mediated instead. Also, the lifetimes are short (typically < 10 fs), and desorption probabilities are smaller than for most examples considered so far.

7.2.1. NO/Pt(111)

NO desorption from Pt(111) is probably *the* prototype system for substrate-mediated DIET from metals. Also here, representative two-state models have been used with one (desorption coordinate Z)[178,180,181,213,214,276,446−449] and two degrees of freedom, either Z and the NO distance r[183,184,281,320,450,451] or Z and the polar angle θ.[452,453] The 2D (r, Z) model has also been used for nonadiabatic scattering of NO from Pt(111).[454]

Model potentials have been used for the ground state V_g and the negative-ion resonance state V_a. In the 1D models, the ground state was chosen as a Morse potential, and the excited state was chosen as a negative-ion resonance potential (eq 112). The excited-state lifetime was also chosen semi-empirically as $\tau_{el} \sim 2{-}10$ fs, depending on model, dimensionality, and author. The substrate-mediated excitation process itself was treated by a singular Franck–Condon transition of the ground-state vibrational wave function to the excited state.

The most striking experimental observation after using 9 ns laser pulses at 355 nm was that the molecules come off the surface vibrationally hot, $T_{vib} \sim 850$ K. This was again attributed to the assumption that during desorption an anion state is temporarily populated, in which the NO bond is stretched.[281,450] However, by assuming in simulations a bond elongation of $\Delta r \sim 0.1$ Å, which is typical for NO$^-$ in the gas phase, this leads to much larger vibrational excitation than actually found.[455] In fact, with this assumption, a population inversion of vibrational levels is predicted, while experimentally only the lowest two levels are significantly populated, and a ratio $P_1/P_0 \sim 0.04$ is observed. A number of possibilities, including partial charge transfer only and coordinate-dependent quenching, have been suggested[183] to resolve this issue.

Another possibility is vibrational relaxation of the NO bond at the surface. This possibility was investigated in ref 320 within the two-state (r, Z) model. The NO vibrational lifetime was estimated from ab initio cluster calculations and eq 127 as $\tau_{vib} \sim 500$ fs. It was found that this vibrational relaxation lowers the desorption probability and, more importantly, favors $v = 0$ for desorbing NO(v), in expense of higher v. Thus, vibrational cooling of the NO bond may help to explain the observed, relatively moderate vibrational excitation of desorbing NO molecules.[21,22] In ref 320, also, an analytical solution of the LvN equations for DIET with coordinate-independent Lindblad dissipation was given.

The vibrational relaxation of the NO–Pt bond was the subject of a few studies.[451,117] The vibrational lifetime was assumed to be in the order of picoseconds. In ref 451, Gao's relaxation operator (eq 51) in the harmonic approximation was used. In ref 117, the anharmonic raising and lowering operators of eqs 47 and 48 were adopted instead. NO–surface relaxation led again to a reduction of the desorption probability of several percent and, more importantly, to a saturation of Y, which is otherwise often not reached in finite-time propagations. The desorption probability itself is small, $\sim 10^{-4}$ per absorbed photon in the 1D model with $\tau_{el} = 2$ fs.[181]

7.2.2. NH₃/Cu

The DIET of ammonia from surfaces also has a rich experimental[282–286,456–458] and theoretical history.[287–290,459,460] For copper surfaces, one of the most striking features is that there is a pronounced isotope effect when replacing NH₃ with ND₃. The isotope effect not only refers to the total DIET yield, i.e., $Y(\text{NH}_3)/Y(\text{ND}_3) \sim 4$,[285] but also to the vibrational state distribution of photodesorbed ammonia. For NH₃/ND₃/Cu(111), for example, it was found that symmetric and antisymmetric levels of the "umbrella" (ν_2) mode of photodesorbing ammonia are unequally populated, with NH₃ preferring symmetric and ND₃ preferring antisymmetric levels.[286]

These findings have been modeled theoretically with bimodal two-state models in conjunction with the jumping wave packet scheme. A lifetime of about 1.5 fs reproduces the isotope effects and other experimental findings as well. In contrast to NO/Pt(111), for example, for NH₃ desorbing from surfaces, it is essential to take at least one internal mode, namely, the umbrella mode ν_2 (vibration along the inversion coordinate x; see Figure 16), into account. Accordingly, after
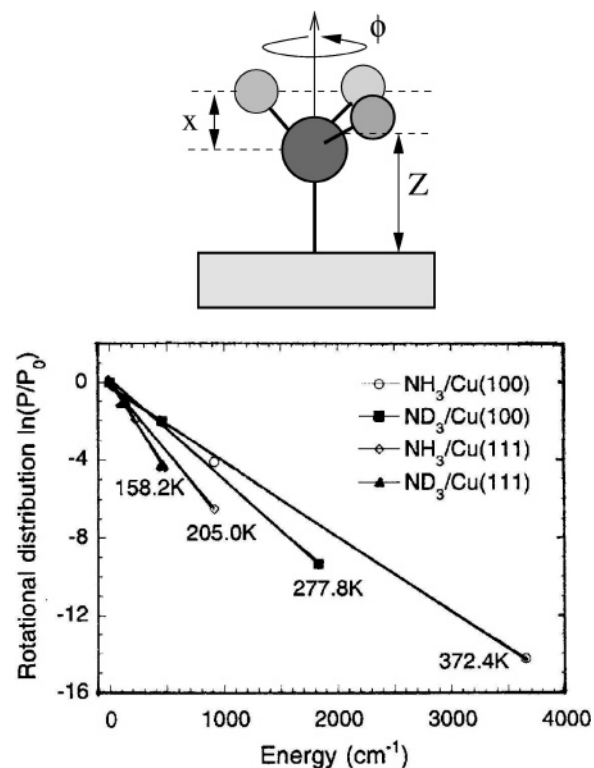

Figure 16. Coordinates (top) and Boltzmann plot (bottom) of rotational level populations of NH₃ and ND₃ desorbing from Cu-(100) and Cu(111). The bottom panel was reprinted with permission from ref 290. Copyright 2001 American Institute of Physics.

Franck–Condon excitation, the molecule moves from the initial N down/H up configuration toward planarity, causing vibrational excitation after desorption.

The 2D model is, however, not sufficient to explain the rotational excitation of the desorbing molecules, and their experimentally observed dependence on surface indices. When desorbing from Cu(111), the molecules are rotationally by more than a factor of 2 colder than when desorbing from Cu(100).[457] To explain this experimental fact, Li and Guo have used 3D model potentials for ammonia/Cu(111) and Cu(100),[290] where in addition to Z and x, also the azimuthal angle ϕ as shown in Figure 16 was considered. For Cu(111), the 3-fold symmetry of the surface is compatible with the C_{3v} symmetry of the ammonia adsorbing on top, while for Cu(100) with its 4-fold rotation axis there is a symmetry mismatch. As a consequence, there is a much larger potential corrugation for Cu(100) along ϕ than for Cu(111). The result is the observed higher rotational excitation of NH₃ when desorbing from Cu(100) rather than Cu(111), as indicated in Figure 16.

From the figure, one first notes that the population of rotational levels follows a Boltzmann plot, so it is reasonable to assign a rotational temperature T_{rot}, a finding consistent with experiment.[457] Furthermore, the computed rotational temperatures for NH₃ are $T_{rot} = 372$ K for Cu(100) and T_{rot}

= 205 K for Cu(111), again in reasonable agreement with the experimental values of 540 and 220 K, respectively. The ND_3 molecules come off rotationally colder. Other computed observables, such as the total desorption yield, are not much affected by the extra degree of freedom.

7.2.3. O_2 on Metal Surfaces

The photochemistry of molecular oxygen on metal surfaces is interesting, because of several possible intermediate oxidation states of oxygen. All of them give rise to their own (diabatic) PES and to possibly different reaction pathways. The most important oxidation states are neutral O_2 (the physisorption state), O_2^- (superoxide), and O_2^{2-} (peroxide); see section 3.2. The neutral state is bound along the O−O distance r and gives O_2 plus the metal surface for $Z \rightarrow \infty$. The superoxide state with one electron attached to the antibonding π^* orbital is typically bound along r and Z. The peroxide state is bound along Z and gives two dissociated O^- ions when r is extended. This is at least the situation that applies for O_2/Pt(111), according to experimental findings.[277]

In ref 277, a 2D (r, Z) three-state model was developed, for O_2 oriented parallel on an uncorrugated surface. The three potentials stand for O_2 [$V_g(r, Z)$], O_2^- [V_m, (r, Z), m = molecularly adsorbed], and O_2^{2-} [$V_a(r, Z)$, dissociative state], with nondiabatic coupling functions $V_{am}(r, Z)$ and $V_{gm}(r, Z)$ between a/m and g/m accounted for. The potential and coupling parameters were chosen such that the ground-state *adiabatic* potential function, i.e., the lowest root obtained from diagonalizing the potential matrix

$$\underline{\underline{V}} = \begin{pmatrix} V_g & V_{gm} & 0 \\ V_{gm} & V_m & V_{am} \\ 0 & V_{am} & V_a \end{pmatrix} \quad (156)$$

reproduces experimental facts, such as geometries and vibrational frequencies. The adiabatic ground-state surface is also consistent with periodic DFT calculations.[461] Initially, the molecule resides as adsorbed species O_2^- approximately at the minimum of V_m, separated by barriers from a physisorption well (minimum of V_g) and the dissociated state (minimum valley of V_a). The barrier to dissociation is 0.34 eV, and the one toward desorption is 0.38 eV. An analogous multistate model was devised by Kosloff and co-workers for similar systems.[462]

A DIET scenario arising from *electron* excitation for O_2/Pt(111) was modeled by Franck−Condon transition of the inital wave function to the dissociative excited state V_a, which corresponds to an attachment $O_2^- \rightarrow O_2^{2-}$.[277] It was then time-evolved under the influence of the Hamiltonian $\underline{\underline{H}} = \underline{\underline{1}}\hat{T}_R + \underline{\underline{V}}$ for a residence time τ_R, and Gadzuk's averaging scheme was applied. Similarly, a resonance *hole* excitation was modeled by Franck−Condon exciting the inital wave function to the neutral excited state V_g and proceeding as above. One can then calculate the branching ratio between desorption and dissociation,

$$B = \frac{Y_{des}}{Y_{dis}} \quad (157)$$

under different excitation conditions (electron or hole). In the Gadzuk averaging, a sub-femtosecond excited-state lifetime was assumed for the excited states, but a single, "representative" residence time $\tau_R = 2$ fs without averaging

gave results close to the averaged quantities. Vibrational damping was accounted for by a simplified scheme, in which fluxes going in r and Z directions were phenomenologically damped with exponential damping factors $e^{-t/\tau_{vib}}$, with $\tau_{vib}^r = 0.25$ ps and $\tau_{vib}^Z = 3$ ps. It was thus assumed that vibrational relaxation along r is faster than along Z.

In refs 211 and 277, the branching ratio under DIET conditions was calculated as $B < 1$, comparable to the experimental value of $B \sim 0.5-1$. This corresponds to more dissociation than desorption after excitation with nanosecond pulses.[32] The branching ratio, however, depends sensitively on details of vibrational damping. Under hole resonance conditions, similar results were obtained.

The dependence of the branching ratio on vibrational damping was further analyzed in ref 211, based on dissipative Lindblad functionals as described in eq 51[121,122] to treat nonlinear vibrational relaxation and a stochastic wave packet approach to solve the open-system LvN equation. In particular, the experimental finding was of interest that under FL conditions, the branching ratio increases to $B \sim 5-30$, i.e., $Y_{des} \gg Y_{dis}$.[34] Similar findings apply to O_2/Pd.[31,135] The FLD/DIMET was modeled in a simplified way, by assuming that a second electronic excitation took place after some delay time. Figure 17 shows the branching ratio B, as a function
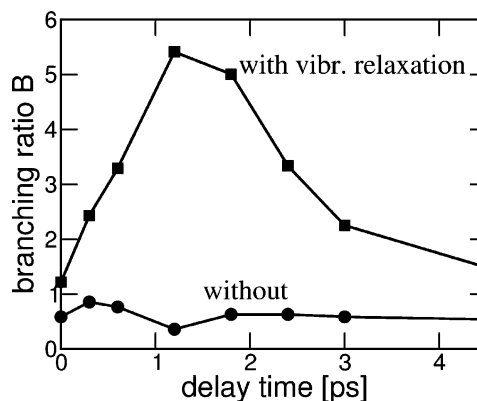

Figure 17. Branching ratio B for O_2/Pt(111) as a function of delay time between two subsequent excitations. The two curves are without (bullets) and with (filled squares) vibrational relaxation taken into account (solid); after ref 211.

of delay time, for two different cases: without vibrational relaxation and with vibrational relaxation. Note that in the latter case, $B > 1$ for all delays, in agreement with experiments. This behavior has its origin in the anisotropic vibrational relaxation: Because $\tau_{vib}^Z > \tau_{vib}^r$, the Z mode is still vibrationally "hot" when the second electronic excitation takes place. In contrast, the r mode has already relaxed. Therefore, the desorption (along Z) is greatly enhanced over dissociation (along r), under FLD conditions.

7.3. DIMET

This last example makes the connection to FLD from metal surfaces, which has been realized for many other systems.

7.3.1. NO on Metal Surfaces

The first system for which DIMET has been observed is NO/Pd(111), with a nonlinear scaling of the yield with fluence according to eq 1 and an exponent $n = 3.3$.[23] This and the other DIMET hallmarks as described in the Introduction, notably the higher DIMET yield as compared to DIET,

were reproduced and explained in ref 25 with the help of stochastic trajectory simulations, using two-state models. The stochastic trajectory calculations are the classical analogues to the quantum mechanical DIMET models based on open-system density matrix theory as described in section 2.3.4, when realized by a MCWP algorithm.[178] The classical particles undergo random jumps between two potentials V_g-(Z) (neutral state) and $V_a(Z)$ (anion state). These jumps are governed by the upward rate $W_{g \to a}^{el}$ that depends on the time-dependent electronic temperature $T_{el}(t)$, and the downward rate $W_{a \to g}^{el}$. The latter was assumed to be $\tau_{el} = 2$ fs in ref 25. The electronic temperature was calculated from the 2TM.

Another important hallmark of DIMET is the ultrashort, sub-picosecond response in FLD, recorded by 2PC. For NO/Pd(111), 2PC was measured and simulated, using Arrhenius type rate equations and the 2TM in ref 24.

The open-system density matrix approach was applied in refs 117, 180, 181, and 448 for FLD of NO/Pt(111) within a 1D model and extended in refs 183 and 184 to two modes (r, Z). Also, here, $\tau_{el} = 2$ fs was assumed (in the 1D model), and the 2TM was applied to obtain the upward rate in eq 110. The LvN equations were solved either by direct density matrix propagation,[181] by stochastic wave packet methods,[178,184] or by a variational wave packet method.[212] The use of stochastic wave packets also allowed us to quantify the notion of "multiple" in DIMET. As a result, for realistic $T_{el}(t)$ profiles, it was found that the average number M per pulse is surprisingly small.[181] This is consistent with an independent analysis of Gadzuk.[463]

Again, the nonlinear scaling law (eq 1) could be reproduced within the 1D two-state matrix model.[117,448] A scaling exponent in eq 1 of $n \approx 4.4$ was found, in reasonable agreement with the experimental value of $n = 6 \pm 1$.[27]

Unlike in direct photochemistry, where n can be interpreted as the number of photons needed to break the bond, in the indirect, hot-electron-mediated process, n has no simple physical interpretation. The excitation rate $W_{g \to a}^{el}$ depends exponentially on $T_{el}(t)$, which itself depends nonlinearly on the laser field. To be more quantitative, in Figure 18, the
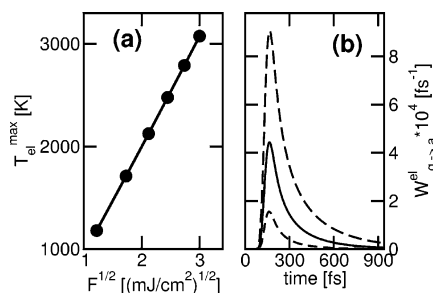
Figure 18. (a) Maximal electronic temperature T_{el}^{max} as a function of laser fluence F. (b) Time dependence of the excitation rate $W_{g \to a}^{el}(t)$ for three laser fluences 4.5, 6, and 7.5 mJ/cm² (from bottom to top); after ref 117.

maximum electronic temperature T_{el}^{max} is shown for Pt(111), when 80 fs Gaussian pulses with increasing fluence are used, together with the corresponding excitation rates. In Figure 18a, $T_{el}^{max}(t)$ is plotted against $F^{1/2}$. From the almost perfect linear relationship, one finds $T_{el}^{max} \propto F^{1/2}$, in excellent agreement with an estimate $T_{el}^{max} \propto \sqrt{F}$ given by Corkum et al.[464] and also in ref 131. In Figure 18b corresponding, selected excitation rates are given.

In ref 117, besides electronic relaxation, also vibrational relaxation of the NO-surface vibration was accounted for, leading to a reduction of the desorption yield also in DIMET. In ref 117, it was further found, based on calculation of the vibrational state distribution $P_v(t)$ of the NO-substrate vibration from the full density matrix, that $P_v(t)$ is nonthermal, at least for hundreds of femtoseconds, rendering the notion of a vibrational temperature T_{vib} in FLD somewhat questionable—See Figure 19.
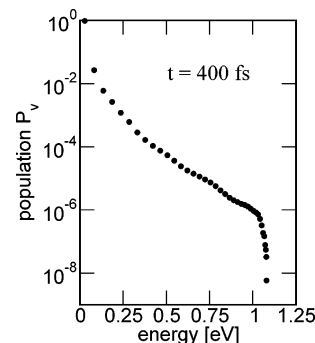
Figure 19. Populations P_v of the vibrational states of the NO−Pt bond at $t = 400$ fs, according to a density matrix model.[117] A Gaussian laser pulse with fwhm 80 fs and a fluence $F = 6$ mJ/cm² and wavelength $\lambda = 619$ nm has been used for excitation. All states up to the desorption continuum of NO−Pt, starting at $E = D = 1.08$ eV, are shown.

As mentioned above, "phononic" vs "electronic" mechanisms of FLD or other reactions can experimentally be discriminated by 2PC measurements. Again, for NO/Pt, 2PC traces of desorption yields were calculated, using the 1D two-state density matrix/2TM.[117] An observed, rapid initial falloff of the $Y(\Delta t)$ curve on the time scale of a few hundred femtoseconds is indicative of the electronic mechanism. It was also found, however, that the initial steep decay of $Y(\Delta t)$ is followed by a very slow decay extending far into the picosecond and probably even nanosecond regime. Nevertheless, also in this regime, the mechanism is electronic in the model, since no phonons were accounted for. The reason for this behavior can be traced back to the prediction of the 2TM, of a fast decay of $T_{el}(t)$ due to electron−phonon coupling, followed by a slow decay as soon as $T_{el} \approx T_{ph}$, when diffusive cooling begins to dominate. As a consequence, the second pulse finds the electrons "warm", for long times, which in turn leads to larger yields than expected for two uncorrelated laser pulses. This finding suggests that the classification as "phononic" or "electronic" mechanisms from time scale arguments is not entirely straightforward.

To go beyond the concept of bath and system temperatures, Koch et al. applied their surrogate Hamiltonian for FLD of NO from NiO(100). As mentioned earlier, however, because the substrate is no metal, direct dipole excitation of the system dominates,[399,400] and DIMET cannot be observed. This is consistent with FLD experiments for NO from NiO, where at most a slight superlinear dependence of the yield on the laser fluence was observed.[465−467] In refs 399 and 400, on the other hand, a dependence of computed observables such as desorption probability and velocity distribution, on the pulse length (rather than only the fluence), was predicted.

7.3.2. O₂ on Metal Surfaces

FLD in the DIMET regime was also observed for O_2 at metal surfaces, as said earlier. In refs 149 and 152, the

"weakly nonadiabatic" theory of section 2.2 was applied to DIMET of O_2 from Pt(111), in a 1D model, assuming the validitiy of the concept of a vibrational temperature during desorption. Both the perturbative model described above and a nonperturbative, scattering-theoretic approach for the transition rates $W_{\alpha \to \beta}$ were used. In this latter approach, the inelastic transition rates $W_{\alpha \to \beta}$ are calculated as[468,469]

$$W_{\alpha \to \beta} = \sum_{k,k'} 2 \frac{2\pi}{\hbar} f_k (1 - f_{k'}) |T_{\beta k', \alpha k}|^2 \, \delta(E_\beta + \epsilon_{k'} - E_\alpha - \epsilon_k) \quad (158)$$

Here, the scattering matrix element from initial vibrational state $|\alpha\rangle$ and metal electronic state $|k\rangle$, to final state $|\beta\rangle$, $|k'\rangle$ is

$$T_{\beta k', \alpha k} = \sum_m \frac{\langle \beta | m \rangle \langle m | \alpha \rangle V_{ak'}^* V_{ak}}{\epsilon_k + E_\alpha - (\epsilon_a + \Lambda_a) - E_m + i\Delta_a} \quad (159)$$

where the V_{ak} values are the coupling matrix elements defined in the Newns–Anderson Hamiltonian (eq 66). In eq 158, f_k is the occupation number of metal electron state $|k\rangle$ at temperature T_{el}, and $(1 - f_{k'})$ is the corresponding probability for state $|k'\rangle$ to be empty. Furthermore, Λ_a is the shift and Δ_a is the broadening of the resonance level $|a\rangle$, as defined earlier. The intermediate states $|m\rangle$ in the eq 159 are the eigenstates of the negative ion resonance state, which are temporarily occupied.

It was found that the two approaches (called models A and B in refs 149 and 152), give quite similar results, while a classical treatment underestimates the "vibrational heating". In ref 149, it was also argued that, if initially no off-diagonals of the density matrix are present, they do also play no big role during the FLD process, making a master equation approach valid.

In ref 149, a nonlinear scaling law $Y \propto F^{5.6 \pm 0.4}$ was found for DIMET with single 80 fs pulses, as compared to the experimental observation $Y \propto F^{6.4}$. Also, 2PC traces were modeled. For O_2/Pt(111), the 2PC yield shows a feature about 0.6 ps (hwhm) wide, which was well-reproduced by the model.[149]

Another theory toward FLD has been presented in ref 470. Nonequilibrium Green's functions were used in conjunction with DFT, to compute from first principles the probability of desorption or dissociation of O_2 on Ag(110), as a function of photon energy.

7.3.3. CO on Metal Surfaces

The FLD of CO from metal surfaces in the nonlinear fluence regime has been the subject of numerous investigations. Again, the nonlinear yield-fluence dependence according to eq 1 and the ultrashort response times in 2PC traces were the most striking experimental results. For CO/Cu(111), the exponent n in (eq 1) is $n = 3.7$.[28] For CO/Cu-(100), at a coverage of 0.5, one finds $n = 8 \pm 1$ in the (absorbed) fluence range between 4.3 and 4.6 mJ/cm² and a 2PC halfwidth of about 2 ps.[29]

The theoretical modeling of these processes/systems ranges from Arrhenius expressions (eq 24 or 58) in conjunction with temperature models (section 2.2.1), over the more sophisticated MD with electronic friction method (also section 2.2.1), to coupled wave packet schemes (section 2.3.2) and open-system density matrix theory (section 2.3.4).

In refs 29 and 471, the Arrhenius eq 24 has been used, and eqs 59 and 60 applied to various adsorbate modes of CO/Cu(100). For the CO–Cu mode, electron–vibration and phonon–vibration couplings $\eta_{el} = (6 \text{ ps})^{-1}$ and $\eta_{ph} = (3 \text{ ps})^{-1}$ were chosen. For the C–O mode, $\eta_{el} = (2 \text{ ps})^{-1}$ was assumed, and η_{ph}^{-1} was found to be very long. By assuming that the CO–Cu mode is the vibrational coordinate along which desorption occurs and using the appropriate frequency factor B in eq 24 and the vibrational temperature of that mode, the exponent n found in eq 1 was $n = 8.4$, in agreement with the experimental value.[29] It was also argued in ref 29 that other modes of adsorbed CO, namely, the frustrated rotations and translations, cannot be fully excluded as possible desorption modes.

The procedure applied in ref 29, namely, applying one of the Arrhenius expressions (eq 24 or 58) to a selected (guessed) desorption mode, with parameters (η_{el}, η_{ph}, B, and/or E_a) either fitted or taken from other sources, is an established technique to rationalize the experimental outcome of FL-induced reactions at surfaces.[6,9,10] Of course, this approach is somewhat empirical and relies on a 1D reaction path.

For CO/Cu(100), Head-Gordon et al. found by MD simulation with electronic friction and all six, coupled adsorbates modes included (see eq 64), $n \sim 5.6$ for half coverage.[144,145] Their model has the additional advantage that also the translational, rotational, and vibrational energies of the desorbing molecules can be obtained. In the MD simulations, the frictions were chosen consistent with the friction tensor computed in ref 140.

The FLD of CO from Cu(100) in the nonlinear regime was also the subject of a number of quantum mechanical investigations, using "strongly nonadiabatic" models. Micha and co-workers adopted modified open-system density matrix theory and/or dissipative wave packet models, the latter with up to four modes (Z, θ, X, ϕ), finding an exponent $n \sim 3$.[472–478] In their modeling, the excitation is through an "effective dipole", suggesting a more direct dependence of the desorption dynamics on laser parameters than in other models. Such a more direct dependence, however, is questionable in the case of indirect, e.g.m hot-electron-mediated mechanisms, where, for example, no dependence of the cross-sections on the laser polarization and hence dipole orientation is found. The hot-electron-mediated FLD of CO from Cu surfaces was also studied in ref 479, by a three-state dissipative wave packet model, where one state represents a metal excitation.

7.3.4. Other Systems

Apart from the systems mentioned, for a number of other adsorbates and surfaces, hot-electron-mediated FLD has been observed and, in most cases, also modeled by Arrhenius type rate equations and electronic friction models. One example is the associative desorption of H_2 from Ru(0001),[6] where a large isotope effect was observed after replacing H_2 by D_2. Recently, this system has also been treated with two-mode MD with electronic friction.[480] This work showed good agreement between theory and experiment as far as the scaling of the yield with fluence and the internal energy distribution of the desorbing molecules is concerned.

Another example is FLD of CO from Pt(111), where the fluence dependence of the yield is again strongly nonlinear, but the actual exponent n depends on the pulse length.[481] This is therefore an example where not only the fluence but

also the pulse shape counts. However, no difference in the desorption yield was found when chirping the pulse.[481] Furthermore, in ref 482, NH_3 and ND_3 were desorbed from Pt(111) with FL pulses. Interestingly, here, no dependence on the pulse length was observed, and also the clear isotope effect reported for DIET with nanosecond lasers is not found.

8. Related Processes: STM-Induced Desorption and ESD

8.1. STM-Induced Desorption

It has been stated that STM-induced desorption or analogous reactions are closely related to DIET when the STM operates in the "above threshold regime", and related to DIMET when operating "below threshold". As a concrete example, the desorption and switching of H at Si(100) have been mentioned.

Ultrafast STM desorption was not only observed for H/Si but for larger molecules as well. An example is the desorption of benzene from Si(100)2 × 1, at negative voltages.[39,40,203] The desorption yield depends linearly on current, indicative of a single-electron process.

A 2D two-state model has been devised,[39,40,203] with (dimensionless) desorption coordinate Z and a "butterfly" mode X. The first is related to the molecule−surface distance, the second one is related to the buckling of the benzene molecule, as indicated in Figure 20.
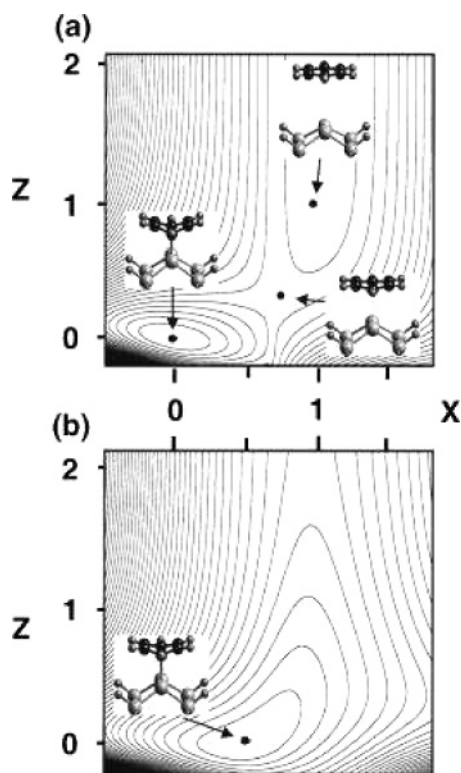

Figure 20. Neutral ground state (a) and positive ion state (b), for benzene on Si(100)2 × 1 in the two-mode model. The calculations were done with a cluster on the B3LYP/6-31G** level of theory. Stationary points are indicated by dots, and the corresponding geometries are shown.[203] Reprinted with permission from ref 203. Copyright 2000 American Institute of Physics.

At negative sample bias, the HOMO is being depopulated; therefore, a positive ion is expected to be a good representa-

tive of the excited-state resonance. Gadzuk's jumping wave packet model was used for STM-induced DIET. A lifetime τ_{el} of the positive ion resonance of $\tau_{el} \sim 7-20$ fs was assumed, to rationalize the observed, high efficiency of the desorption process. Mechanistically, it was suggested that the molecule, which is buckled in the ground state, tends to planarize after Franck−Condon excitation and then desorbs from the surface vibrationally excited, in the butterfly mode. Further examples, and the perhaps more interesting STM-DIMET regime, will not be covered here beyond what already has been said.

8.2. Electron-Induced Desorption

Instead, I briefly turn to electron-induced processes such as ESD, which are also often described by jumping wave packet models analogous to DIET, with an initial, impulsive excitation. An example is the ESD of CO from Ru(0001) by 150 eV electrons,[72,73] which was studied theoretically in refs 204 and 205.

In contrast to the "low-energy" excitations considered so far, the high-energy electrons probably lead to a double-excitation of the CO molecule.[72] As a consequence, not only vibrational excitation, but in fact a vibrational population inversion for the desorbing molecule was found experimentally, with a maximum around $\nu = 30$. The possibility that some of the molecules might dissociate was mentioned.[72]

In refs 204 and 205, a 2D two-state model was developed with Z, the CO−surface distance, and the C−O distance, r, i.e., desorption and dissociation mode. The excited state was assumed to be the $3\sigma^{-1} 4\sigma^{-1} 2\pi^{+2}$ doubly excited state, with a strongly elongated C−O bond and CO−surface distance.[483] After Franck−Condon excitation and subsequent relaxation, the molecule desorbs with enormous vibrational energy, as shown in Figure 21. The vibrational excitation is a conse-
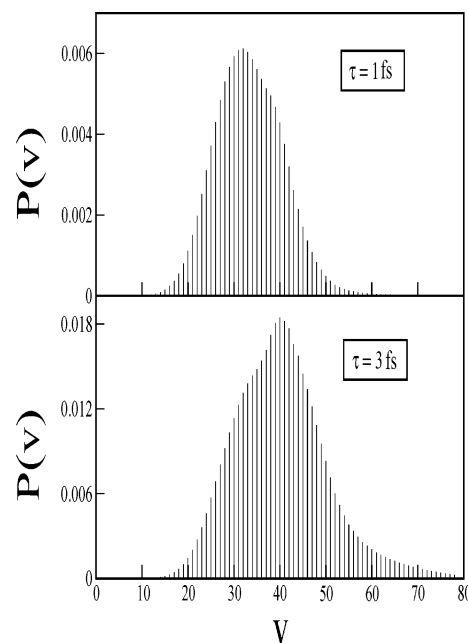

Figure 21. Vibrational state distributions $P(\nu)$ for CO desorbing from Ru(0001), for two different excited-state lifetimes.[204]

quence of the substantial bond lengthening in the doubly excited state, of about $\Delta r \sim 0.6$ Å. Also, dissociation occurs to some extent. The excited state lifetime is essentially unknown and was assumed to be in the few femtoseconds range.

A more recent example of ESD is that of CH_3Br from O/Ru(001). Here, pronounced steric effects were predicted,[206] with a Br-up configuration desorbing with a much higher probability than a Br-down configuration. Also, in this example, bimodal two-state models were employed. The excited state was assumed to be an anion state.

9. Controlling Surface Reactivity

We close this review by describing several actual developments toward the *control* of ultrafast molecular desorption from surfaces.

9.1. Control by Nanostructuring

While ideal, extended surfaces are a useful reference, and they may not be ideal for practical applications of surface photochemistry. Here, as in heterogeneous catalysis, confined structures such as clusters or films can offer advantages.

For example, it has been found that NO molecules desorb from amorphous or ordered aggregates (5−80 Å in diameter) of Pd atoms on alumina surfaces, very efficiently when stimulated with nanosecond UV light (DIET conditions).[484] The photodesorption cross-section increases with decreasing aggregate size over at least 1 order of magnitude. It has been conjectured that this may be due to additional binding sites with low adsorption energy, but electronic effects may also play a role.[484]

Electronic effects are clearly responsible for the high photoreactivity of Ag nanoparticles, where plasmon-enhanced photochemistry was observed experimentally. Plasmons are collective excitations of the metal electrons, which resonantly enhance the electric field at the surface. As a consequence, the direct photoreaction cross-section increases. This mechanism was predicted theoretically some time ago.[485,486] Other enhancement channels are due to the coupling of plasmons to electron−hole pairs, or phonons, leading to indirect, *incoherent* adsorbate excitation. A plasmon-enhanced, phonon-induced reaction is the FLD of water from quartz-supported Ag clusters, as demonstrated in ref 487. An example of direct excitation of a short-lived surface plasmon, possibly coupled to hot electrons, leads to desorption of NO molecules from Ag clusters on alumina.[488] Surface plasmons were already known to enhance the photoreactivity of adsorbates on roughened Ag surfaces.[489]

In addition, the photoreactivity of an adsorbate may be enhanced by other mechanisms: (i) The lifetime of intermediate states could be dramatically influenced by quantum size effects. For metal films, for example, it is known from calculations that the density of electronic states in the solid varies discontinuously with film thickness, thus causing a discontinuous behavior also for the lifetimes.[375,395,490] Similarly, for metal clusters, it was shown by DFT, the jellium model, and the self-energy formalism that small metal clusters show a nonmonotonic lifetime as a function of cluster size.[491] In cases for which the lifetime is very long, the molecule can gain more energy in the excited state; therefore, the desorption cross-section increases.

(ii) In the case of "hot-electron"-mediated FL chemistry, the confinement may have an influence on the $T_{el}(t)$ curve. This latter effect was demonstrated in ref 448. In Figure 22a, I show the time-resolved electronic temperature $T_{el}(t)$, at the surface of Pt(111) films several to many nanometers thick, after excitation by FL pulses.[448] For the calculation, the 2TM was used with a thickness-dependent source term $S(t)$
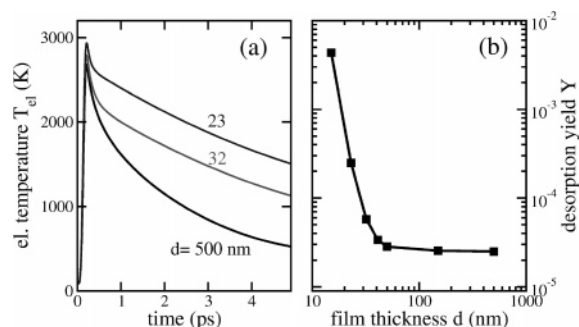

Figure 22. (a) $T_{el}(t)$ curves for thin Pt films, obtained with the 2TM.[448] A Gaussian laser pulse polarized perpendicular to the substrate was used with fluence $F = 6$ mJ/cm^2, fwhm $= 80$ fs, and $\lambda = 619$ nm. The $d = 500$ nm result is indistinguishable from the bulk. (b) Desorption yields resulting from the open-system density matrix model, for different film thicknesses d.

according to eq 56. It is first of all seen that with decreasing film thickness, the maximum electronic temperature, T_{el}^{max}, increases. From Figure 18a, I recall that T_{el}^{max} is proportional to $\sqrt{F}$, now one finds an approximate relation $T_{el}^{max} \propto \sqrt{F/d}$, suggesting that lowering d has as similar effect as increasing F. From Figure 22a, it is also evident that the electronic temperature is high for a longer time, before heat diffusion can cool the electrons down. As a consequence, the hot-electron-mediated desorption depends sensitively on film thickness, as shown in Figure 22b. Here, the desorption probability has been calculated with the open-system density matrix approach of above.

Another way of how to enhance photoreaction cross-sections has been suggested in ref 492. Accordingly, when depositing an ultrathin metal film on a semiconductor, UV/vis photons would create hot electrons or holes in the semiconductor. These will then tunnel through the metal layer to the adsorbate to form an ion resonance by electron or hole attachment. It was argued that this leads to an enhancement factor $\propto 1/d$, and for films a few tens of Ångstroms thick, the reaction cross-section might increase a factor of about 10. A related but different proposal to enhance reaction cross-sections is due to Gadzuk,[493,494] who suggested to use metal−insulator−metal tunnel junction devices to tune electron (hole) energies into resonance.

9.2. Laser Control of Surface Reactions

There are also attempts to control surface photoreactivity by the light source itself. A difficulty arising in the case substrate-mediated photochemistry is that the adsorbate is excited only indirectly; that is, *coherent control* is evidently not easily possible. Of course, there is the "trivial" control by laser frequency and fluence. Also, the reaction cross-section of FLD will be enhanced by a sequence of laser pulses, rather than a single pulse, as observed in 2PC experiments.

Similar ways of *incoherent control* have been predicted in ref 448, where the *shape* of the laser pulse envelope was proposed as a possible control parameter, in agreement with the experimental finding for CO/Pt(111) as mentioned above.[481] The predicted controllability of FL-desorption by chirped pulses,[473] on the other hand, was not supported by experiment: Neither a positive nor a negative chirp had any effect on the desorption of CO/Pt(111), at least in the range of experimental parameters considered.[481]

While UV/vis photons penetrate most metal surfaces thus favoring hot-electron mechanisms, IR photons couple directly to the adsorbate−surface bond. It has therefore been suggested to use a IR + UV/vis strategy to first vibrationally excite the adsorbate and then to desorb it by electronic excitation.[180,181,201,202,260,404,405,449] From DIMET, one knows that vibrational excitation favors desorption. This is also consistent with a number of experimental findings for DIET, where vibrational preparation was achieved by surface heating.[495−497] As an example, it was shown that the DIET yield of CH_3 radicals desorbing from GaAs increases by a factor of about 10 when heating the substrate from 100 to 580 K.[496]

In the realm of molecular reaction control, the IR + UV strategy is known as "vibrationally mediated chemistry".[498−500] For surface science, it was suggested that IR preexcitation will not only lead to larger UV/vis desorption yields but may also be used for isomerization reactions[208,406] and for isotope-selective chemistry.[404,405]

In most of these cases, IR pulses in the picosecond domain were optimized by assuming a certain shape, e.g., Gaussian or $\sin^2$, and a fixed frequency. Only recently, OCT was adopted.[449] In ref 449, a hybrid quantum control scheme for NO/Pt(111) was suggested, namely, coherent excitation of the NO−Pt vibration with IR pulses obtained from OCT, followed by the incoherent electronic excitation by hot electrons. Again, the 1D two-state model within open-system density matrix theory with Lindblad excitation/deexcitation operators[181] was used. It was found that the optimal IR pulse prepares the NO molecule such that it moves toward the surface at the moment when the hot-electron excitation sets in. By this preparation, the Antoniewicz mechanism is enhanced, and the desorption yields are found to increase by a factor of about 8.

It is expected that an entirely coherent control of surface photoreactions would be more effective. This requires, however, a direct electronic excitation. The latter is possible for Cs/Cu(111), which, as outlined above, can be *directly* excited from the SS to the Cs−Cu antibonding state (A) by a FL pulse and for which coherent phase control of desorption has been predicted.[329] Another example where coherent laser control of desorption, in this case of halogens from alkali halides via a surface exciton mechanism has been realized and modeled, was described in ref 501.

Direct control of photoreactions on semiconductors has also been suggested, as outlined earlier. Examples are the photodesorption of H from Si(100) and the lateral switching of H on the same surface[208] by FL pulses. Both reactions were found to sensitively depend on whether the H−Si bond was preexcited by IR pulses or not.

10. Conclusions

Desorption of atoms and molecules from surfaces, despite comparatively simple, is one of the key reactions in surface science. It can be initiated by various sources, ranging from simple heating over direct excitation with light sources or blackbody radiation, to hot electrons, high-energy electron beams, and other energetic particles. The time scales for desorption span a wide range from femtoseconds to seconds and longer, depending on the system and source of excitation. Furthermore, desorption serves as a model reaction for many other dynamical processes at adsorbate-covered surfaces.

There are many actual developments in the field, both experimentally and from the theoretical point of view. One

example is that the time limit of ultrafast processes is more and more being pushed into the attosecond domain, also for surfaces.[398] Attosecond processes are very popular at present in atomic and molecular physics, because they define the natural time scale of electronic motion.[502] From the theory point of view, powerful methods are being developed to follow electronic motion in real time.[503−514] This will be very beneficial also for adsorbate systems, where the direct monitoring of electron dynamics after photoexcitation plays an increasingly important role. Apart from the examples given above, this also becomes evident for "solvated electron" dynamics at surfaces.[515−522]

Another line of research, connected with scanning tunneling microscopy but also with molecular junctions, aims at pushing the spatial resolution to the molecular limit. The combination of STM or molecular devices with light holds promises, for example, for the light-induced switching of electronic currents through adsorbed molecules.[523]

The (quantum) theoretical models and methods of all of these phenomena, as different as they seem at first glance, share many common aspects. One trend for the future seems to be that the more generic, model-like theories of previous years are being complemented by the first-principles modeling of concrete systems. Still, the underlying concepts form the basis for numerical investigations and often provide a deeper understanding.

11. Acknowledgments

12. References

(1) Zimmermann, F. M.; Ho, W. *Surf. Sci. Rep.* **1995**, *22*, 127.
(2) Guo, H.; Saalfrank, P.; Seideman, T. *Prog. Surf. Sci.* **1999**, *62*, 239.
(3) Tully, J. C. *Annu. Rev. Phys. Chem.* **2000**, *51*, 153.
(4) Watanabe, K.; Takagi, N.; Matsumoto, Y. *Chem. Phys. Lett.* **2002**, *366*, 606.
(5) Camillone, N., III; Khan, K. A.; Lasky, P. J.; Wu, L.; Moryl, J. E.; Osgood, R. M., Jr. *J. Chem. Phys.* **1998**, *109*, 8045.
(6) Denzler, D. N.; Frischkorn, Ch.; Hess, C.; Wolf, M.; Ertl, G. *Phys. Rev. Lett.* **2003**, *91*, 226102.
(7) Denzler, D. N.; Frischkorn, Ch.; Wolf, M.; Ertl, G. *J. Phys. Chem. B* **2004**, *108*, 14503.
(8) Bartels, L.; Wang, F.; Möller, D.; Knoesel, E.; Heinz, T. F. *Science* **2004**, *305*, 648.
(9) Stépán, K.; Güdde, J.; Höfer, U. *Phys. Rev. Lett.* **2005**, *94*, 236103.
(10) Bonn, M.; Funk, S.; Hess, C.; Denzler, D. N.; Stampfl, C.; Scheffler, M.; Wolf, M.; Ertl, G. *Science* **1999**, *285*, 1042.
(11) Sauvage, J.-P. *Molecular Machines Motors*; Springer: Berlin, 2001.
(12) Hoki, K.; Yamaki, M.; Fujimura, Y. *Angew. Chem., Int. Ed.* **2003**, *42*, 2976.

(13) Hoki, K.; Sato, M.; Yamaki, M.; Sahnoun, R.; González, L.; Koseki, S.; Fujimura, Y. *J. Phys. Chem. B* **2004**, *108*, 4916.
(14) Huck, N. P. M.; Jager, W. F.; de Lange, B.; Feringa, B. L. *Science* **1996**, *273*, 1686.
(15) Koumura, N.; Zijlstra, R. W.; van Delden, R. A.; Harada, N.; Feringa, B. L. *Nature* **1999**, *401*, 152.
(16) Joachim, C.; Gimzewski, J. K.; Aviram, A. *Nature* **2000**, *408*, 541.
(17) Hussla, I.; Seki, H.; Chuang, T. J.; Gortel, Z. W.; Kreuzer, H. J.; Piercy, P. *Phys. Rev. B* **1985**, *32*, 3489.
(18) Niedermayer, T.; Schlichting, H.; Menzel, D.; Payne, S. H.; Kreuzer, H. J. *Phys. Rev. Lett.* **2002**, *89*, 12610.
(19) Hassel, M.; Svensson, K.; Persson, M.; Andersson, S. *Phys. Rev. Lett.* **1998**, *80*, 2481.
(20) Vondrak T.; Zhu, X.-Y. *Phys. Rev. Lett.* **1999**, *82*, 1967.
(21) Buntin, S. A.; Richter, L. J.; Cavanagh, R. R.; King, D. S. *Phys. Rev. Lett.* **1988**, *61*, 1321.
(22) Buntin, S. A.; Richter, L. J.; King, D. S.; Cavanagh, R. R. *J. Chem. Phys.* **1989**, *91*, 6429.
(23) Prybyla, J. A.; Heinz, T. F.; Misewich, J. A.; Loy, M. M. T.; Glownia, J. H. *Phys. Rev. Lett.* **1990**, *64*, 1537.
(24) Budde, F.; Heinz, T. F.; Loy, M. M. T.; Misewich, J. A.; de Rougemont, F.; Zacharias, H. *Phys. Rev. Lett.* **1991**, *66*, 3024.
(25) Misewich, J. A.; Heinz, T. F.; Newns, D. M. *Phys. Rev. Lett.* **1992**, *68*, 3737.
(26) Budde, F.; Heinz, T. F.; Kalamarides, A.; Loy, M. M. T.; Misewich, J. A. *Surf. Sci.* **1993**, *283*, 143.
(27) Ho, W. *Surf. Sci.* **1996**, *363*, 166.
(28) Prybyla, J. A.; Tom, H. W. K.; Aumiller, G. D. *Phys. Rev. Lett.* **1992**, *68*, 503.
(29) Struck, L. M.; Richter, L. J.; Buntin, S. A.; Cavanagh, R. R.; Stephenson, J. C. *Phys. Rev. Lett.* **1996**, *77*, 4576.
(30) Misewich, J. A.; Heinz, T. F.; Weigand, P.; Kalamarides, A. In *Laser Spectroscopy on Metal Surfaces*; Dai, H. L., Ho, W., Eds.; World Scientific: Singapore, 1995.
(31) Misewich, J. A.; Nakabayashi, S.; Weigand, P.; Wolf, M.; Heinz, T. F. *Surf. Sci.* **1996**, *363*, 204.
(32) Kao, F.-J.; Busch, D. G.; Cohen, D.; Gomes da Costa, D. C.; Ho, W. *Phys. Rev. Lett.* **1993**, *71*, 2094.
(33) Kao, F. J.; Busch, D. G.; Gomes da Costa, D. C.; Ho, W. *Phys. Rev. Lett.* **1993**, *70*, 4098.
(34) Busch, D. G.; Ho, W. *Phys. Rev. Lett.* **1996**, *77*, 1338.
(35) Shen, T.-C.; Wang, C.; Abeln, G. C.; Tucker, J. R.; Lyding, J. W.; Avouris, Ph.; Walkup, R. E. *Science* **1995**, *268*, 1590.
(36) Foley, E. T.; Kam, A. F.; Lyding, J. W.; Avouris, Ph. *Phys. Rev. Lett.* **1998**, *80*, 1336.
(37) Persson, B. N. J.; Avouris, Ph. *Surf. Sci.* **1997**, *390*, 45.
(38) Avouris, Ph.; Walkup, R. E.; Rossi, A. R.; Akpati, H. C.; Nordlander, P.; Shen, T.-C.; Abeln, G. C.; Lyding, J. W. *Surf. Sci.* **1996**, *363*, 368.
(39) Alavi, S.; Rousseau, R.; Patitsas, S. N.; Lopinski, G. P.; Wolkow, R. A.; Seideman, T. *Phys. Rev. Lett.* **2000**, *85*, 5372.
(40) Alavi, S.; Rousseau, R.; Lopinski, G. P.; Wolkow, R. A.; Seideman, T. *Faraday Discuss.* **2000**, *117*, 213.
(41) Sloan, P. A.; Hedouin, M. F. G.; Palmer, R. E.; Persson, M. *Phys. Rev. Lett.* **2003**, *91*, 118301.
(42) Pascual, J. I.; Lorente, N.; Song, Z.; Conrad, H.; Rust, H.-P. *Nature* **2003**, *423*, 525.
(43) Thirstrup, C.; Sakurai, M.; Nakayama, T.; Stokbro, K. *Surf. Sci.* **1999**, *424*, L329.
(44) Quaade, U. J.; Stokbro, K.; Thirstrup, C.; Grey, F. *Surf. Sci.* **1998**, *415*, L1037.
(45) Stokbro, K.; Quaade, U. J.; Lin, R.; Thirstrup, C.; Grey, F. *Faraday Discuss.* **2000**, *117*, 231.
(46) Eigler, D. M.; Schweizer, E. K. *Nature* **1990**, *344*, 524.
(47) Stroscio, J. A.; Eigler, D. M. *Science* **1991**, *254*, 1319.
(48) Bartels, L.; Meyer, G.; Rieder, K.-H. *Phys. Rev. Lett.* **1997**, *79*, 697.
(49) Eigler, D. M.; Lutz, C. P.; Rudge, W. E. *Nature* **1991**, *352*, 600.
(50) Bartels, L.; Meyer, G.; Rieder, K.-H.; Velic, D.; Knoesel, E.; Hotzel, A.; Wolf, M.; Ertl, G. *Phys. Rev. Lett.* **1998**, *80*, 2004.
(51) Akiyama, R.; Matsumoto, T.; Kawai, T. *Surf. Sci.* **1998**, *418*, L73.
(52) Carpinelli, J. M.; Swartzentruber, B. S. *Phys. Rev. B* **1998**, *58*, R13423.
(53) Ho, W. *J. Chem. Phys.* **2002**, *117*, 11033.
(54) Stipe, B. C.; Rezaei, M. A.; Ho, W. *Science* **1998**, *280*, 1732.
(55) Stipe, B. C.; Rezaei, M. A.; Ho, W. *Phys. Rev. Lett.* **1998**, *81*, 1263.
(56) Stipe, B. C.; Rezaei, M. A.; Ho, W. *Phys. Rev. Lett.* **1999**, *82*, 1724.
(57) Lauhon, L. J.; Ho, W. *J. Chem. Phys.* **1999**, *111*, 5633.
(58) Stipe, B. C.; Rezaei, M. A.; Ho, W. *Science* **1998**, *279*, 1907.
(59) Moresco, F.; Meyer, G.; Rieder, K.-H.; Tang, H.; Gourdon, A.; Joachim, Ch. *Phys. Rev. Lett.* **2001**, *87*, 088302.
(60) Dujardin, G.; Walkup, R. E.; Avouris, Ph. *Science* **1992**, *255*, 1232.
(61) Martel, R.; Avouris, Ph.; Lyo, I.-W. *Science* **1996**, *272*, 385.
(62) Stipe, B. C.; Rezaei, M. A.; Ho, W.; Gao, S.; Persson, M.; Lundquist, B. I. *Phys. Rev. Lett.* **1997**, *78*, 4410.
(63) Lauhon, L. J.; Ho, W. *J. Phys. Chem. A* **2000**, *104*, 2463.
(64) Lauhon, L. J.; Ho, W. *Surf. Sci.* **2000**, *451*, 219.
(65) Hla, S. W.; Bartels, L.; Meyer, G.; Rieder, K.-H. *Phys. Rev. Lett.* **2000**, *85*, 2777.
(66) Gaudioso, J.; Ho, W. *Angew. Chem., Int. Ed.* **2001**, *40*, 4080.
(67) Nitzan, A. *Annu. Rev. Phys. Chem.* **2001**, *52*, 681.
(68) Reichert, J.; Ochs, R.; Beckmann, D.; Weber, H. B.; Mayor, M.; Löhneysen, H. v. *Phys. Rev. Lett.* **2002**, *88*, 176804.
(69) Heurich, J.; Cuevas, J. C.; Wenzel, W.; Schön, G. *Phys. Rev. Lett.* **2002**, *88*, 256803.
(70) Frederiksen, T.; Brandbyge, M.; Lorente, N.; Jauho, A.-P. *Phys. Rev. Lett.* **2004**, *93*, 256601.
(71) Jortner, J., Ratner, M., Eds. *Molecular Electronics*; Blackwell: Oxford 1997.
(72) Wurm, S.; Feulner, P.; Menzel, D. *Phys. Rev. Lett.* **1995**, *74*, 2591.
(73) Wurm, S.; Feulner, P.; Menzel, D. *Surf. Sci.* **1998**, *400*, 155.
(74) Romm, L.; Asscher, M.; Zeiri, Y. *J. Chem. Phys.* **1999**, *110*, 3153.
(75) Lorente, N.; Teillet-Billy, D.; Gauyacq, J. P. *Surf. Sci.* **1999**, *432*, 155.
(76) Seideman, T. *J. Chem. Phys.* **1993**, *99*, 4766.
(77) Seideman, T. *J. Chem. Phys.* **1997**, *106*, 417.
(78) Feibelman, P. J. *Phys. Rev. B* **1980**, *22*, 3654.
(79) Levinson, H. J.; Plummer, E. W.; Feibelman, P. J. *J. Vac. Sci. Technol.* **1980**, *17*, 216.
(80) Feibelman, P. J. *Phys. Rev. B* **1981**, *23*, 2629.
(81) Feibelman, P. J. *Prog. Surf. Sci.* **1982**, *12*, 287.
(82) Ishida, H.; Liebsch, A. *Phys. Rev. B* **1992**, *45*, 6171.
(83) Kosloff, R. *J. Phys. Chem.* **1988**, *92*, 2087.
(84) Mohan, V.; Sathyamurthy, N. *Comput. Phys. Rep.* **1988**, *48*, 213.
(85) Heidberg, J.; Stein, H.; Riehl, E.; Szilagyi, Z.; Weiss, H. *Surf. Sci.* **1985**, *158*, 553.
(86) Meyer, H.-D.; Manthe, U.; Cederbaum, L. S. *Chem. Phys. Lett.* **1990**, *165*, 73.
(87) Manthe, U.; Meyer, H.-D.; Cederbaum, L. S. *J. Chem. Phys.* **1992**, *97*, 9062.
(88) Nest, M.; Meyer, H.-D. *J. Chem. Phys.* **2003**, *119*, 24.
(89) Berman, M.; Kosloff, R. *Comput. Phys. Commun.* **1991**, *63*, 1.
(90) Hellsing, B.; Metiu, H. *Chem. Phys. Lett.* **1986**, *127*, 45.
(91) Raab, A.; Meyer, H.-D. *J. Chem. Phys.* **2000**, *112*, 10718.
(92) Cattarius, C.; Meyer, H.-D. *J. Chem. Phys.* **2004**, *121*, 9283.
(93) Peirce, A. P.; Dahleh, M. A.; Rabitz, H. *Phys. Rev. A* **1988**, *37*, 4950.
(94) Kosloff, R.; Rice, S. A.; Gaspard, P.; Tersigni, S.; Tannor, D. J. *Chem. Phys.* **1989**, *139*, 201.
(95) Shi, S.; Rabitz, H. *J. Chem. Phys.* **1990**, *92*, 364.
(96) Yan, Y. J.; Gillilan, R. E.; Whitnell, R. M.; Wilson, K. R.; Mukamel, S. *J. Phys. Chem.* **1993**, *97*, 2320.
(97) Ohtsuki, Y.; Zhu, W.; Rabitz, H. *J. Chem. Phys.* **1999**, *110*, 9825.
(98) Ohtsuki, Y.; Nakagami, K.; Zhu, W.; Rabitz, H. *Chem. Phys.* **2003**, *287*, 197.
(99) Efrima, S.; Freed, K. F.; Jedrzejek, C.; Metiu, H. *Chem. Phys. Lett.* **1980**, *74*, 43.
(100) Jedrzejek, C.; Freed, K. F.; Efrima, S.; Metiu, H. *Chem. Phys. Lett.* **1981**, *79*, 227.
(101) Efrima, S.; Jedrzejek, C.; Freed, K. F.; Hood, E.; Metiu, H. *J. Chem. Phys.* **1983**, *79*, 2436.
(102) Korzeniewski, G. E.; Hood, E.; Metiu, H. *J. Chem. Phys.* **1984**, *80*, 6274.
(103) Zwanzig, R. *Lect. Theor. Phys.* **1960**, *3*, 106.
(104) Blum, K. *Density Matrix Theory and Applications*; Plenum Press: New York, 1996.
(105) Redfield, A. G. *IBM J. Res. Dev.* **1957**, *1*, 19.
(106) Pollard, W. T.; Felts, A. K.; Friesner, R. A. *Adv. Chem. Phys.* **1996**, *93*, 77.
(107) Kohen, D.; Marston, C. C.; Tannor, D. J. *J. Chem. Phys.* **1997**, *107*, 5236.
(108) Gaspard, P.; Nagaoka, M. *J. Chem. Phys.* **1999**, *111*, 5668.
(109) Lindblad, G. *Commun. Math. Phys.* **1976**, *48*, 119.
(110) Gorini, V.; Kossakowski, A.; Sudarshan, E. C. G. *J. Math. Phys.* **1976**, *17*, 821.
(111) Alicki, R.; Lendi, K. *Quantum Dynamical Semigroups and Applications*; Springer: Berlin, 1987.
(112) Frigerio, A.; Gorini, V. *J. Math. Phys.* **1976**, *17*, 2123.
(113) Kosloff, R.; Ratner, M. A.; Davis, W. B. *J. Chem. Phys.* **1997**, *106*, 7036.
(114) Huffacker, J. N.; Dwivedi, P. H. *J. Math. Phys.* **1975**, *16*, 862.
(115) Nest, M.; Saalfrank, P. *J. Chem. Phys.* **2000**, *113*, 8753.
(116) Nest, M.; Saalfrank, P. *Chem. Phys.* **2001**, *268*, 65.
(117) Nest, M.; Saalfrank, P. *J. Chem. Phys.* **2002**, *116*, 7189.
(118) Gelfand, Y. A.; Likhtman, E. P. *JETP Lett.* **1971**, *13*, 323.
(119) Caldeira, A. O.; Leggett, A. J. *Physica A* **1983**, *121*, 587.
(120) Gao, S. *Phys. Rev. Lett.* **1997**, *79*, 3101.

(121) Gao, S. *Phys. Rev. B* **1998**, *57*, 4509.
(122) Gao, S. *Phys. Rev. B* **1999**, *60*, 15609.
(123) Dum, R.; Zoller, P.; Ritsch, H. *Phys. Rev. A* **1992**, *45*, 4879.
(124) Dalibard, J.; Castin, Y.; Mølmer, K. *Phys. Rev. Lett.* **1992**, *68*, 580.
(125) Mølmer, K.; Castin, Y.; Dalibard, J. *J. Opt. Soc. Am. B* **1993**, *10*, 524.
(126) Steinbach, J.; Garraway, B.; Knight, P. *Phys. Rev. A* **1995**, *51*, 3302.
(127) Wolfseder, B. Ph.D. Thesis, Technische Universität München, 1997.
(128) Andrianov, I.; Saalfrank, P. *Chem. Phys. Lett.* **2003**, *367*, 455.
(129) Kaganov, M. I.; Lifshitz, I. M.; Tanatarov, L. V. *Sov. Phys. JETP* **1957**, *4*, 173.
(130) Anisimov, S. I.; Kapeliovich, B. L.; Perel'man, T. L. *Zh. Eksp. Teor. Fiz.* **1974**, *66*, 776.
(131) Hohlfeld, J.; Wellershoff, S.-S.; Güdde, J.; Conrad, U.; Jähnke, V.; Matthias, E. *Chem. Phys.* **2000**, *251*, 237.
(132) Weaver, J. H.; et al. *Physics Data*; Fachinformationszentrum: Karlsruhe, 1981.
(133) Brandbyge, M.; Hedegård, P.; Heinz, T. F.; Misewich, J. A.; Newns, D. M. *Phys. Rev. B* **1995**, *52*, 6042.
(134) Fann, W. S.; Storz, R.; Tom, H. W. K.; Bokor, J. *Phys. Rev. Lett.* **1992**, *68*, 2834.
(135) Weik, F.; de Meijere, A.; Hasselbrink, E. *J. Chem. Phys.* **1993**, *99*, 682.
(136) Bejan, D.; Raseev, G. *Phys. Rev. B* **1997**, *55*, 4250.
(137) Lugovskoy, A. V.; Bray, I. *Phys. Rev. B* **1999**, *60*, 3279.
(138) Knorren, R.; Bouzerar, G.; Bennemann, K.-H. *Phys. Rev. B* **2001**, *63*, 094306.
(139) Gao, S.; Lundquist, B. I.; Ho, W. *Surf. Sci.* **1995**, *341*, L1031.
(140) Tully, J. C.; Gomez, M.; Head-Gordon, M. *J. Vac. Sci. Technol. A* **1993**, *11*, 1914.
(141) Fox, R. F.; Gatland, I. R.; Roy, R.; Vemuri, G. *Phys. Rev. A* **1988**, *38*, 5938.
(142) Diekhöner, L.; Hornekær, L.; Mortensen, H.; Jensen, E.; Baurichter, A.; Petrunin, V. V.; Luntz, A. C. *J. Chem. Phys.* **2002**, *117*, 5018.
(143) Luntz, A. C.; Persson, M. *J. Chem. Phys.* **2005**, *123*, 074704.
(144) Springer, C.; Head-Gordon, M.; Tully, J. C. *Surf. Sci.* **1994**, *320*, L57.
(145) Springer, C. M.; Head-Gordon, M. *Chem. Phys.* **1996**, *205*, 73.
(146) Anderson, P. W. *Phys. Rev.* **1961**, *124*, 41.
(147) Newns, D. M. *Phys. Rev.* **1969**, *178*, 1123.
(148) Gadzuk, J. W. *Phys. Rev. B* **1991**, *44*, 13466.
(149) Gao, S. *Phys. Rev. B* **1997**, *55*, 1876.
(150) Chow, K. S.; Browne, D. A.; Ambegaokar, V. *Phys. Rev. B* **1988**, *37*, 1624.
(151) Goychuk, I. A.; Petrov, E. G.; Teslenko, V. I. *Phys. Rev. E* **1994**, *49*, 3894.
(152) Gao, S.; Busch, D. G.; Ho, W. *Surf. Sci.* **1995**, *344*, L1252.
(153) Persson, B. N. J.; Demuth, J. E. *Solid State Commun.* **1986**, *57*, 769.
(154) Persson, B. N. J.; Baratoff, A. *Phys. Rev. Lett.* **1987**, *59*, 339.
(155) Gao, S.; Persson, M.; Lundquist, B. I. *Solid State Commun.* **1992**, *84*, 271.
(156) Gao, S.; Persson, M.; Lundquist, B. I. *J. Electron Spectrosc. Relat. Phenom.* **1993**, *64/65*, 665.
(157) Salam, G. P.; Persson, M.; Palmer, R. E. *Phys. Rev. B* **1994**, *49*, 10655.
(158) Gao, S.; Persson, M.; Lundquist, B. I. *Phys. Rev. B* **1997**, *55*, 4825.
(159) Walkup, R. E.; Newns, D. M.; Avouris, P. *Phys. Rev. B* **1993**, *48*, 1858.
(160) Walkup, R. E.; Newns, D. M.; Avouris, P. *J. Electron Spectrosc. Relat. Phenom.* **1993**, *64/65*, 523.
(161) Teillet-Billy, D.; Gauyacq, J. P.; Persson, M. *Phys. Rev. B* **2000**, *62*, R13306.
(162) Lorente, N.; Persson, M. *Phys. Rev. Lett.* **2000**, *85*, 2997.
(163) Lorente, N.; Persson, M.; Lauhon, L. J.; Ho, W. *Phys. Rev. Lett.* **2001**, *86*, 2593.
(164) Alavi, S.; Larade, B.; Taylor, J.; Guo, H.; Seideman, T. *Chem. Phys.* **2002**, *281*, 293.
(165) Seideman, T. *J. Phys.: Condens. Matter* **2003**, *15*, R521.
(166) Alavi, S.; Seideman, T. *J. Chem. Phys.* **2001**, *115*, 1882.
(167) Alavi, S.; Larade, B.; Taylor, J.; Guo, H.; Seideman, T. *Chem. Phys.* **2002**, *281*, 293.
(168) Tikhodeev, S. G.; Ueba, H. *Phys. Rev. B* **2004**, *70*, 125414.
(169) Kaun, C.; Seideman, T. *Phys. Rev. Lett.* **2005**, *94*, 226801.
(170) Seideman, T. *Isr. J. Chem.* **2005**, *45*, 227.
(171) Liu, K.; Gao, S. *Phys. Rev. Lett.* **2005**, *95*, 226102.
(172) Schinke, R. *Photodissociation Dynamics*; Cambridge University Press: New York, 1993.
(173) Heller, E. J. *Acc. Chem. Res.* **1981**, *14*, 368.
(174) Polanyi, J. C.; Williams, R. J. *J. Chem. Phys.* **1988**, *88*, 3363.
(175) Brenig, W. *Z. Phys. B* **1976**, *23*, 361.
(176) Schuck, P.; Brenig, W. *Z. Phys. B: Condens. Matter* **1982**, *46*, 137.
(177) Gortel, Z. W.; Teshima, R.; Kreuzer, H. J. *Phys. Rev. B* **1988**, *37*, 3183.

(178) Saalfrank, P. *Chem. Phys.* **1995**, *193*, 119.
(179) Gertitschke, P. L.; Domcke, W. *Phys. Rev. A* **1993**, *47*, 1031.
(180) Saalfrank, P.; Baer, R.; Kosloff, R. *Chem. Phys. Lett.* **1994**, *230*, 463.
(181) Saalfrank, P.; Kosloff, R. *J. Chem. Phys.* **1996**, *105*, 2441.
(182) Saalfrank, P. *Chem. Phys.* **1996**, *211*, 265.
(183) Finger, K.; Saalfrank, P. *Chem. Phys. Lett.* **1997**, *268*, 291.
(184) Saalfrank, P.; Boendgen, G.; Finger, K.; Pesce, L. *Chem. Phys.* **2000**, *251*, 51.
(185) Bach, C.; Klüner, T.; Gross, A. *Chem. Phys. Lett.* **2003**, *376*, 424.
(186) Bach, C.; Klüner, T.; Gross, A. *Appl. Phys. A* **2004**, *78*, 231.
(187) Bach, C.; Carbogno, C.; Gross, A. *Isr. J. Chem.* **2005**, *45*, 45.
(188) Tully, J. C.; Preston, R. K. *J. Chem. Phys.* **1971**, *55*, 562.
(189) Tully, J. C. *Faraday Discuss.* **1998**, *110*, 407, and references therein.
(190) Tully, J. C. *J. Chem. Phys.* **1990**, *93*, 1061.
(191) Bach, C.; Gross, A. *Faraday Discuss.* **2000**, *117*, 99.
(192) Bach, C.; Gross, A. *J. Chem. Phys.* **2001**, *114*, 6396.
(193) Sholl, D. S.; Tully, J. C. *J. Chem. Phys.* **1998**, *109*, 7702.
(194) Newton, R. G. *Scattering Theory of Waves and Particles*; McGraw-Hill: New York, 1966.
(195) Harris, S.; Holloway, S.; Darling, G. R. *J. Chem. Phys.* **1995**, *102*, 8235.
(196) van Dishoeck, E. F.; van Haemert, M. C.; Allison, A. C.; Dalgarno, A. *J. Chem. Phys.* **1984**, *81*, 825.
(197) Baer, M. *Adv. Chem. Phys.* **1992**, *82*, 187.
(198) Saalfrank, P. *Chem. Phys.* **1995**, *193*, 119.
(199) Domcke, W., Yarkony, D. R., Köppel, H., Eds. *Advanced Series in Physical Chemistry, Vol. 15, Conical Intersections: Electronic Structure, Dynamics and Spectroscopy*; World Scientific: New Jersey, 2004; references therein.
(200) Klamroth, T.; Kröner, D.; Saalfrank, P. *Phys. Rev. B* **2005**, *72*, 205407.
(201) Boendgen, G.; Saalfrank, P. *J. Phys. Chem. B* **1998**, *102*, 8029.
(202) Saalfrank, P.; Boendgen, G.; Corriol, C.; Nakajima, T. *Faraday Discuss.* **2000**, *117*, 65.
(203) Alavi, S.; Rousseau, R.; Seideman, T. *J. Chem. Phys.* **2000**, *113*, 4412.
(204) Corriol, C.; Darling, G. R.; Holloway, S.; Brenig, W.; Andrianov, I.; Klamroth, T.; Saalfrank, P. *J. Chem. Phys.* **2002**, *117*, 4489.
(205) Corriol, C.; Darling, G. R.; Holloway, S.; Andrianov, I.; Klamroth, T.; Saalfrank, P. *Surf. Sci.* **2003**, *528*, 27.
(206) Jørgensen, S.; Dubnikova, F.; Kosloff, R.; Zeiri, Y.; Libach, Y.; Asscher, M. *J. Phys. Chem. B* **2004**, *108*, 14056.
(207) Ma, G.; Guo, H. *Chem. Phys. Lett.* **2000**, *317*, 315.
(208) Abe, A.; Yamashita, K.; Saalfrank, P. *Phys. Rev. B* **2003**, *67*, 235411.
(209) Pesce, L.; Saalfrank, P. *J. Chem. Phys.* **1998**, *108*, 3045.
(210) Huisinga, W.; Pesce, L.; Kosloff, R.; Saalfrank, P. *J. Chem. Phys.* **1999**, *110*, 5538.
(211) Gao, S.; Strömquist, J.; Lundquist, B. I. *Phys. Rev. Lett.* **2001**, *86*, 1805.
(212) Pesce, L.; Gerdts, T.; Manthe, U.; Saalfrank, P. *Chem. Phys. Lett.* **1998**, *288*, 383.
(213) Guo, H.; Liu, L. *Surf. Sci.* **1997**, *372*, 337.
(214) Gadzuk, J. W.; Richter, L. J.; Buntin, S. A.; King, D. S.; Cavanagh, R. R. *Surf. Sci.* **1990**, *235*, 317.
(215) Hohenberg, P.; Kohn, W. *Phys. Rev.* **1964**, *136*, B8646.
(216) Kohn, W.; Sham, L. J. *Phys. Rev.* **1965**, *140*, A1133.
(217) te Velde, G.; Baerends, E. J. *Chem. Phys.* **1993**, *177*, 399.
(218) Neugebauer, J.; Scheffler, M. *Phys. Rev. B* **1992**, *46*, 16067.
(219) Becke, A. D. *Phys. Rev. A* **1988**, *38*, 3098.
(220) Perdew, J. D. *Phys. Rev. B* **1986**, *33*, 8822.
(221) Kresse, G.; Hafner, J. *Surf. Sci.* **2000**, *459*, 287.
(222) Løvvik, O. M.; Olsen, R. A. *Phys. Rev. B* **1998**, *58*, 10890.
(223) Dong, W.; Ledentu, V.; Sautet, Ph.; Eichler, A.; Hafner, J. *Surf. Sci.* **1998**, *411*, 123.
(224) Rivière, P.; Busnengo, H. F.; Martín, F. *J. Chem. Phys.* **2004**, *121*, 751.
(225) Strømquist, J.; Bengtsson, L.; Persson, M.; Hammer, B. *Surf. Sci.* **1998**, *387*, 382.
(226) Jacobsen, K. W.; Stoltze, P.; Nørskov, J. K. *Surf. Sci.* **1996**, *366*, 394.
(227) Klamroth, T.; Saalfrank, P. *J. Chem. Phys.* **2000**, *112*, 10571.
(228) Daw, M. S.; Baskes, M. I. *Phys. Rev. B* **1984**, *29*, 6643.
(229) Gross, A.; Wilke, S.; Scheffler, M. *Phys. Rev. Lett.* **1995**, *75*, 2718.
(230) Gross, A. *Surf. Sci. Rep.* **1998**, *32*, 291.
(231) Kroes, G. J.; Baerends, E. J.; Mowrey, R. C. *Phys. Rev. Lett.* **1997**, *78*, 3583.
(232) Kroes, G. J. *Prog. Surf. Sci.* **1999**, *110*, 8696.
(233) Pijper, E.; Kroes, G. J.; Olsen, R. A.; Baerends, E. J. *J. Chem. Phys.* **2002**, *117*, 5885.
(234) Pijper, E.; Somers, M. F.; Kroes, G. J.; Olsen, R. A.; Baerends, E. J.; Busnengo, H. F.; Salin, A.; Lemoine, D. *Chem. Phys. Lett.* **2001**, *347*, 277.

(235) Busnengo, H. F.; Pijper, E.; Somers, M. F.; Kroes, G. J.; Salin, A.; Olsen, R.; Lemoine, D.; Dong, W. *Chem. Phys. Lett.* **2002**, *356*, 515.
(236) Vincent, J. K.; Olsen, R. A.; Kroes, G. J.; Luppi, M.; Baerends, E.-J. *J. Chem. Phys.* **2005**, *122*, 044701.
(237) van Harrevelt, R.; Honkola, K.; Nørskov, J. K.; Manthe, U. *J. Chem. Phys.* **2005**, *122*, 234702.
(238) Behler, J.; Delley, B.; Lorenz, S.; Reuter, K.; Scheffler, M. *Phys. Rev. Lett.* **2005**, *94*, 036104.
(239) Szabo, A.; Ostlund, N. S. *Modern Quantum Chemistry*; Dover Publications: New York, 1989.
(240) Jensen, F. *Introduction to Computational Chemistry*; Wiley: New York, 1999.
(241) Cramer, C. J. *Essentials of Computational Chemistry*; Wiley: New York, 2002.
(242) Panas, I.; Siegbahn, P.; Wahlgren, U. *Theor. Chim. Acta* **1988**, *74*, 167.
(243) Brivio, G. P.; Trioni, M. I. *Rev. Mod. Phys.* **1999**, *71*, 231.
(244) Nakatsuji, H. *J. Chem. Phys.* **1987**, *87*, 4995.
(245) Nakatsuji, H.; Nakai, H.; Fukunishi, Y. *J. Chem. Phys.* **1991**, *95*, 640.
(246) Fukunishi, Y.; Nakatsuji, H. *J. Chem. Phys.* **1992**, *97*, 6535.
(247) Nakatsuji, H.; Nakai, H. *J. Chem. Phys.* **1993**, *98*, 2423.
(248) Govind, N.; Wang, Y. A.; da Silva, A. J. R.; Carter, E. A. *Chem. Phys. Lett.* **1998**, *295*, 129.
(249) Klüner, T.; Freund, H.-J.; Freitag, J.; Staemmler, V. *J. Chem. Phys.* **1996**, *104*, 10030.
(250) Abe, A.; Yamashita, K. *Chem. Phys. Lett.* **2001**, *343*, 143.
(251) de Lara-Castells, M. P.; Krause, J. L. *Chem. Phys. Lett.* **2002**, *354*, 483.
(252) de Lara-Castells, M. P.; Krause, J. L. *J. Chem. Phys.* **2003**, *119*, 9710.
(253) de Lara-Castells, M. P.; Mitrushenkov, A. O.; Roncero, O.; Krause, J. L. *Isr. J. Chem.* **2005**, *45*, 59.
(254) Dominguez-Ariza, D.; Lopez, N.; Illas, F.; Pacchioni, G.; Madey, T. E. *Phys. Rev. B* **2004**, *69*, 075405.
(255) Runge, E.; Gross, E. K. U. *Phys. Rev. Lett.* **1984**, *52*, 997.
(256) Kröner, D.; Mehdaoui, I.; Freund, H.-J.; Klüner, T. *Chem. Phys. Lett.* **2005**, *415*, 150.
(257) Thiel, S.; Pykavy, M.; Klüner, T.; Freund, H.-J.; Kosloff, R.; Staemmler, V. *Phys. Rev. Lett.* **2001**, *87*, 077601.
(258) Pykavy, M.; Thiel, S.; Klüner, T. *J. Phys. Chem. B* **2002**, *106*, 12556.
(259) Aizawa, H.; Tsuneyuki, S. *Surf. Sci.* **1996**, *363*, 223.
(260) Saalfrank, P.; Klamroth, T. *Ber. Bunsen-Ges. Phys. Chem.* **1995**, *99*, 1347.
(261) Nakatsuji, H.; Morita, H.; Nakai, H.; Murata, Y.; Fukutani, K. *J. Chem. Phys.* **1996**, *104*, 714.
(262) Whitten, J. L. *J. Phys. Chem. A* **2001**, *105*, 7091.
(263) Buenker, R. J.; Liebermann, H.-P.; Kokh, D. B.; Izgorodina, E. I.; Whitten, J. L. *Chem. Phys.* **2003**, *291*, 115.
(264) Kokh, D. B.; Buenker, R. J.; Liebermann, H.-P.; Pichl, L.; Whitten, J. L. *J. Phys. Chem. B* **2005**, *109*, 18070.
(265) Besley, N. A. *Chem. Phys. Lett.* **2004**, *390*, 124.
(266) Besley, N. A. *J. Chem. Phys.* **2005**, *122*, 184706.
(267) Klüner, T.; Govind, N.; Wang, Y. A.; Carter, E. A. *Phys. Rev. Lett.* **2001**, *86*, 5954.
(268) Petsalakis, I. D.; Polanyi, J. C.; Theodorakopoulos, G. *Surf. Sci.* **2003**, *504*, 162.
(269) Petsalakis, I. D.; Polanyi, J. C.; Theodorakopoulos, G. *Isr. J. Chem.* **2005**, *45*, 111.
(270) Becke, A. *J. Chem. Phys.* **1993**, *98*, 5648.
(271) Nara, J.; Higai, S.; Morikawa, Y.; Ohno, T. *J. Chem. Phys.* **2004**, *120*, 6705.
(272) Kühnle, A.; Linderoth, T. R.; Hammer, B.; Besenbacher, F. *Nature* **2002**, *415*, 891.
(273) Menzel, D.; Gomer, R. *J. Chem. Phys.* **1964**, *41*, 3311.
(274) Redhead, P. A. *Can. J. Phys.* **1964**, *42*, 886.
(275) Antoniewicz, P. R. *Phys. Rev.* **1980**, *B21*, 3811.
(276) Gadzuk, J. W. *Surf. Sci.* **1995**, *342*, 345.
(277) Strömquist, J.; Gao, S. *J. Chem. Phys.* **1996**, *106*, 5751.
(278) Katz, G.; Zeiri, Y.; Kosloff, R. *J. Chem. Phys.* **2004**, *120*, 3931.
(279) Katz, G.; Zeiri, Y.; Kosloff, R. *Isr. J. Chem.* **2005**, *45*, 27.
(280) Katz, G.; Zeiri, Y.; Kosloff, R. *J. Phys. Chem. B* **2005**, *109*, 18876.
(281) Chakrabarti, N.; Balasubramanian, V.; Sathyamurthy, N.; Gadzuk, J. W. *Chem. Phys. Lett.* **1995**, *242*, 490.
(282) Burns, A. R.; Jennison, D. R.; Stechel, E. B.; Li, Y. S. *Phys. Rev. Lett.* **1994**, *72*, 3895.
(283) Burns, A. R.; Stechel, E. B.; Jennison, D. R.; Li, Y. S. *J. Chem. Phys.* **1994**, *101*, 6318.
(284) Jennison, D. R.; Stechel, E. B.; Burns, A. R.; Li, Y. S. *Nucl. Instrum. Methods Phys. Res., Sect. B* **1995**, *101*, 22.
(285) Hertel, T.; Wolf, M.; Ertl, G. *J. Chem. Phys.* **1995**, *102*, 3414.
(286) Bornscheuer, K.-H.; Nessler, W.; Binetti, M.; Hasselbrink, E.; Saalfrank, P. *Phys. Rev. Lett.* **1997**, *78*, 1174.

(287) Saalfrank, P.; Holloway, S.; Darling, G. R. *J. Chem. Phys.* **1995**, *103*, 6720.
(288) Guo, H. *Chem. Phys. Lett.* **1995**, *240*, 393.
(289) Guo, H.; Seideman, T. *J. Chem. Phys.* **1995**, *103*, 9062.
(290) Li, S.; Guo, H. *J. Chem. Phys.* **2001**, *115*, 3330.
(291) Persson, B. N. J.; Gadzuk, J. W. *Surf. Sci.* **1998**, *410*, L779.
(292) Chang, H.-C.; Ewing, G. E. *Phys. Rev. Lett.* **1990**, *65*, 2125.
(293) Chang, H.-C.; Ewing, G. E. *Chem. Phys.* **1989**, *139*, 55.
(294) Lass, K.; Han, X.; Hasselbrink, E. *J. Chem. Phys.* **2005**, *123*, 051102.
(295) Morin, M.; Levinos, N. J.; Harris, A. L. *J. Chem. Phys.* **1992**, *96*, 3950.
(296) Ashcroft, N. W.; Mermin, N. D. *Solid State Physics*; Da Holt, Rinehart and Winston: Orlando, 1976.
(297) Guyot-Sionnest, P.; Lin, P.; Miller, E. *J. Chem. Phys.* **1995**, *102*, 4269.
(298) Persson, B. N. J. *J. Phys. C: Solid State Phys.* **1984**, *17*, 4741.
(299) Head-Gordon, M.; Tully, J. C. *J. Chem. Phys.* **1992**, *96*, 3939.
(300) Head-Gordon, M.; Tully, J. C. *Phys. Rev. B* **1992**, *46*, 1853.
(301) Gai, H.; Voth, J. *J. Chem. Phys.* **1993**, *99*, 740.
(302) Guan, Y.; Muckerman, J. T.; Uzer, T. *J. Chem. Phys.* **1990**, *93*, 4383.
(303) Car, R.; Parrinello, M. *Phys. Rev. Lett.* **1985**, *55*, 2471.
(304) Muckerman, J. T.; Uzer, T. *J. Chem. Phys.* **1989**, *90*, 1968.
(305) Jackson, B. *J. Chem. Phys.* **1991**, *94*, 5126.
(306) Jackson, B. *Comput. Phys. Commun.* **1994**, *80*, 119.
(307) Billing, G. D. *J. Phys. Chem.* **1995**, *99*, 15378.
(308) Corcelli, S. A.; Tully, J. C. *J. Phys. Chem. A* **2002**, *106*, 10849.
(309) Corcelli, S. A.; Tully, J. C. *J. Chem. Phys.* **2002**, *116*, 8079.
(310) Sun, Y.-C.; Lu, H.-F.; Ho, M.-S. *Chem. Phys. Lett.* **2000**, *318*, 7.
(311) Andrianov, I.; Saalfrank, P. *Chem. Phys. Lett.* **2001**, *350*, 191.
(312) Andrianov, I.; Saalfrank, P. *J. Chem. Phys.* **2006**, *124*, 034710.
(313) Brenner, D. W. *Phys. Rev. B* **1990**, *42*, 9458.
(314) Dyson, A.; Smith, P. *Mol. Phys.* **1999**, *96*, 1491.
(315) Sbraccia, C.; Silvestrelli, P.; Ancilotto, F. *Surf. Sci.* **2002**, *516*, 147.
(316) Sun, Y.-C.; Gai, H.; Voth, G. A. *J. Chem. Phys.* **1994**, *100*, 3247.
(317) Lu, H.-F.; Ho, M.-S.; Hong, S.-C.; Liu, A.-H.; Wu, P.-F.; Sun, Y.-C. *J. Chem. Phys.* **1998**, *109*, 6898.
(318) Chiang, S.; Tobin, R. G.; Richards, P. L. *J. Electron Spectrosc.* **1983**, *29*, 113.
(319) Persson, B. N. J.; Persson, M. *Solid State Commun.* **1980**, *36*, 175.
(320) Abe, A.; Yamashita, K. *J. Chem. Phys.* **2003**, *119*, 9710.
(321) Hellsing, B.; Persson, M. *Phys. Scr.* **1984**, *29*, 360.
(322) Trail, J. R.; Graham, M. C.; Bird, D. M.; Persson, M.; Holloway, S. *Phys. Rev. Lett.* **2002**, *88*, 166802.
(323) Trail, J. R.; Bird, D. M.; Persson, M.; Holloway, S. *J. Chem. Phys.* **2003**, *119*, 4539.
(324) Mizielinski, M. S.; Bird, D. M.; Persson, M.; Holloway, S. *J. Chem. Phys.* **2005**, *122*, 084710.
(325) Schönhammer, K.; Gunnarson, O. *Phys. Rev. B* **1981**, *24*, 7084.
(326) Schönhammer, K.; Gunnarson, O. *Surf. Sci.* **1982**, *117*, 53.
(327) Nienhaus, H. *Surf. Sci. Rep.* **2002**, *45*, 1.
(328) Wolf, M.; Aeschlimann, M. *Phys. Bl.* **1998**, *54*, 145.
(329) Petek, H.; Weida, M. J.; Nagano, H.; Ogawa, S. *Science* **2000**, *288*, 1402.
(330) Höfer, U.; Shumay, I. L.; Reuss, Ch.; Thomann, U.; Wallauer, W.; Fauster, Th. *Science* **1997**, *277*, 1480.
(331) Fauster, T.; Reuss, Ch.; Shumay, I. L.; Weinelt, M. *Chem. Phys* **2000**, *251*, 111.
(332) Echenique, P. M.; Berndt, R.; Chulkov, E. V.; Fauster, T.; Goldmann, A.; Höfer, U. *Surf. Sci. Rep.* **2004**, *52*, 219.
(333) Quinn, J. J.; Ferrell, R. A. *Phys. Rev.* **1958**, *112*, 812.
(334) Campillo, I.; Pitarke, J. M.; Rubio, A.; Zarate, E.; Echenique, P. M. *Phys. Rev. Lett.* **1999**, *83*, 2230.
(335) Schöne, W.-D.; Keyling, R.; Bandić, M.; Eckart, W. *Phys. Rev. B* **1999**, *60*, 8616.
(336) Zarate, E.; Apell, P.; Echenique, P. M. *Phys. Rev. B* **1999**, *60*, 2326.
(337) Keyling, R.; Schöne, W. D.; Eckart, W. *Phys. Rev. B* **2000**, *61*, 1670.
(338) Hedin, L.; Lundquist, S. *Solid State Phys.* **1969**, *23*, 1.
(339) Campillo, I.; Silkin, V. M.; Pitarke, J. M.; Chulkov, E. V.; Rubio, A.; Echenique, P. M. *Phys. Rev. B* **2000**, *61*, 13484.
(340) Echenique, P. M.; Pitarke, J. M.; Chulkov, E. V.; Rubio, A. *Chem. Phys.* **2000**, *251*, 1.
(341) García-Lekue, A.; Pitarke, J. M.; Chulkov, E. V.; Liebsch, A.; Echenique, P. M. *Phys. Rev. B* **2003**, *68*, 045103.
(342) Campillo, I.; Pitarke, J. M.; Rubio, A.; Echenique, P. M. *Phys. Rev. B* **2000**, *62*, 1500.
(343) Gurtubay, I.; Pitarke, J. M.; Echenique, P. M. *Phys. Rev. B* **2004**, *69*, 245106.
(344) Zhukov, V. P.; Aryasetiawan, F.; Chulkov, E. V.; Echenique, P. M. *Phys. Rev. B* **2002**, *65*, 115116.
(345) Zhukov, V. P.; Chulkov, E. V.; Echenique, P. M. *Phys. Rev. Lett.* **2004**, *93*, 096401.
(346) Zhukov, V. P.; Andreyev, O.; Hoffmann, D.; Bauer, M.; Aeschlimann, M.; Chulkov, E. V.; Echenique, P. M. *Phys. Rev. B* **2004**, *70*, 233106.

(347) Spataru, C. D; Cazalilla, M. A.; Rubio, A.; Benedict, L. X.; Echenique, P. M.; Louie, S. G. *Phys. Rev. Lett.* **2001**, *87*, 246405.

(348) Gerlach, A.; Berge, K.; Goldmann, A.; Campillo, I.; Rubio, A.; Pitarke, J. M.; Echenique, P. M. *Phys. Rev. B* **2001**, *64*, 085423.

(349) Zhukov, V. P.; Chulkov, E. V.; Echenique, P. M. *Phys. Rev. B* **2003**, *68*, 045102.

(350) Echenique, P. M.; Pendry, J. B. *J. Phys. C* **1978**, *11*, 2065.

(351) Klamroth, T.; Saalfrank, P.; Höfer, U. *Phys. Rev. B* **2001**, *64*, 035420.

(352) Hotzel, A.; Wolf, M.; Gauyacq, J. P. *J. Phys. Chem. B* **2000**, *104*, 8438.

(353) Marinica, D. C.; Ramseyer, C.; Borisov, A. G.; Tellet-Billy, D.; Gauyacq, J. P.; Berthold, W.; Feulner, P.; Höfer, U. *Phys. Rev. Lett.* **2002**, *89*, 046802.

(354) Chulkov, E. V.; Sarría, I.; Silkin, V. M.; Pitarke, J. M.; Echenique, P. M. *Phys. Rev. Lett.* **1998**, *80*, 4947.

(355) Sarría, I.; Osma, J.; Chulkov, E. V.; Pitarke, J. M.; Echenique, P. M. *Phys. Rev. B* **1999**, *60*, 11795.

(356) Osma, J.; Sarría, I.; Chulkov, E. V.; Pitarke, J. M.; Echenique, P. M. *Phys. Rev. B* **1999**, *59*, 10591.

(357) Echenique, P. M.; Osma, J.; Silkin, V. M.; Chulkov, E. V.; Pitarke, J. M. *Appl. Phys. A* **2000**, *71*, 503.

(358) Keyling, R.; Schöne, W.-D.; Eckart, W. *Chem. Phys. Lett.* **2002**, *354*, 376.

(359) Chulkov, E. V.; Kliewer, J.; Berndt, R.; Silkin, V. M.; Hellsing, B.; Crampin, S.; Echenique, P. M. *Phys. Rev. B* **2003**, *68*, 195422.

(360) Wolf, M.; Knoesel, E.; Hertel, T. *Phys. Rev. B* **1996**, *54*, R5295.

(361) Bauer, M.; Pawlik, S.; Aeschlimann, M. *Phys. Rev. B* **1997**, *55*, 10040.

(362) Ogawa, S.; Nagano, H.; Petek, H. *Phys. Rev. Lett.* **1999**, *82*, 1931.

(363) Borisov, A. G.; Gauyacq, J. P.; Kazansky, A. K.; Chulkov, E. V.; Silkin, V. M.; Echenique, P. M. *Phys. Rev. Lett.* **2001**, *86*, 488.

(364) Borisov, A. G.; Gauyacq, J. P.; Chulkov, E. V.; Silkin, V. M.; Echenique, P. M. *Phys. Rev. B* **2002**, *65*, 235434.

(365) Borisov, A. G.; Kazansky, A. K.; Gauyacq, J. P. *Phys. Rev. B* **2001**, *64*, 201105.

(366) Gauyacq, J. P.; Kazansky, A. K. *Phys. Rev. B* **2005**, *72*, 045418.

(367) Borisov, A. G.; Gauyacq, J. P.; Chulkov, E. V.; Silkin, V. M.; Echenique, P. M. *Phys. Rev. B* **2002**, *65*, 235434.

(368) Borisov, A. G.; Kazansky, A. K.; Gauyacq, J. P. *Phys. Rev. B* **1999**, *59*, 10935.

(369) Borisov, A. G.; Kazansky, A. K.; Gauyacq, J. P. *Appl. Phys. A* **2004**, *78*, 141.

(370) Borisov, A. G.; Gauyacq, J. P. *Phys. Rev. B* **2000**, *62*, 4265.

(371) Sjakste, J.; Borisov, A. G.; Gauyacq, J. P. *Phys. Rev. Lett.* **2004**, *92*, 156101.

(372) Canário, A. R.; Borisov, A. G.; Gauyacq, J. P.; Esaulov, V. A. *Phys. Rev. B* **2005**, *71*, 121401(R).

(373) Hecht, T.; Winter, H.; Borisov, A. G.; Gauyacq, J. P.; Kazansky, A. K. *Phys. Rev. Lett.* **2000**, *84*, 2517.

(374) Borisov, A. G.; Gauyacq, J. P.; Sidis, V.; Kazansky, A. K. *Phys. Rev. B* **2001**, *63*, 045407.

(375) Usman, E. Yu.; Urazgil'din, I. F.; Borisov, A. G.; Gauyacq, J. P. *Phys. Rev. B* **2001**, *64*, 205405.

(376) Gadzuk, J. W.; Metiu, H. *Phys. Rev. B* **1980**, *22*, 2603.

(377) Gerber, R. B. *Chem. Rev.* **1987**, *87*, 29.

(378) Bahrim, B.; Teillet-Billy, D.; Gauyacq, J. P. *Surf. Sci.* **1999**, *431*, 193.

(379) Lorente, N.; Borisov, A. G.; Teillet-Billy, D.; Gauyacq, J. P. *Surf. Sci.* **1999**, *429*, 46.

(380) Lorente, N.; Teillet-Billy, D.; Gauyacq, J. P. *J. Chem. Phys.* **1999**, *111*, 7075.

(381) Teillet-Billy, D.; Gauyacq, J. P. *Surf. Sci.* **1990**, *239*, 343.

(382) Nestmann, B.; Nesbet, R. K.; Peyerimhoff, S. D. *J. Phys. B: At. Mol. Opt. Phys.* **1991**, *24*, 5133.

(383) Nestmann, B. *J. Phys. B: At. Mol. Opt. Phys.* **1998**, *31*, 3929.

(384) Berman, M.; Mündel, C.; Domcke, W. *Phys. Rev. A* **1985**, *31*, 641.

(385) Teillet-Billy, D.; Stibbe, D. T.; Tennyson, J.; Gauyacq, J. P. *Surf. Sci.* **1999**, *443*, 57.

(386) Nordlander, P. *Phys. Rev. B* **1992**, *46*, 2584.

(387) Hanssen, J.; Martin, C. F.; Nordlander, P. *Surf. Sci.* **1999**, *423*, L271.

(388) Braun, J.; Nordlander, P. *Surf. Sci.* **2000**, *448*, L193.

(389) Hill, S. B.; Haich, C. B.; Zhou, Z.; Nordlander, P.; Dunning, F. B. *Phys. Rev. Lett.* **2000**, *85*, 5444.

(390) Oubre, C.; Nordlander, P.; Dunning, F. B. *J. Phys. Chem. B* **2002**, *106*, 8338.

(391) Shao, H.; Langreth, D. C.; Nordlander, P. *Phys. Rev. B* **1994**, *49*, 13929.

(392) Ustaze, S.; Guillemot, L.; Esaulov, V. A.; Nordlander, P.; Langreth, D. C. *Surf. Sci.* **1998**, *415*, L1027.

(393) Klamroth, T.; Saalfrank, P. *Surf. Sci.* **1998**, *410*, 21.

(394) More, W.; Merino, J.; Monreal, R.; Pou, P.; Flores, F. *Phys. Rev. B* **1998**, *58*, 7385.

(395) Taylor, M.; Nordlander, P. *Phys. Rev. B* **2001**, *64*, 115422.

(396) Niedfeldt, K.; Carter, E. A.; Nordlander, P. *J. Chem. Phys.* **2004**, *121*, 3751.

(397) Wurth, W. *Appl. Phys. A* **1997**, *65*, 597.

(398) Föhlisch, A.; Feulner, P.; Hennies, F.; Fink, A.; Menzel, D.; Sánchez-Portal, D.; Echenique, P. M.; Wurth, W. *Nature* **2005**, *463*, 373.

(399) Koch, C. P.; Klüner, T., Freund, H.-J.; Kosloff R. *Phys. Rev. Lett.* **2003**, *90*, 117601.

(400) Koch, C. P.; Klüner, T.; Freund, H.-J.; Kosloff R. *J. Chem. Phys.* **2003**, *119*, 1750.

(401) Bonn, M.; Hess, C.; Wolf, M. *J. Chem. Phys.* **2001**, *115*, 7725.

(402) Beyvers, S.; Ohtsuki Y.; Saalfrank P. *J. Chem. Phys.* **2006**, *124*, 234706.

(403) Saalfrank, P. *J. Chem. Phys.* **2000**, *113*, 3780.

(404) Saalfrank, P.; Paramonov, G. K. *J. Chem. Phys.* **1997**, *107*, 10723.

(405) Paramonov, G. K.; Saalfrank, P. *J. Chem. Phys.* **1999**, *110*, 6500.

(406) Paramonov, G. K.; Saalfrank, P. *Chem. Phys. Lett.* **1999**, *301*, 509.

(407) Saalfrank, P. *Int. J. Quantum Chem.* **2000**, *80*, 210.

(408) Pearlstine, K. A.; McClelland, G. M. *Surf. Sci.* **1983**, *134*, 389.

(409) Liu, L.; Feldman, L. C.; Tolk, N. H.; Zhang, Z.; Cohen, P. I. *Science* **2006**, *312*, 1024.

(410) Tully, J. C. *Science* **2006**, *312*, 1004.

(411) Heidberg, J.; Stein, H.; Riehl, E. *Phys. Rev. Lett.* **1982**, *49*, 666.

(412) Gortel, Z. W.; Kreuzer, H. J.; Piercy, P.; Teshima, R. *Phys. Rev. B* **1983**, *27*, 5066.

(413) Dzegilenko, F.; Herbst, E. *J. Chem. Phys.* **1994**, *100*, 9205.

(414) Dzegilenko, F.; Herbst, E.; Uzer, T. *J. Chem. Phys.* **1995**, *102*, 2593.

(415) Brivio, G. P.; Rossi, M. L.; Torri, M.; Gortel, Z. W. *Phys. Rev. Lett.* **1996**, *76*, 3376.

(416) Ohtsuki, Y.; Kato, T.; Fujimura, Y.; Lin, S. H. *J. Chem. Phys.* **1997**, *106*, 4339.

(417) Nakagami, K.; Ohtsuki, Y.; Fujimura, Y.; Lin, S. H. *Phys. Chem. Chem. Phys.* **2003**, *5*, 528.

(418) Woittequand, S.; Toubin, C.; Pouilly, B.; Monnerville, M.; Briquez, S.; Meyer, H.-D. *Chem. Phys. Lett.* **2005**, *406*, 202.

(419) Kosloff, R.; Zeiri, Y. *J. Chem. Phys.* **1992**, *97*, 1719.

(420) Seideman, T. *J. Chem. Phys.* **1993**, *99*, 4766.

(421) Guo, H.; Schatz, G. C. *J. Chem. Phys.* **1991**, *94*, 379.

(422) Seideman, T.; Guo, H. *J. Chem. Phys.* **1995**, *103*, 2745.

(423) Hintendender, M.; Rebentrost, F.; Kosloff, R.; Gerber, R. B. *J. Chem. Phys.* **1996**, *105*, 11347.

(424) Giorgi, J. B.; Künemuth, R.; Polanyi, J. C.; Wang, J.-X. *J. Chem. Phys.* **1997**, *106*, 3129.

(425) Giorgi, J. B.; Künemuth, R.; Polanyi, J. C. *J. Chem. Phys.* **1999**, *110*, 598.

(426) García-Vela, A.; Gerber, R. B. *J. Chem. Phys.* **1993**, *98*, 427.

(427) Schröder, T.; Schinke, R.; Bačić, Z. *Chem. Phys. Lett.* **1995**, *235*, 316.

(428) Pouilly, B.; Monnerville, M.; Gatti, F.; Meyer, H.-D. *J. Chem. Phys.* **2005**, *122*, 184313.

(429) Manz, J.; Saalfrank, P.; Schmidt, B. *J. Chem. Soc., Faraday Trans.* **1997**, *93*, 957.

(430) Kroes, G. J.; Clary, D. C. *J. Phys. Chem.* **1992**, *96*, 7079.

(431) Cárdenas, A.; Coalson, R. D. *J. Chem. Phys.* **1999**, *110*, 11542.

(432) Lu, G. Q.; Linsbigler, A.; Yates, Y. T., Jr. *J. Chem. Phys.* **1995**, *102*, 4657.

(433) Petek, H.; Ogawa, S. *Prog. Surf. Sci.* **1997**, *56*, 239, and references therein.

(434) Petek, H.; Nagano, H.; Weida, M. J.; Ogawa, S. *J. Phys. Chem. A* **2000**, *104*, 10234.

(435) Watanabe, K.; Matsumoto, Y. *Faraday Discuss.* **2000**, *117*, 203.

(436) Klüner, T. *Isr. J. Chem.* **2005**, *45*, 77.

(437) Menges, M.; Baumeister, B.; Al-Shamery, K.; Freund, H.-J.; Fischer, C.; Andresen, P. *J. Chem. Phys.* **1994**, *101*, 3318.

(438) Thiel, S.; Pykavy, M.; Klüner, T.; Freund, H.-J.; Kosloff, R.; Staemmler, V. *J. Chem. Phys.* **2002**, *116*, 762.

(439) Borowski, S.; Klüner, T.; Freund, H.-J. *J. Chem. Phys.* **2003**, *119*, 10367.

(440) Borowski, S.; Klüner, T.; Freund, H.-J.; Klinkmann, I.; Al-Shamery, K.; Pykavy, M.; Staemmler, V. *Appl. Phys. A* **2004**, *78*, 223.

(441) Borowski, S.; Klüner, T. *Chem. Phys.* **2004**, *304*, 51.

(442) Mull, T.; Baumeister, B.; Menges, M.; Freund, H.-J.; Weide, D.; Fischer, C.; Andresen, P. *J. Chem. Phys.* **1992**, *96*, 7108.

(443) Klüner, T.; Freund, H.-J.; Staemmler, V.; Kosloff, R. *Phys. Rev. Lett.* **1998**, *80*, 5208.

(444) Klüner, T.; Thiel, S.; Freund, H.-J.; Staemmler, V. *Chem. Phys. Lett.* **1998**, *294*, 413.

(445) Mehdaoui, I.; Kröner, D.; Pykavy, M.; Freund, H.-J.; Klüner, T. *Phys. Chem. Chem. Phys.* **2005**, *8*, 1584.

(446) Kühn, O.; May, V. *Chem. Phys.* **1996**, *208*, 117.

(447) Howe, P.-T.; Dai, H.-L. *Surf. Sci.* **2000**, *451*, 12.

(448) Nest, M.; Saalfrank, P. *Phys. Rev. B* **2004**, *69*, 235405.

(449) Nakagami, K.; Ohtsuki, Y.; Fujimura, Y. *Chem. Phys. Lett.* **2002**, *360*, 91.

(450) Guo, H. *J. Chem. Phys.* **1997**, *106*, 1967.
(451) Guo, H.; Ma, G. *Surf. Sci.* **2000**, *451*, 7.
(452) Guo, H.; Chen, F. *Faraday Discuss.* **1997**, *108*, 309.
(453) Chen, F.; Guo, H. *Chem. Phys. Lett.* **1998**, *286*, 205.
(454) Li, S.; Guo, H. *J. Chem. Phys.* **2002**, *117*, 4499.
(455) Zimmermann, F. M. *Surf. Sci.* **1997**, *390*, 174.
(456) Zhu, X.-Y.; White, J. M. *Phys. Rev. Lett.* **1992**, *68*, 3359.
(457) Bornscheuer, K.-H.; Binetti, M.; Hasselbrink, E. *Isr. J. Chem.* **1998**, *38*, 329.
(458) Nessler, W.; Bornscheuer, K.-H.; Hertel, T.; Hasselbrink, E. *Chem. Phys.* **1996**, *205*, 205.
(459) Hasselbrink, E.; Wolf, M.; Holloway, S.; Saalfrank, P. *Surf. Sci.* **1996**, *363*, 179.
(460) Torri, M.; Gortel, Z. W.; Teshima, R. *Phys. Rev. B* **1998**, *58*, 13982.
(461) Eichler, A.; Hafner, J. *Phys. Rev. Lett.* **1997**, *79*, 4481.
(462) Kosloff, R.; Katz, G.; Zeiri, Y. *Faraday Discuss.* **2000**, *117*, 291.
(463) Gadzuk, J. W. *Chem. Phys.* **2000**, *251*, 87.
(464) Corkum, P. B.; Brunel, F.; Sherman, N. K.; Srinivasan-Rao, T. *Phys. Rev. Lett.* **1988**, *61*, 2886.
(465) Eichhorn, G.; Richter, M.; Al-Shamery, K.; Zacharias, H. *Surf. Sci.* **1996**, *368*, 67.
(466) Eichhorn, G.; Richter, M.; Al-Shamery, K.; Zacharias, H. *Chem. Phys. Lett.* **1998**, *289*, 367.
(467) Eichhorn, G.; Richter, M.; Al-Shamery, K.; Zacharias, H. *J. Chem. Phys.* **1999**, *111*, 386.
(468) Domcke, W.; Cederbaum, L. S. *J. Phys. B: At. Mol. Phys.* **1977**, *10*, L47.
(469) Domcke, W.; Cederbaum, L. S. *J. Phys. B: At. Mol. Phys.* **1980**, *13*, 2829.
(470) Nakamura, H.; Yamashita, K. *J. Chem. Phys.* **2005**, *122*, 194706.
(471) Germer, T. A.; Stephenson, J. C.; Heilweil, E. J.; Cavanagh, R. R. *J. Chem. Phys.* **1994**, *101*, 1704.
(472) Bekčić, D.; Micha, D. A. *J. Chem. Phys.* **1995**, *103*, 3795.
(473) Micha, D. A.; Yi, Z. *Chem. Phys. Lett.* **1998**, *298*, 250.
(474) Yi, Z.; Micha, D. A.; Sund, J. *J. Chem. Phys.* **1999**, *110*, 10562.
(475) Micha, D. A. *Int. J. Quantum Chem.* **2000**, *80*, 394.
(476) Micha, D. A.; Santana, A. *J. Phys. Chem. A* **2001**, *105*, 2468.
(477) Micha, D. A.; Santana, A.; Salam, A. *J. Chem. Phys.* **2002**, *116*, 5173.
(478) Micha, D. A.; Santana, A. *J. Phys. Chem. A* **2003**, *107*, 7311.
(479) Bejan, D.; Raseev, G.; Monnerville, M. *Surf. Sci.* **2001**, *470*, 293.
(480) Luntz, A.; Persson, M.; Wagner, S.; Frischkorn, C.; Wolf, M. *J. Chem. Phys.* **2006**, accepted for publication.
(481) Cai, L.; Xiao, X.; Loy, M. M. T. *Surf. Sci.* **2000**, *464*, L727.
(482) Cai, L.; Xiao, X.; Loy, M. M. T. *J. Chem. Phys.* **2001**, *115*, 9490.
(483) Hilf, M. Diploma thesis, Technische Universität München, 1996.
(484) Kampling, M.; Al-Shamery, K.; Freund, H.-J.; Wilde, M.; Fukutani, K.; Murata, Y. *Phys. Chem. Chem. Phys.* **2002**, *4*, 2629.
(485) Das, P. C.; Puri, A.; George, T. F. *J. Chem. Phys.* **1990**, *93*, 9106.
(486) Nitzan, A.; Brus, L. E. *J. Chem. Phys.* **2005**, *75*, 2205.
(487) Kwiet, S.; Starr, D. E.; Grujic, A.; Wolf, M.; Hotzel, A. *Appl. Phys. B* **2005**, *80*, 115.
(488) Rakete, C. Ph.D. Thesis, Freie Universität Berlin, 2004.
(489) Kidd, R. T.; Lennon, D.; Meech, S. R. *J. Chem. Phys.* **2000**, *113*, 8276.
(490) Thumm, U.; Kürpick, P.; Wille, U. *Phys. Rev. B* **2000**, *61*, 3067.

(491) Quijada, M.; Díez Muiño, R.; Echenique, P. M. *Nanotechnology* **2005**, *16*, S176.
(492) Zhdanov, V. P.; Kasemo, B. *Surf. Sci.* **1999**, *432*, L599.
(493) Gadzuk, J. W. *Phys. Rev. Lett.* **1996**, *76*, 4234.
(494) Gadzuk, J. W. *J. Vac. Sci. Technol. A* **1997**, *15*, 1520.
(495) Menzel, D. *Surf. Sci.* **1969**, *14*, 340.
(496) Xin, Q.-S.; Zhu, X.-Y. *Chem. Phys. Lett.* **1997**, *265*, 259.
(497) Thiel, S.; Klüner, T.; Wilde, M.; Al-Shamery, K.; Freund, H.-J. *Chem. Phys.* **1998**, *228*, 185.
(498) Letokhov, V. S. *Science* **1973**, *180*, 451.
(499) Crim, F. F. *Science* **1990**, *249*, 1387.
(500) Shapiro, M.; Brumer, P. *J. Chem. Phys.* **1993**, *98*, 201.
(501) Beck, K. M.; Joly, A. G.; Dupuis, N. F.; Perozzo, P.; Hess, W. P.; Sushko, P. V.; Shluger, A. L. *J. Chem. Phys.* **2004**, *120*, 2456.
(502) Drescher, M.; Hentschel, M.; Kienberger, R.; Uiberacker, M.; Yakovlev, V.; Scrinzi, A.; Westerwalbesloh, T.; Kleineberg, U.; Heinzmann, U.; Krausz, F. *Nature* **2002**, *419*, 803.
(503) Runge, E.; Gross, E. K. U. *Phys. Rev. Lett.* **1984**, *52*, 997.
(504) Kulander, K. C. *Phys. Rev. A* **1987**, *36*, 2726.
(505) Calvayrac, F.; Reinhard, P.-G.; Suraud, E.; Ullrich, C.-A. *Phys. Rep.* **2000**, *337*, 493.
(506) Harumiya, K.; Kawata, I.; Kono, H.; Fujimura, Y. *J. Chem. Phys.* **2000**, *113*, 8953.
(507) Zanghellini, J.; Kitzler, M.; Fabian, C.; Brabec, T.; Scrinzi, A. *Laser Phys.* **2003**, *13*, 1064.
(508) Klamroth, T. *Phys. Rev. B* **2003**, *68*, 245421.
(509) Colgan, J.; Loch, S. D.; Pindzola, M. S.; Ballance, C. P.; Griffin, D. C. *Phys. Rev. A* **2003**, *68*, 032712.
(510) Breidbach, J.; Cederbaum, L. S. *J. Chem. Phys.* **2003**, *118*, 3983.
(511) Kato, T.; Kono, H. *Chem. Phys. Lett.* **2004**, *392*, 533.
(512) Castro, A.; Marques, M. A. L.; Alonso, J. A.; Bertsch, G. F.; Rubio, A. *Eur. Phys. J. D* **2004**, *28*, 211.
(513) Nest, M.; Klamroth, T.; Saalfrank, P. *J. Chem. Phys* **2005**, *122*, 124102.
(514) Krause, P.; Klamroth, T.; Saalfrank, P. *J. Chem. Phys* **2005**, *123*, 074105.
(515) Harris, C. B.; Ge, N.-H.; Lingle, R. L., Jr.; McNeill, J. D.; Wong, C. M. *Annu. Rev. Phys. Chem.* **1997**, *48*, 711.
(516) Ge, N.-H.; Wong, C. M.; Lingle, R. L., Jr.; McNeill, J. D.; Gaffney, K. J.; Harris, C. B. *Science* **1998**, *279*, 202.
(517) Miller, A. D.; Bezel, I.; Gaffney, K. J.; Garrett-Roe, S.; Liu, S. H.; Szymanski, P.; Harris, C. B. *Science* **2002**, *297*, 1163.
(518) Gahl, C.; Bovensiepen, U.; Frischkorn, C.; Wolf, M. *Phys. Rev. Lett.* **2002**, *89*, 107402.
(519) Bovensiepen, U.; Gahl, C.; Wolf, M. *J. Phys. Chem. B* **2003**, *107*, 8706.
(520) Dutton, G.; Pu, J.; Truhlar, D. G.; Zhu, X.-Y. *J. Chem. Phys.* **2003**, *118*, 4337.
(521) Bezel, I.; Gaffney, K. J.; Garrett-Roe, S.; Liu, S. H.; Miller, A. D.; Szymanski, P.; Harris, C. B. *J. Chem. Phys.* **2004**, *120*, 845.
(522) Andrianov, I.; Klamroth, T.; Saalfrank, P.; Bovensiepen, U.; Gahl, C.; Wolf, M. *J. Chem. Phys.* **2005**, *122*, 234710.
(523) Zhang, C.; Du, M.-H.; Cheng, H.-P.; Zhang, X.-G.; Roitberg, A. E.; Krause, J. L. *Phys. Rev. Lett.* **2004**, *92*, 158301.